Nanocellulose-Enhanced Asymmetric Organocatalysis in Michael Additions and Aldol Reactions

ナリハリフェチャ, ジェシカ, ラナイブアリマナナ

Nanocellulose-Enhanced Asymmetric Organocatalysis in Michael Additions and Aldol Reactions

by

Naliharifetra Jessica Ranaivoarimanana

A Ph.D. Thesis Submitted to Faculty of Agriculture

Department of Agro-environmental Sciences

Graduate School of Bioresource and Bioenvironmental Sciences

Kyushu University, Japan

in partial fulfillment of the requirements for the degree of

Doctor of Philosophy

in

Agricultural Science

Prof. Takuya Kitaoka, Chair

Prof. Tetsuo Kondo

Assoc. Prof. Hirofumi Ichinose

Fukuoka 2020

Acknowledgements

I would like to express my deepest feeling of gratitude to my supervisor, Professor Takuya Kitaoka for the tremendous amount of knowledge he passed on me, his advices his support throughout my entire stay at Kyushu University. It is an honor and a pleasure to work under his guidance. Thank you for this great opportunity.

I would like to thank Professor Tetsuo Kondo for the time a dedication he gave for reviewing my work, but also for his advices and teachings even though we shared just short time. Nonetheless, I would like to thank Associate Professor Hirofumi Ichinose for his comments, guidance throughout my stay at Kyushu University. It is an honor to have you two as part of the reviewing committee.

In addition, my special thanks to Xin Habaki, my colleague and friend with whom I had hours of fruitful exchange and collaboration. I am also grateful to my good friend Hirayama Yusaku, for his support in many aspects of my stay in Japan, on or off campus. My special thanks to Mayumi Hatakeyama, Ph.D. who was especially kind to me since the first day I arrived at the Laboratory of Bioresources Chemistry, to Naoya Fukuda who also helped me at the end of my thesis.

I am also grateful to Kyohei Kanomata, Ph.D. for his guidance, his strict but sound critics.

I would like to thank the Japanese Government who supported this research and my stay *via* the MEXT scholarship program.

To all my laboratory mates, former and present, my gratitude for the enthusiasm and the particularly nice atmosphere we had in the laboratory.

To my family and friends, for the love and care, thank you.

Last but not least, I would like to send my thoughts to my moms who hold a special place in my heart.

I dedicate this work to my wife Zo. You're always there to cheer me up, for long extrapolations about research and fun subjects, to help me make that next step. Words cannot describe how grateful I am to have you.

Fukuoka, September 25th, 2020

Naliharifetra Jessica Ranaivoarimanana

Table of contents

Abbreviations

CNC	Cellulose nanocrystals
CNF	Cellulose nanofibrils
CsNF	Chitosan Nanofiber
CsP	Chitosan Powder
DFT	Density Functional Theory
dr	Diastereomeric ratio
ee	Enantiomeric excess
MD	Molecular Dynamics
MM	Molecular Mechanics
NMR	Nuclear Magnetic Resonance
NP	Nanoparticles
PMF	Potential of Mean Force
QM	Quantum Mechanics
SDGs	Sustainable Developpement Goals
SFC	Supercritical Fluid Chromatography
SMD	Steered Molecular Dynamics
TEM	Transmission Electronic Microscopy
TEMPO	2,2,6,6-tetramethylpiperidine 1-oxyl
TLC	Thin Layer Chromatography

TOCNF	TEMPO oxidized cellulose nanofibrils
TOCNF-H	protonated TEMPO oxidized cellulose nanofibrils
XRD	X-Ray diffraction

List of Figures

List of Schemes

List of Tables

Chapter 1

Introduction

Sustainable Developpement Goals (SDGs) are for now farfetched for many in the industry or academic circle. However, the Earth is gifted with natural polysaccharides, a class of molecule which is so abundant and renewable that tapping into it would substantially contribute to the SDGs in terms of materials production but also energy [1]. This study will expand celluloses rather lightly explored potentials which will constitute one face of the coin to buy an entrance in the achievement of SDGs with the other face constituted by organocatalytic reactions.

1.1. Cellulose

1.1.1. Background

The term ‘cellulose’ was first used by Anselm Payen in 1838 when he discovered a fibrous material obtained after treating plant tissue, cotton linters, root tips, pit and ovules from the flowers of trees with acid-ammonia followed by extraction in water [2]. Cellulose, a natural polysaccharide, is the most abundant and renewable natural polymer on Earth because it is the main constituent of green plants’ cell walls. It can be present in the leaf (e.g., sisal), in the fruit (e.g., cotton) or in the stalk or the rigid structure of plants (e.g., wood, flax) [3]. Through the ages, this substance found various applications as heating source, clothing, writing support and building material. Although the main source of cellulose are woods and plant fibers (cotton, hemp, flax, etc.), it can also be extracted from marine animals (tunicate), algae, fungi,

invertebrates, and bacteria [4,5]. Nowadays, the annual industrial production of cellulose is estimated to be over 75 billion tons [6]. The majority is extracted from wood as cellulose pulp for papermaking. However, a growing interest is noticed in the field of energy production [7] due to cellulose's renewability and abundance but also in the developpement of advanced functional material as nanosized cellulose presents outstanding properties such as low density but having high stiffness, high specific surface area, transparency etc. [8]

Regardless of its origin, cellulose is a linear homopolymer of D-glucose connected by acetal functions at C4 and C1 positions or *β*-1,4 linkages also named *O*-glycosidic bonds (**Figure 1. 1**).

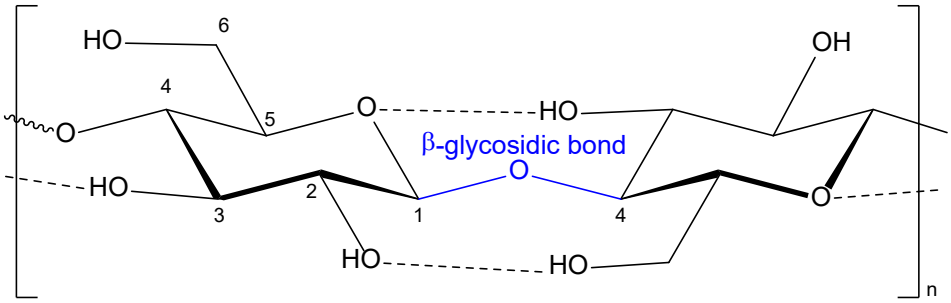

Figure 1. 1 Schematic of a single cellulose chain repeat unit with atom numbering, showing the directionality of the *β*-1,4 linkage and intrachain hydrogen bonding (dotted line). (Adapted from Ref. 9 with permission from Springer).

The regular assembly of dozens of cellulose molecule chains in one direction bundled together by strong hydrogen bonds forms highly crystalline cellulose microfibrils of 3 to 4 nm in width and several microns in length (**Figure 1. 2**).

1.1.2. Nano-sized cellulose or cellulose nanofibrils (CNF) production

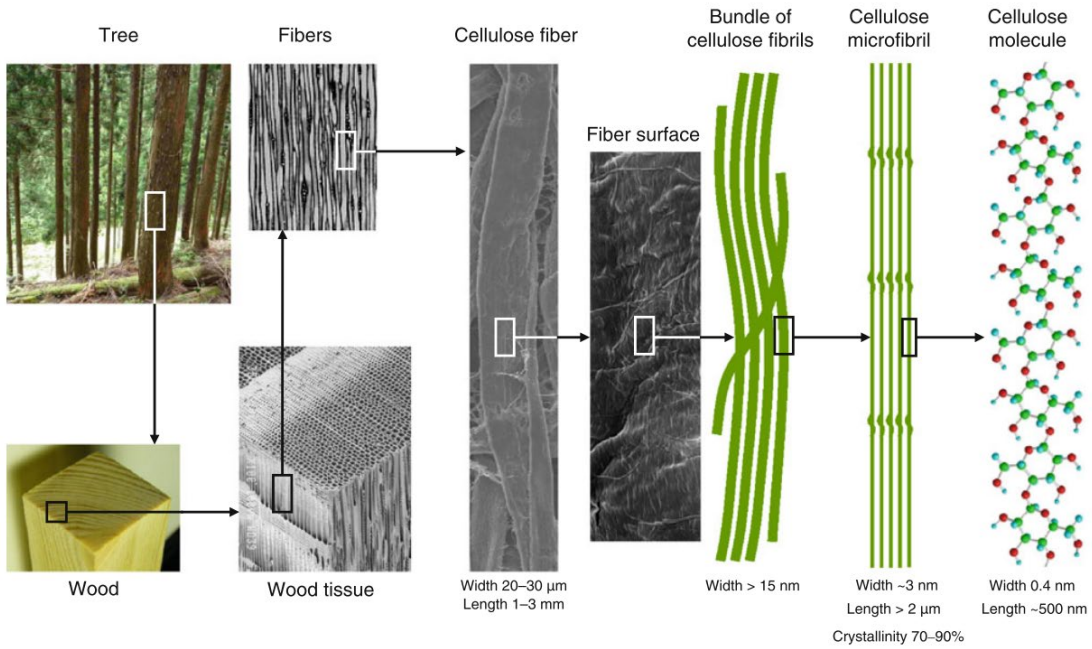

Figure 1. 2 Hierarchical structure of wood cellulose from a tree to a cellulose chain (Reprinted from Ref. 8 with permission from Springer).

CNF can be produced by some bacteria and algae or extracted from plants, e.g. wood, in two general steps: (1) a portion of hemicellulose and most of the lignin covering CNFs in the cell walls are removed from the plant chips by pulping techniques (mechanical pulping, kraft or sulfite process); (2) as CNF are strongly bonded together by hydrogen bonds, strong mechanical treatment are applied subsequently with chemical treatments to individualize them from the pulp. Some example of devices to mechanically tear down the fibers includes super-grinders, microfluidizers, high-pressure homogenizers [9–11].

The chemical treatment's purpose is to introduce anionic charges on the surface of the material. This will cause strong repulsion between fibers and reduce the energy required by the mechanical treatment to produce individualized nanosized cellulose. The diversity of CNF properties depend on two main factors: (1) the biosynthesis of the crystalline cellulose microfibrils, which is dependent on cellulose source, and (2) the extraction process of the CNF

from the cellulose microfibrils, which includes aforementioned mechanical/chemical treatments [12].

The pioneering method for charge introduction is acid hydrolysis [13,14]. For example, the use of a 63.5% (w/w) sulfuric acid at 40 to 80°C for the hydrolysis with subsequent sonication results in needle shaped cellulose called cellulose nanocrystals (CNC). The nanoparticles have lengths between 200 and 400 nm, widths lesser than 10 nm and a the recovery yield is in the order of 30% [15]. Taking advantage of these physicochemical properties, CNF and CNC have been widely explored in polymer nanocomposite reinforcement, high performance purification systems [16,17]. Tremendous efforts have been made towards industrial production of CNF, although it is still hampered by the enormous energy requirement in the mechanical treatment requirement to individualize the fibers due to strong interfibrillar hydrogen bonds. The solution in energy reduction provided by acid hydrolysis also raise concerns about the generation of hazardous effluents inherent to this method. Additionally, the yield is relatively low and the control of uniformity in shape of obtained particles is difficult because of the harsh treatment. Such features are crucial for CNF applications. These issues are being addressed by a mild but efficient chemical pretreatment named TEMPO mediated oxidation.

1.1.3. TEMPO-oxidized cellulose nanofibrils (TOCNF) production

The method consists of introducing carboxylates on the surface of native cellulose crystals then applying mechanical treatment to individualize the nanofibrils. In this process, catalytic amounts of 2,2,6,6-tetramethylpiperidine 1-oxyl (TEMPO) and NaBr are dissolved in aqueous suspension of the cellulose pulp at pH 10–11, and the oxidation is initiated by the addition of NaClO solution as a primary oxidant at room temperature. The result is a complete selective transformation of glucose into glucuronic acid units at a regular interval on the surface of the native crystalline cellulose bundles (**Figure 1. 3**) [18]. The application of

TEMPO/NaBr/NaClO is then followed by mild mechanical treatment. The treatment using household blenders for 4 minutes is enough to yield more than 95% of individual nanofibrils [19]. Among reported CNF, TOCNF have the narrowest width (3-4 nm). The nanofibril width is almost uniform across different wood species. The length can be adjusted depending on the oxidation and disintegration conditions and can reach several microns yielding aspect ratios over 100. Furthermore, the mildness of the approach leaves the original cellulose crystal unchanged permitting high crystallinity in the final product. Therefore, well-defined nanoarchitecture confer to TOCNF-derived materials superior physical properties in gas-barrier films [20], free-standing aerogels [21], nanocomposites [22], purification membranes [23,24], and in the confection of electroactive paper [25,26].

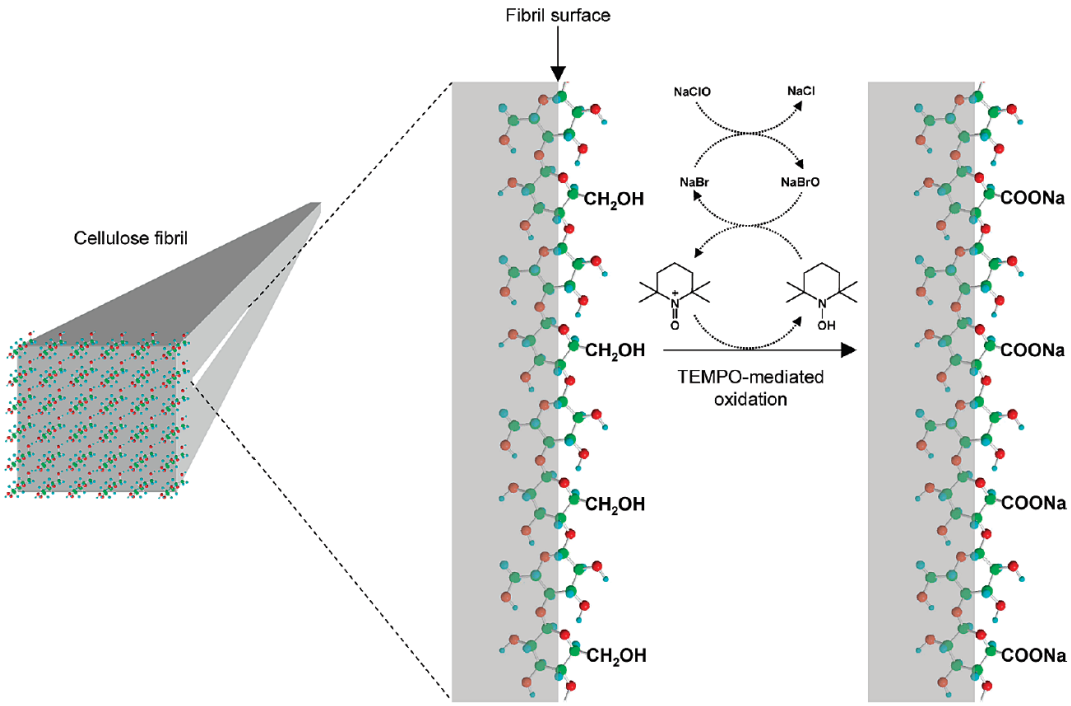

Figure 1. 3 Schematic model of oxidation of C6 primary hydroxyl on cellulose microfibril surfaces by TEMPO/NaClO/NaBr system (Reprinted with permission from Ref. 18. Copyright (2010) American Chemical Society).

1.1.4. CNF's abilities to interact with various substrates

The last decade has seen nanocellulose established as an excellent environmentally friendly nanofillers for the reinforcement in polymer matrixes, membranes, and other materials. This is made possible by their high aspect ratio, low thermal expansion, highly crystalline structure and the presence of numerous hydroxy groups and functions introduced by the chemical treatment during their preparation. Material-oriented applications of CNF have been extensively studied. Nonetheless, the application derived by the surface chemistry of nanocellulose are gaining more attention.

The hydroxy groups from native cellulose give CNF their main hydrophilic character. These functions can form hydrogen bonds that are the key function in binder applications related to adhesion between cellulose nanoparticles and other materials [27].

An important feature of cellulose is its chirality. Cellulose chains present a regular helical structure. The material, not in its nanofibril form but 6-trityl-cellulose dissolved in chloroform, is often used to coat silica gel to make chiral stationary phases of separation columns for high-performance liquid chromatography [28]. The performance of the separation of chiral substances depends on the highly regular helical structure induced by cellulose with various hydrogen bonding and π-π interactions from the functionalized surface [29]. On the other hand, bundled and individualized cellulose nanofibrils exhibit right-handed twisted nanostructure [30]. In addition, negatively charged chiral surface of nanocelluloses promote a self-organization phenomenon known as chiral-nematic ordering (**Figure 1. 4**). The chirality sparkled optical applications of CNFs [31], but more importantly, the chiral nanocellulose structure was reported to induce conformational changes on adsorbed dyes such as Congo red [32]. The free and optically inactive dye showed a red shift once adsorbed on the chiral CNF's

surface. Transfer of the intrinsic structural chirality from nanocelluloses is much expected in the making of chiral materials and chiral catalysis or asymmetric catalysis [33].

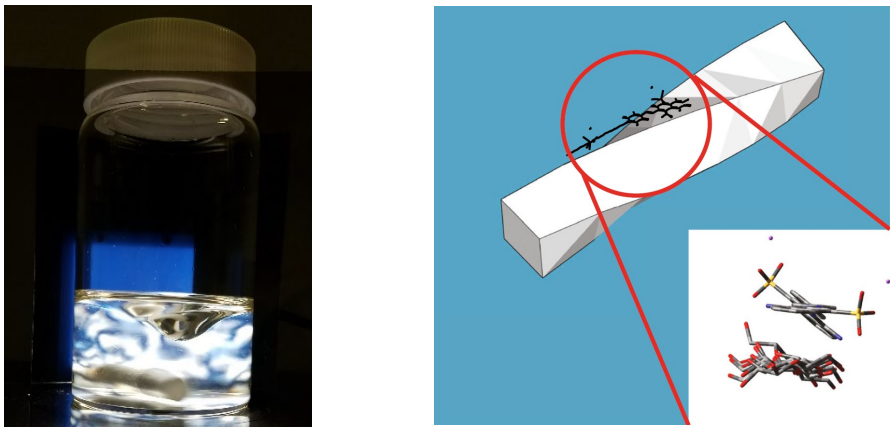

Figure 1. 4 On the left: TOCNF water suspension observed between cross-polarized filters showing birefringence, characteristic to chiral nematic ordered suspensions; on the right: computational model from Density Functional Theory calculations (DFT) of the conformation of Congo red when adsorbed on a twisted CNF. The dye molecule adopted a twisted conformation reflecting CNF's chirality (Reprinted from Ref. 32 with permission from Springer).

The readily functionalizable nature of cellulose makes CNFs, especially TOCNFs, a matrix of choice for the immobilization of metal nanoparticles (NP) and cations as catalysts [34]. Indeed, the surface hydroxy groups on the nanocelluloses itself and the carboxylate groups from TEMPO-mediated oxidation are very effective at reducing and stabilizing metal precursors. As an example, palladium NP were successfully immobilized on CNC with covalent bonding and the composite was used in the hydrogenation of ketones [35]. It is important to point that the use of cellulose in the domain of catalytic reactions has been only lightly explored. The field in still in its infancy and the application of nanocellulose in organocatalysis is highly awaited [35–37].

1.2. Organocatalysis

1.2.1. Organocatalyst

Organocatalysis is the use of non-metallic catalysts to accelerate chemical reactions. The term refers to catalyst solely composed of C N H or P atoms, without metals[38]. Heavy metal pollution resulting from industrial solid waste disposal is a major environmental problem the modern world face [39]. In addition, metal catalysts are expensive and very sensible to air and moisture. Despite being highly reactive and selective, they require inert conditions where the reactions are conducted under argon or nitrogen atmosphere to fully exploit their potential.

The rush for the developpement of organocatalyst started in the 1970s with the Hajos–Parrish–Eder–Sauer–Wiechert reaction [40]:

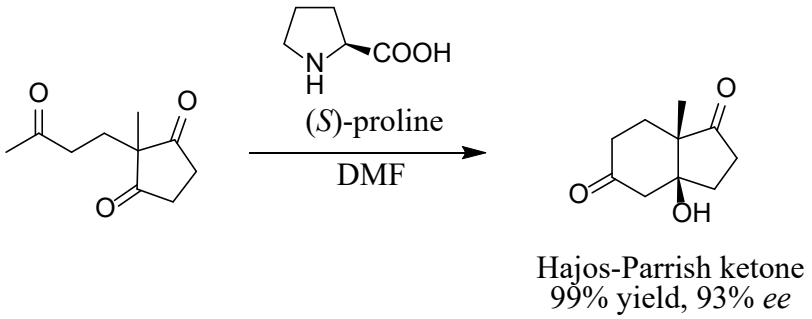

Hajos-Parrish ketone
99% yield, 93% *ee*

Scheme 1. 1 Hajos–Parrish–Eder–Sauer–Wiechert reaction catalyzed by (*S*)-Proline for the synthesis of Hajos-Parrish ketones and Wieland-Miescher ketones [40].

The particularity in this synthesis of the Hajos-Parrish ketones or Wieland-Miescher ketones is the use of proline, a molecule devoid of metal, to achieve highly enantioselective aldol reaction (**Scheme 1. 1**). Enantioselectivity (*ee*) is the degree to which one enantiomer of a chiral product is preferentially formed in a reaction. These types of reactions are also noted asymmetric reactions. An enantiomer is one of a pair of chemical compounds whose molecular

structures have a mirror-image relationship to each other. This property is often linked to the presence of a chiral center in the compound e.g. a carbon linked to four different substituents. In the production of natural compounds *via* asymmetric synthesis, seeking for the highest *ee* is of paramount interest because each enantiomer often possess drastically different therapeutic effects [41].

The transfer of the chirality of nanocellulose in chemical reactions has only been seldomly reported. The following few studies showed that nanosized cellulose materials can affect the enantioselectivity in catalytic processes. Serizawa and coworkers reported that the hydrolysis of chiral peptides for several days showed different reaction rates for each enantiomer when the hydrolytic reaction was directly catalyzed by cellulose nanowhiskers [36]. Furthermore, Kaushik and coworkers showed that the hydrogenation of ketones catalyzed by nanocomposites formed by palladium nanoparticles supported on cellulose nanowhiskers afforded the products with some enantioselectivity [35]. Although the nanocomposites does not fall in the realm of organocatalysts and that the reactions' selectivities were insufficient from the viewpoint of asymmetric synthesis, these two reports clearly indicated that nanocellulose has the potential to induce enantioselectivity, possibly owing to its inherent chiral nanoarchitecture [31,42–44].

The high specific surface area and structural rigidity of nanocellulose are key to enhancing catalytic efficiency in heterogeneous reactions [45]. Although nanocellulose has only been reported as a solid support in immobilized catalysts to date, the direct contribution of nanocellulose to heterogeneous catalysis [46] will attract much attention in academia and industry because such novel chiral catalytic systems would expand the potential practical applications of nanocellulose and will open up new horizons in nanocellulose engineering and asymmetric catalysis science.

Proline sparked a number of publication and organocatalytic systems development. Notably, in the domain of carbon–carbon bond forming reactions such as aldol reactions, Michael addition, Mannich reactions, and Diels–Alder reactions to name a few[47].

(*S*)-Proline is industrially produced by precipitation from gelatin hydrolysate or fermentation using *Brevibacterium flavum* mutants [48]. The amino acid is an attractive cheap and readily available organocatalyst that can and already contributes to sustainable processes. Despite these advantages, the common trait to its use as a catalyst is the requirement of a high amount paired with moderate to low selectivity. A new strategy for CNF based organocatalyst with proline is then much attractive. The Michael additions of ketones to nitroolefins and the aldol reaction of ketones to aldehydes are good candidates for this purpose due to the nature of their substrates susceptible to interact with CNF.

1.2.2. Michael addition

The Michael addition is one of the most studied carbon–carbon bond-forming reaction along with the aldol reaction. In fact, the nucleophilic addition to nitroolefin in the Michael addition represents a direct and attractive approach for the construction of versatile β-functionalized intermediates in organic synthesis because the nitro group can undergo further transformations [49]:

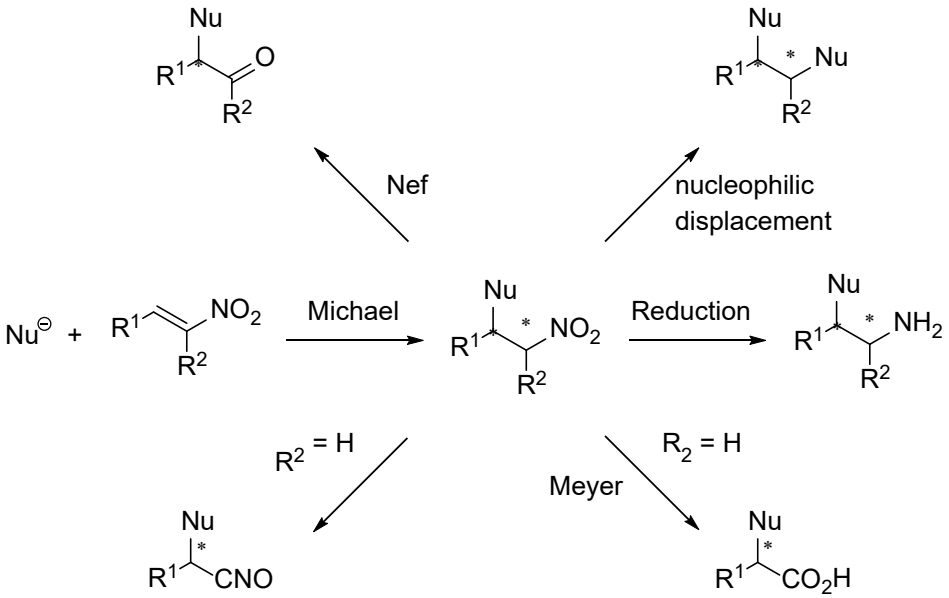

Scheme 1. 2 Possible transformations that nitro groups can undergo after the Michael addition (Adapted from Ref. 49 with permission from John Wiley and Sons).

The first use of (*S*)-proline to catalyze the Michael addition was discovered the same year by List *et al.* and Barbas *et al*., two different research groups [50,51].

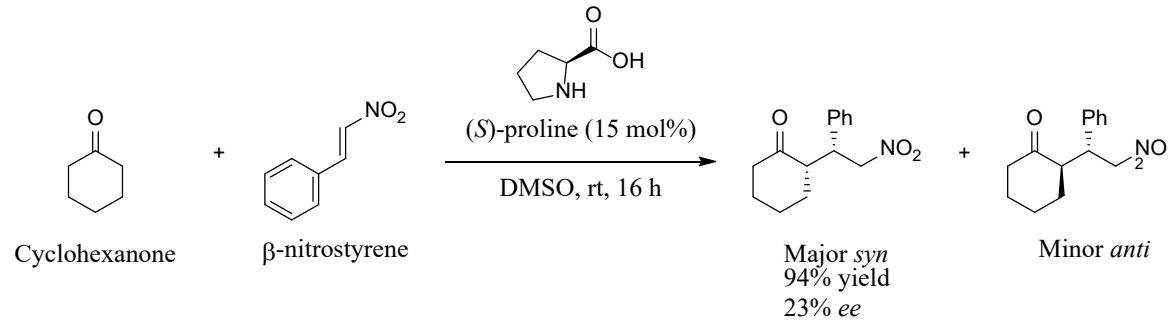

Scheme 1. 3 (S)-Proline catalyzed Michael addition between cyclohexanone and β-nitrostyrene in DMSO at room temperature [50].

The reaction is the formation of a new C–C bond between a ketone and an α-β unsaturated compound (**Scheme 1. 3**). The result is the production of two pair of enantiomers where the *syn* configuration is predominant when catalyzed by (*S*)-proline.

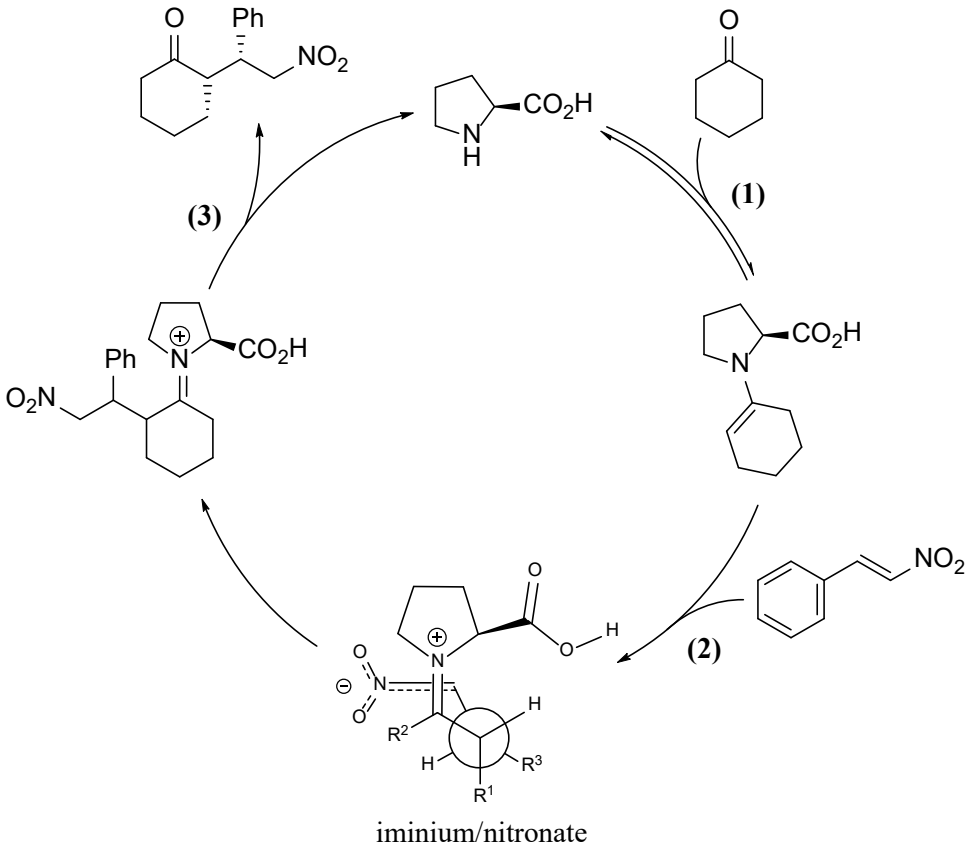

Scheme 1. 4 Commonly adopted mechanism of the (*S*)-Proline catalyzed Michael addition between cyclohexanone and β-nitrostyrene.

The adopted mechanism of the reaction starts with the formation of an enamine intermediate between proline and the ketone substrate (step 1 in **Scheme 1. 4**). The enamine is then subjected to nucleophilic attack by the nitroolefin to form an iminium/nitronate transition state (step 2). This step is considered to be the enantioselective step and stabilization of the

transition step would enable high enantioselectivity [52]. The last part of the mechanism is a hydrolysis to release the product and regenerate (*S*)-proline (step 3).

The main drawback of the reaction is poor enantioselectivity and a high catalyst loading. However, good enantiocontrol is highly desirable because the Michael addition offers the possibility to synthesize γ-nitro carbonyl compounds which are valuable building blocks for the preparation of various pharmaceutically relevant compounds such as the anti-influenza drug (－)-Oseltamivir [53].

1.2.3. Aldol reaction

The asymmetric aldol reaction is frequently employed as a crucial step of enantioselective C–C bond formation in the total synthesis of natural products [54]. Constituting one of the key milestones of organocatalysis, the (*S*)-proline catalyzed intermolecular aldol reactions *via* an enamine mechanism was also discovered the same year by Lis *et al.* and Barbas *et al*. in 2001 (**Scheme 1. 5**) [55,56]:

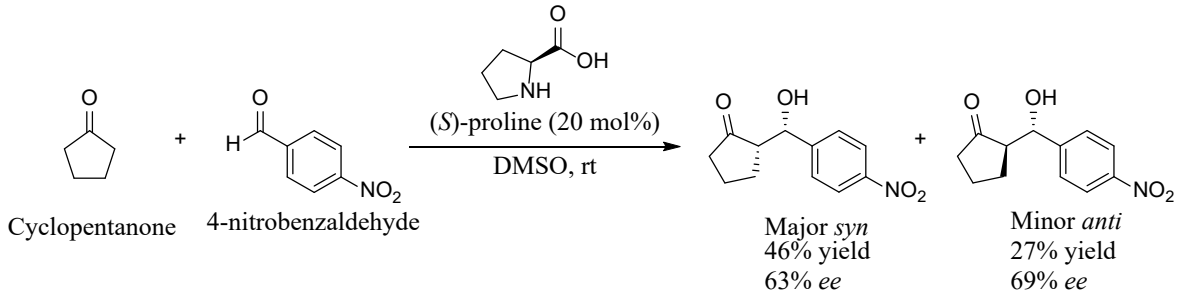

Scheme 1. 5 (*S*)-Proline catalyzed aldol reaction between cyclopentanone and 4-benzaldehyde in DMSO at room temperature [55,56].

The mechanism of the reaction is commonly admitted starting with the reversible formation of an enamine between proline and the ketone substrate (step 1 in **Scheme 1. 6**). The orientation on the approach of the enamine on the attack on the aldehyde substrate is the enantioselective step (step 2).

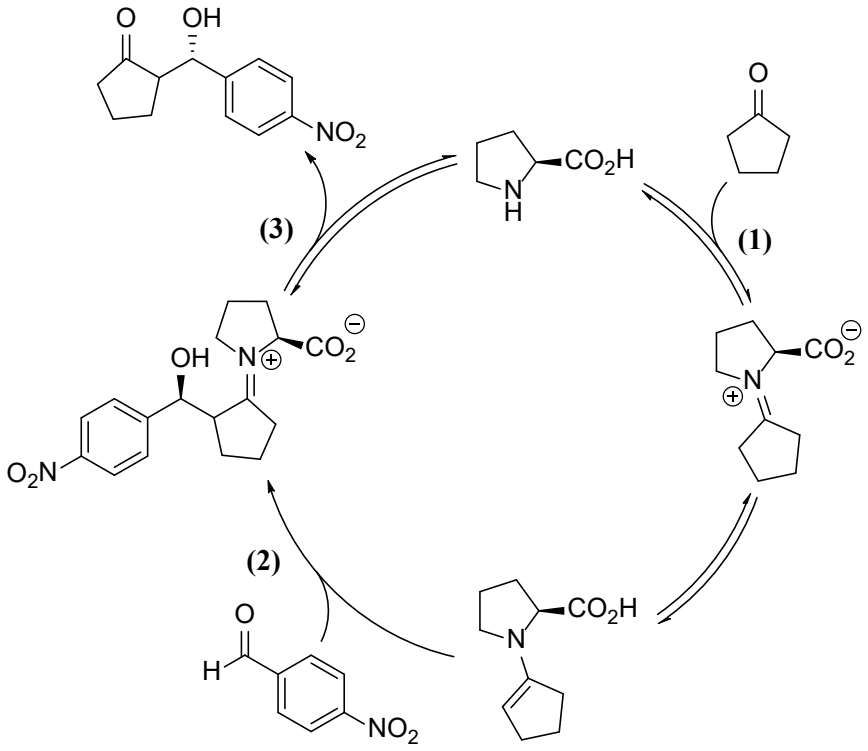

Scheme 1. 6 Commonly adopted mechanism of the (*S*)-Proline catalyzed Aldol reaction between cyclopentanone and 4-nitrobenzaldehyde.

It is important to notice that (*S*)-proline can form oxazolidinones with two molecules of the aldehyde substrate in the case of the aldol reaction (**Scheme 1. 7**). The process is irreversible thus induce deactivation of the catalyst overtime.

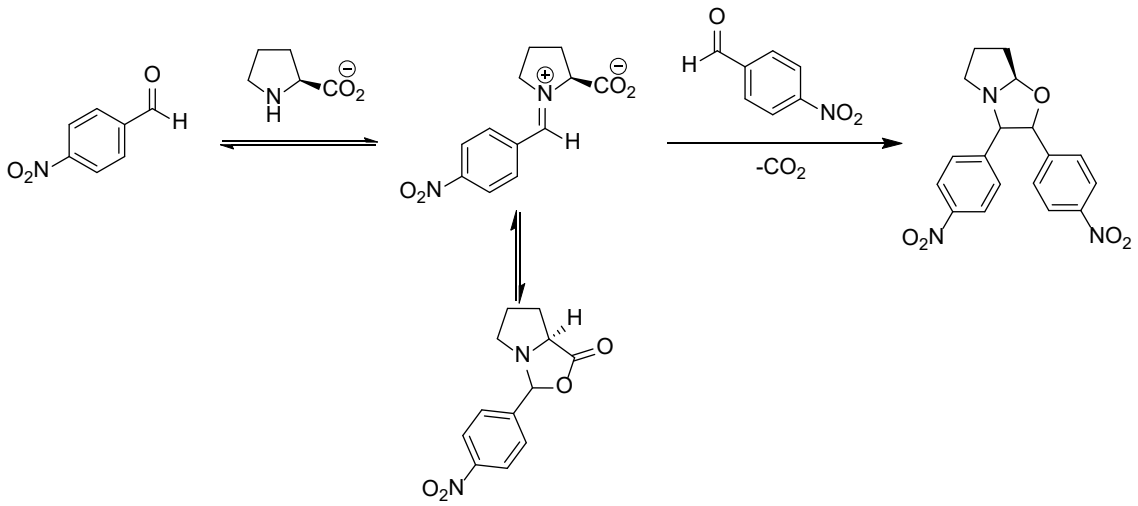

Scheme 1. 7 Commonly adopted mechanism of the formation of oxazolidinone in the (*S*)-Proline catalyzed Aldol reaction with 4-nitrobenzaldehyde.

1.3. Dissertation overview

This thesis is an overview of the results reported in two publications supported with some unpublished data. The target of this work is to bring to light novel functionality of cellulose nanofibrils and widen the application of these materials in a more ecological way. In other words, to contribute to asymmetric organocatalysis with green and sustainable polysaccharide nanofibers.

In the first publication which constitutes the second chapter [57], TOCNF was used in conjunction with (*S*)-proline in the asymmetric Michael addition. In the second publication comprised in the third chapter, TOCNF-H was used combined with (*S*)-proline in the asymmetric aldol reaction. The two chapters represents attempts on transferring nanocellulose's intrinsic chirality by using them as matrix for the respective reactions.

The fourth chapter focus on using different polysaccharide nanofibers as catalyst. The materials were tested as chiral source and promoter of a collection of few organocatalytic reactions.

The manuscript consists of the identification of the suitable nanocellulose or polysaccharide nanofibers enhancer, and reaction condition optimizations. Additionally, an application of the new catalytic system to different substrates is reported. Furthermore, attempts on investigations of the reaction's mechanism is also provided.

References

1. Ashby, M.F. Scaling Up Biopolymer Production. In *Materials and Sustainable Development*; Elsevier, **2016**; pp. 117–133.

2. Eichhorn, S.J.; Baillie, C.A.; Zafeiropoulos, N.; Mwaikambo, L.Y.; Ansell, M.P.; Dufresne, A.; Entwistle, K.M.; Herrera-Franco, P.J.; Escamilla, G.C.; Groom, L.; et al. Current international research into cellulosic fibres and composites. *J. Mater. Sci.* **2001**, *36*, 2107–2131.

3. Lavoine, N.; Desloges, I.; Dufresne, A.; Bras, J. Microfibrillated cellulose - Its barrier properties and applications in cellulosic materials: A review. *Carbohydr. Polym.* **2012**, *90*, 735–764.

4. Klemm, D.; Kramer, F.; Moritz, S.; Lindström, T.; Ankerfors, M.; Gray, D.; Dorris, A. Nanocelluloses: A new family of nature-based materials. *Angew. Chemie - Int. Ed.* **2011**, *50*, 5438–5466.

5. Klemm, D.; Heublein, B.; Fink, H.-P.; Bohn, A. Cellulose: Fascinating Biopolymer and Sustainable Raw Material. *Angew. Chem. Int. Ed* **2005**, *44*, 3358–3393.

6. Habibi, Y.; Lucia, L.A.; Rojas, O.J. Cellulose nanocrystals: Chemistry, self-assembly, and applications. *Chem. Rev.* **2010**, *110*, 3479–3500.

7. Balat, M. Production of bioethanol from lignocellulosic materials via the biochemical pathway: A review. *Energy Convers. Manag.* **2011**, *52*, 858–875.

8. Isogai, A. Wood nanocelluloses: Fundamentals and applications as new bio-based nanomaterials. *J. Wood Sci.* **2013**, *59*, 449–459.

9. Turbak, A.F.; Snyder, F.W.; Sandberg, K.R. Microfibrillated cellulose, a new cellulose product: Properties, uses, and commercial potential. *J. Appl. Polym. Sci., Appl. Polym.*

Symp. **1983**.

10. Taniguchi, T. Microfibrillation of natural fibrous materials. *J. Soc. Mater. Sci.* **1996**, *45*, 472–473.

11. Missoum, K.; Belgacem, M.; Bras, J. Nanofibrillated Cellulose Surface Modification: A Review. *Materials (Basel).* **2013**, *6*, 1745–1766.

12. Moon, R.J.; Martini, A.; Nairn, J.; Simonsen, J.; Youngblood, J. Cellulose nanomaterials review: Structure, properties and nanocomposites. *Chem. Soc. Rev.* **2011**, *40*, 3941–3994.

13. Nickerson, R.F.; Habrle, J.A. Cellulose intercrystalline structure. *Ind. Eng. Chem.* **1947**, *39*, 1507–1512.

14. Chen, Y.; Liu, C.; Chang, P.R.; Cao, X.; Anderson, D.P. Bionanocomposites based on pea starch and cellulose nanowhiskers hydrolyzed from pea hull fibre: Effect of hydrolysis time. *Carbohydr. Polym.* **2009**, *76*, 607–615.

15. Bondeson, D.; Mathew, A.; Oksman, K. Optimization of the isolation of nanocrystals from microcrystalline cellulose by acid hydrolysis. *Cellulose* **2006**, *13*, 171–180.

16. Eichhorn, S.J.; Dufresne, A.; Aranguren, M.; Marcovich, N.E.; Capadona, J.R.; Rowan, S.J.; Weder, C.; Thielemans, W.; Roman, M.; Renneckar, S.; et al. Review: current international research into cellulose nanofibres and nanocomposites. *J. Mater. Sci.* **2010**, *45*, 1–33.

17. Mondal, S. Preparation, properties and applications of nanocellulosic materials. *Carbohydr. Polym.* **2017**, *163*, 301–316.

18. Okita, Y.; Saito, T.; Isogai, A. Entire surface oxidation of various cellulose microfibrils by TEMPO-mediated oxidation. *Biomacromolecules* **2010**, *11*, 1696–1700.

19. Isogai, A.; Saito, T.; Fukuzumi, H. TEMPO-oxidized cellulose nanofibers. *Nanoscale* **2011**, *3*, 71–85.

20. Fukuzumi, H.; Saito, T.; Iwata, T.; Kumamoto, Y.; Isogai, A. Transparent and High Gas Barrier Films of Cellulose Nanofibers Prepared by TEMPO-Mediated Oxidation. *Biomacromolecules* **2009**, *10*, 162–165.

21. Nemoto, J.; Saito, T.; Isogai, A. Simple Freeze-Drying Procedure for Producing Nanocellulose Aerogel-Containing, High-Performance Air Filters. *ACS Appl. Mater. Interfaces* **2015**, *7*, 19809–19815.

22. Hamou, K. Ben; Kaddami, H.; Dufresne, A.; Boufi, S.; Magnin, A.; Erchiqui, F. Impact of TEMPO-oxidization strength on the properties of cellulose nanofibril reinforced polyvinyl acetate nanocomposites. *Carbohydr. Polym.* **2018**, *181*, 1061–1070.

23. Fukuzumi, H.; Fujisawa, S.; Saito, T.; Isogai, A. Selective Permeation of Hydrogen Gas Using Cellulose Nanofibril Film. *Biomacromolecules* **2013**, *14*, 1705–1709.

24. Ma, H.; Burger, C.; Hsiao, B.S.; Chu, B. Ultrafine Polysaccharide Nanofibrous Membranes for Water Purification. *Biomacromolecules* **2011**, *12*, 970–976.

25. Nyström, G.; Mihranyan, A.; Razaq, A.; Lindström, T.; Nyholm, L.; Strømme, M. A nanocellulose polypyrrole composite based on microfibrillated cellulose from wood. *J. Phys. Chem. B* **2010**, *114*, 4178–4182.

26. Koga, H.; Nogi, M.; Komoda, N.; Nge, T.T.; Sugahara, T.; Suganuma, K. Uniformly connected conductive networks on cellulose nanofiber paper for transparent paper electronics. *NPG Asia Mater.* **2014**, *6*, e93–e93.

27. Favier, V.; Canova, G.R.; Shrivastava, S.C.; Cavaillé, J.Y. Mechanical percolation in cellulose whisker nanocomposites. *Polym. Eng. Sci.* **1997**, *37*, 1732–1739.

28. Shen, J.; Ikai, T.; Okamoto, Y. Synthesis and application of immobilized polysaccharide-based chiral stationary phases for enantioseparation by high-performance liquid chromatography. *J. Chromatogr. A* **2014,** *1363*, 51–61.

29. Kim, B.-H.; Lee, S.U.; Moon, D.C. Chiral Recognition of N -Phthaloyl, N -Tetrachlorophthaloyl, and N -Naphthaloyl α-Amino Acids and Their Esters on Polysaccharide-Derived Chiral Stationary Phases. *Chirality* **2012**, *24*, 1037–1046.

30. Usov, I.; Nyström, G.; Adamcik, J.; Handschin, S.; Schütz, C.; Fall, A.; Bergström, L.; Mezzenga, R. Understanding nanocellulose chirality and structure–properties relationship at the single fibril level. *Nat. Commun.* **2015**, *6*, 7564.

31. Yu, H.; Deng, J. Alkynylated Cellulose Nanocrystals Simultaneously Serving as Chiral Source and Stabilizing Agent for Constructing Optically Active Helical Polymer Particles. *Macromolecules* **2016**, *49*, 7728–7736.

32. Conley, K.; Whitehead, M.A.; van de Ven, T.G.M. Probing the structural chirality of crystalline cellulose with induced circular dichroism. *Cellulose* **2017**, *24*, 479–486.

33. Shopsowitz, K.E.; Qi, H.; Hamad, W.Y.; MacLachlan, M.J. Free-standing mesoporous silica films with tunable chiral nematic structures. *Nature* **2010**, *468*, 422–426.

34. Kaushik, M.; Moores, A. Review: nanocelluloses as versatile supports for metal nanoparticles and their applications in catalysis. *Green Chem.* **2016**, *18*, 622–637.

35. Kaushik, M.; Basu, K.; Benoit, C.; Cirtiu, C.M.; Vali, H.; Moores, A. Cellulose nanocrystals as chiral inducers: Enantioselective catalysis and transmission electron microscopy 3D characterization. *J. Am. Chem. Soc.* **2015**, *137*, 6124–6127.

36. Serizawa, T.; Sawada, T.; Wada, M. Chirality-specific hydrolysis of amino acid substrates by cellulose nanofibers. *Chem. Commun.* **2013**, *49*, 8827–8829.

37. Koga, H.; Namba, N.; Takahashi, T.; Nogi, M.; Nishina, Y. Renewable Wood Pulp Paper Reactor with Hierarchical Micro/Nanopores for Continuous-Flow Nanocatalysis. *ChemSusChem* **2017**, *10*, 2560–2565.

38. Gaunt, M.J.; Johansson, C.C.C.; McNally, A.; Vo, N.T. Enantioselective organocatalysis. *Drug Discov. Today* **2007**, *12*, 8–27.

39. Khan, A.; Khan, S.; Khan, M.A.; Qamar, Z.; Waqas, M. The uptake and bioaccumulation of heavy metals by food plants, their effects on plants nutrients, and associated health risk: a review. *Environ. Sci. Pollut. Res.* **2015**, *22*, 13772–13799.

40. Hajos, Z.G.; Parrish, D.R. Asymmetric Synthesis of Bicyclic Intermediates of Natural product chemistry. *J. Org. Chem.* **1974**, *39*, 1615–1621.

41. Knoche, B.; Blaschke, G. Investigations on the in vitro racemization of thalidomide by high-performance liquid chromatography. *J. Chromatogr. A* **1994**, *666*, 235–240.

42. Hanley, S.J.; Revol, J.F.; Godbout, L.; Gray, D.G. Atomic force microscopy and transmission electron microscopy of cellulose from Micrasterias denticulata; evidence for a chiral helical microfibril twist. *Cellulose* **1997**, *4*, 209–220.

43. Usov, I.; Nyström, G.; Adamcik, J.; Handschin, S.; Schütz, C.; Fall, A.; Bergström, L.; Mezzenga, R. Understanding nanocellulose chirality and structure-properties relationship at the single fibril level. *Nat. Commun.* **2015**, *6*, 7564.

44. Goto, H.; Jwa, J.; Nakajima, K.; Wang, A. Textile-surface interfacial asymmetric polymerization. *J. Appl. Polym. Sci.* **2014**, *131*, n/a-n/a.

45. Koga, H.; Tokunaga, E.; Hidaka, M.; Umemura, Y.; Saito, T.; Isogai, A.; Kitaoka, T. Topochemical synthesis and catalysis of metal nanoparticles exposed on crystalline cellulose nanofibers. *Chem. Commun* **2010**, *46*, 8567–8569.

46. Tamura, Y.; Kanomata, K.; Kitaoka, T. Interfacial Hydrolysis of Acetals on Protonated TEMPO-oxidized Cellulose Nanofibers. *Sci. Rep.* **2018**, *8*, 5021.

47. Notz, W.; Tanaka, F.; Barbas, C.F. Enamine-based organocatalysis with proline and diamines: The development of direct catalytic asymmetric aldol, Mannich, Michael, and Diels-Alder reactions. *Acc. Chem. Res.* **2004**, *37*, 580–591.

48. Stoimenova, A.; Ivanov, K.; Obreshkova, D.; Saso, L. Biotechnology in the production of pharmaceutical industry ingredients: Amino acids. *Biotechnol. Biotechnol. Equip.* **2013**, *27*, 3620–3626.

49. Berner, O.M.; Tedeschi, L.; Enders, D. Asymmetric Michael additions to nitroalkenes. *Eur. J. Org. Chem.* **2002**, *2002*, 1877–1894.

50. List, B.; Pojarliev, P.; Martin, H.J. Efficient Proline-Catalyzed Michael Additions of Unmodified Ketones to Nitro Olefins. *Org. Lett.* **2001**, *3*, 2423–2425.

51. Betancort, J.M.; Sakthivel, K.; Thayumanavan, R.; Barbas, C.F. Catalytic enantioselective direct Michael additions of ketones to alkylidene malonates. *Tetrahedron Lett.* **2001**, *42*, 4441–4444.

52. Yang, H.; Wong, M.W. (S)-Proline-catalyzed nitro-Michael reactions: towards a better understanding of the catalytic mechanism and enantioselectivity. *Org. Biomol. Chem.* **2012**, *10*, 3229.

53. Hayashi, Y.; Ogasawara, S. Time Economical Total Synthesis of (−)-Oseltamivir. *Org. Lett.* **2016**, *18*, 3426–3429.

54. Enders, D.; Fronert, J.; Bisschops, T.; Boeck, F. Asymmetric total synthesis of smyrindiol employing an organocatalytic aldol key step. *Beilstein J. Org. Chem.* **2012**, *8*, 1112–1117.

55. Sakthivel, K.; Notz, W.; Bui, T.; Barbas, C.F. Amino acid catalyzed direct asymmetric aldol reactions: A bioorganic approach to catalytic asymmetric carbon-carbon bond-forming reactions. *J. Am. Chem. Soc.* **2001**, *123*, 5260–5267.

56. List, B.; Pojarliev, P.; Castello, C. Proline-catalyzed asymmetric aldol reactions between ketones and alpha-unsubstituted aldehydes. *Org. Lett.* **2001**, *3*, 573–575.

57. Ranaivoarimanana, N.; Kanomata, K.; Kitaoka, T. Concerted Catalysis by Nanocellulose and Proline in Organocatalytic Michael Additions. *Molecules* **2019**, *24*, 1231.

Chapter 2

TEMPO-oxidized Cellulose Nanofibrils Enhanced Michael Additions

2.1. Introduction

The effect of different types of cellulose nanofibrils with different surface chemistry, –OH groups if only or also with –COONa, were tested in the asymmetric Michael addition as these groups were the most anticipated to interact with the reactants or the transition states.

2.2. Materials and Methods

2.2.1. Chemicals

All chemicals used were of analytical grade. Unless otherwise stated, solvents, substrates and catalysts in all reactions including the Michael addition were purchased from Merck KGaA (Darmstadt, Germany), FUJIFILM Wako Pure Chemical Industries, Ltd. (Osaka, Japan), Sigma-Aldrich Japan GK (Tokyo, Japan), and Tokyo Chemical Industry Co., Ltd. (Tokyo, Japan), and used as received. Water used in this study was purified with an Arium Ultrapure Water System (Sartorius Co., Ltd., Tokyo, Japan).

2.2.2. Nanocellulose

Softwood-derived TEMPO-oxidized cellulose nanofibrils (TOCNF, carboxylate content: 1.61 mmol/g) kindly supplied by Nippon Paper Industries Co., Ltd. (Tokyo, Japan) were mainly used in this study. TOCNF with lower carboxylate content (0.9 mmol/g) were freshly prepared according to a previously reported method for comparison purposes [1,2]. Cellulose nanofibrils (CNF) prepared by mechanical nanofibrillation were purchased from Sugino Machine Limited (BiNFi-s AFo-10002, Uozu, Japan).

2.2.3. TEMPO-oxidized cellulose nanofibrils characterization

The crystallinity of used TOCNF was determined by powder XRD recorded on a Rigaku MultiFlex diffractometer (Rigaku Corporation, Tokyo, Japan) with Ni-filtered Cu Kα radiation (λ= 0.15418 nm) at 40 kV and 20 mA. Freeze-dried TOCNFs samples were pressed to make a pellet for the characterization. Scanning was performed at 0.5° min^{-1} with 0.05° intervals. The crystallinity index (CrI) was calculated according to the method reported by Segal and co-workers [3].

The morphology of TOCNF was analyzed by TEM performed on a JEM-2100HCKM microscope (JEOL, Tokyo, Japan), operated at an accelerating voltage of 200 kV, at the Ultramicroscopy Research Center of Kyushu University. The samples were prepared by dropping TOCNF water dispersion (0.005% w/w, 5 μL) on a glow-discharged carbon-coated Cu grid. The excess liquid was absorbed with a filter paper after 5 min, and a negative staining reagent (1% sodium phosphotungstate, 5 μL), was dropped onto the sample. After standing for 5 min, the excess liquid was absorbed with a filter paper. Deionized water (5 μL) was added dropwise, and removed with a filter paper after 3 min. After air-drying, the coated grid was observed using the TEM apparatus in bright-field mode.

The carboxylate content of the TOCNFs was determined by conductometric titration [2]. A freeze-dried sample (100 mg) was added to deionized water (55 mL) and 0.02 M NaCl (5 mL), and the mixture was vigorously stirred to prepare a well-dispersed slurry. Then, 0.1 M HCl was added to the mixture to set the pH value in the range of 2.5–3.0. A 0.05 M NaOH solution was added at the rate of 0.2 mL/min with a Fusion 100 CX07100 micro syringe pump (Chemyx Inc., Stafford, United States of America) until the pH raised up to 11. The pH and conductivity were monitored by a LAQUA F-74 (HORIBA Advanced Techno Co., Ltd, Kyoto, Japan) during titration. The carboxylate content (mmol/g) of the sample was determined from the pH and conductivity curves.

2.2.4. TOCNF with low carboxylate content preparation

TOCNF with low carboxylate content were prepared according to a previously published method [1,2]. Water suspension of CNF prepared by mechanical nanofibrillation purchased from Sugino Machine Limited (BiNFi-s AFo-10002, Uozu, Japan) were used as starting materials. Wet-state CNFs (3.0 g of dried cellulose) were suspended in deionized water (300 mL) containing TEMPO (48 mg) and NaBr (300 mg). TEMPO-mediated oxidation was started by adding sodium hypochlorite (2.0 mmol/g of cellulose) to the suspension. The mixture was stirred at room temperature for 30 min, while the suspension was maintained at pH 10 using a pH titrator (GT-200 Automatic Titrator, Mitsubishi Chemical Analytech, Yamato, Japan) that was loaded with NaOH (0.5 M). The oxidation was quenched with ethanol (10 mL) and the suspension was washed thoroughly with deionized water by successive centrifugation at 22,540× *g* for 10 min (TOMMY Suprema 21 High-Speed Refrigerated Centrifuge, TOMMY Seiko, Tokyo, Japan).

Nanofibrillation was conducted by aqueous counter collision with a high-pressure water jet system at 245 MPa (0.1-mm diameter dual-nozzle chamber; Star Burst Labo, Sugino Machine Limited, Uozu, Japan) [4]. The obtained mixture was then centrifuged to separate the cellulose nanofibrils as supernatant (0.6 wt%) from the unfibrillized fibers (22,540 ×g, 10 min).

2.2.5. Water removal process from TOCNF

Except otherwise stated, TOCNF in sodium or protonated form were subjected to water removal treatment as water impedes the Michael addition but also the aldol reaction. The applied method was solvent exchange or freeze-drying.

The solvent exchanged TOCNF were prepared by centrifugation (9,200× *g*, 5 min) five times of a mixture of TOCNF water suspension (10 mL, 1.04 wt%) and the solvent to be used in corresponding reaction (30 mL). The supernatant was replaced with fresh solvent after each centrifugation cycle. After the last cycle, the solvent was removed, and the TOCNFs precipitate was recovered and used in reactions.

To obtain freeze-dried samples, TOCNF water suspension (10 mL, 1.04 wt%) was mixed with tertiary butanol (30 mL), frozen in liquid nitrogen, and dried under vacuum (Scanvac CoolSafe LaboGene, Sakuma Seisakusho, Co. Ltd., Tokyo, Japan).

2.2.6. Michael addition substrate synthesis

All substrate used in the Michael addition were commercially available except (*E*)-1-bromo-4-(2-nitrovinyl)benzene (**Table 2. 5**, **2c**) and (*E*)-1-(2-nitrovinyl)naphthalene (**Table 2. 5**, **2d**). These two compounds were synthesized according to previously reported methods [5].

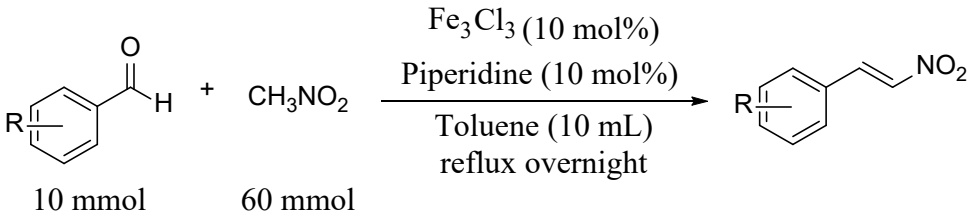

Scheme 2. 1 Piperidine catalyzed Henri reaction for the synthesis of nitroalkene substrates for the TOCNF enhanced Michael addition.

The adequate substituted benzaldehyde (10.0 mmol), CH_3NO_2 (4 mL, 60 mmol), and piperidine (98.8 μL, 1.0 mmol) were added sequentially to an oven-dried round-bottom flask (100 mL) containing toluene (10 mL), then anhydrous $FeCl_3$ (16.2 mg, 0.10 mmol) was poured in. The mixture was refluxed under N_2 atmosphere overnight. After being cooled down to room temperature, the reaction mixture was concentrated under reduced pressure. Purification by column chromatography (hexane and dichloromethane as eluent) of the concentrated organic layer afforded the product. The spectroscopic data of each product were in agreement with previously reported data (see **Appendix**).

2.2.7. Michael addition representative procedure in the presence of TOCNF

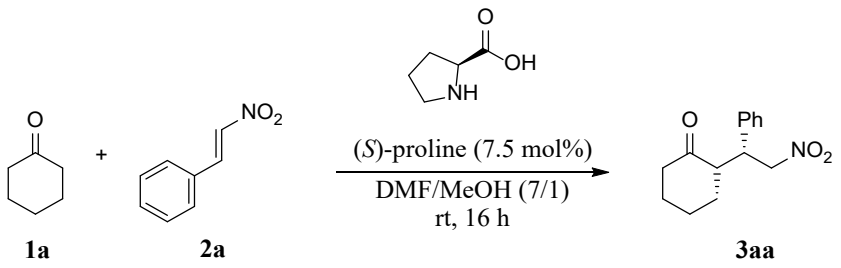

Scheme 2. 2 Representative reaction used in the TOCNF enhanced Michael addition.

If used, freeze-dried TOCNFs or precipitate were dispersed in 14 mL DMF with a double-cylinder-type homogenizer (2 min) to constitute the reaction medium.

Cyclohexanone (**1a**) (4.0 mL, excess) and *trans*-β-nitrostyrene (**2a**) (74.6 mg, 0.50 mmol) were added to the dispersion, followed by a solution of (*S*)-proline (4.4 mg, 7.5 mol% with respect to **2a**) in methanol (2.0 mL) (**Scheme 2. 2**). The resulting mixture was stirred at room temperature and monitored by thin layer chromatography (TLC) on glass-backed plates precoated with silica gel (silica gel 60 GF254, 0.25 mm Merck, Tokyo, Japan). The plates were visualized using combinations of ultraviolet light (254 nm) and chemical stains (*p*-anisaldehyde and potassium permanganate). Upon completion, the reaction was quenched by adding aq. NH_4Cl, extracted with ethyl acetate (30 mL × 3), and dried over Na_2SO_4. The concentrated organic layer was purified by column chromatography on an automated flash chromatography system (Smart Flash EPCLC-AI-580S, Yamazen, Osaka, Japan). Hexane and ethyl acetate were used as eluents and rendered the product **3aa** as a white solid after solvent evaporation (108.8 mg, 88%). The spectroscopic data of each product was in agreement with previously reported data [6,7].

2.2.8. Reaction products characterization

The structure of the products was confirmed by Nuclear Magnetic Resonance spectroscopy (NMR). ^{1}H- and ^{13}C-NMR spectra were recorded on a JNM-ECZ400 spectrometer (JEOL, Tokyo, Japan) at the Center of Advanced Instrumental Analysis, Kyushu University. Chemical shifts in the ^{1}H-NMR spectra are reported in parts per million relatives to the peak of tetramethylsilane (TMS, δ 0.00 ppm), used as an internal standard. ^{13}C-NMR spectra were recorded with complete proton decoupling, and chemical shifts are reported in parts per million relatives to the solvent resonance ($CDCl_3$, δ 77.0 ppm), used as an internal standard.

The enantioselectivity and diastereomeric ratios of products were measured by supercritical fluid chromatography (SFC; ACQUITY UPC2, Waters, Tokyo, Japan) using chiral stationary phases. Each purified Michael addition samples were solved in isopropyl alcohol (IPA) before injection. The Michael addition of cyclohexanone (**1a**) with *trans*-β-nitrostyrene (**2a**) gives four isomers (**Scheme 2. 3**). The enantioselectivity (*ee*) towards the formation of the (*SR*)-*syn* main product (noted a) in **Scheme 2. 3**) is given by the following equation:

$$ee = \left|\frac{[a]-[b]}{[a]+[b]}\right| \times 100$$

where [a] is the integrated peak surface of (*SR*)-*syn* and [b] is the integrated peak surface of (*RS*)-*syn* (noted b) in **Scheme 2. 3**) on the SFC chromatograph.

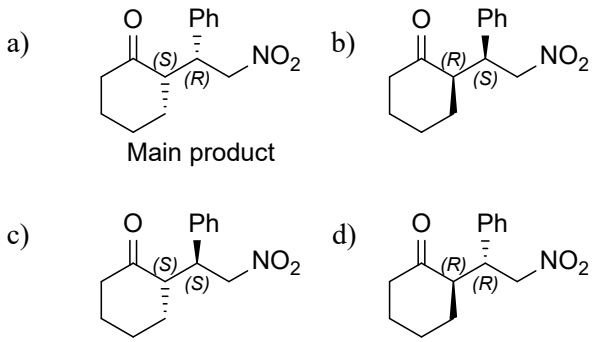

Scheme 2. 3 Products of the Michael addition, where a) and b) are the *syn* diastereomers, c) and d) are the *trans* diastereomers; a) is the mirror image of b) and form a pair of enantiomer, the same rule applies to c) and d).

The diastereoselectivity (*dr*) is the ratio between *syn* and *trans* diastereomers. The value is the ratio of the total surface of a) and b) relative to the total surface of c) and d) peaks from the SFC chromatograph.

2.3. Results and Discussion

2.3.1. TEMPO-oxidized cellulose nanofibrils characterization

The XRD pattern of the TOCNF showed characteristic reflections from cellulose I type structures that can be respectively assigned to the (1 -1 0), (1 1 0), (2 0 0) and (0 0 4) planes (**Figure 2. 1**). The value of the crystallinity index (CrI) was 57.6% with a crystal size of 2.1 nm. These values are within the range of reported TEMPO-oxidized cellulose nanofibrils produced from soft wood [8].

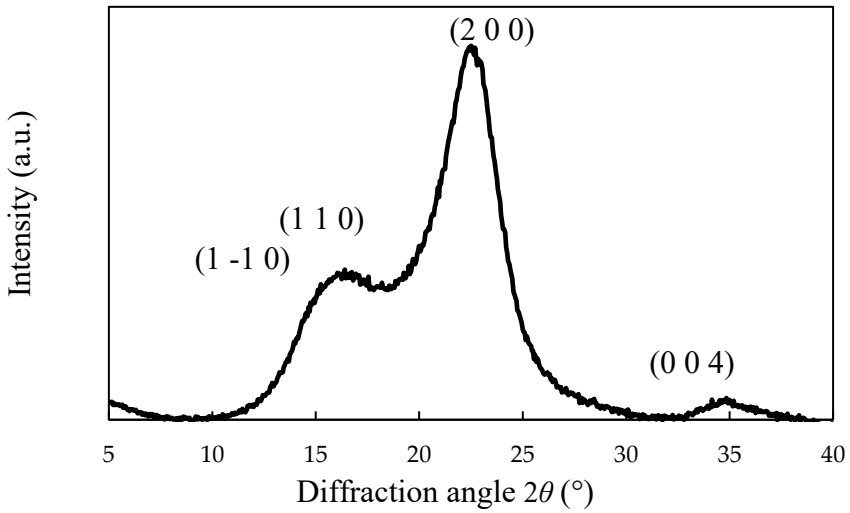

Figure 2. 1 XRD pattern of TOCNF supplied by Nippon Paper Industries Co., Ltd (Tokyo, Japan). CrI = 57.6% and D_{200} = 2.1 nm [9].

The observation of TOCNF by TEM revealed nanofibrils of several hundreds of nanometers length (**Figure 2. 2**). The partially aggregated state of the nanofibril is due to drying during sample preparation.

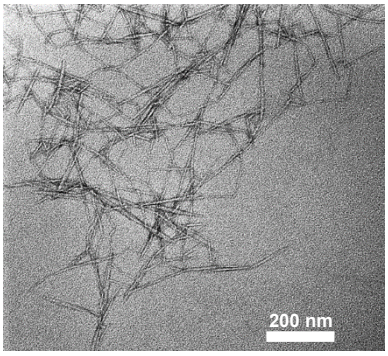

Figure 2. 2 TEM image of TOCNF supplied by Nippon Paper Industries Co., Ltd (Tokyo, Japan).

The carboxylate content of the sample deduced from the pH and conductivity curves was 1.61 mmol/g for TOCNF provided by Nippon Paper Industries Co., Ltd, and 0.9 mmol/g for the freshly prepared TOCNF samples (**Figure 2. 3**).

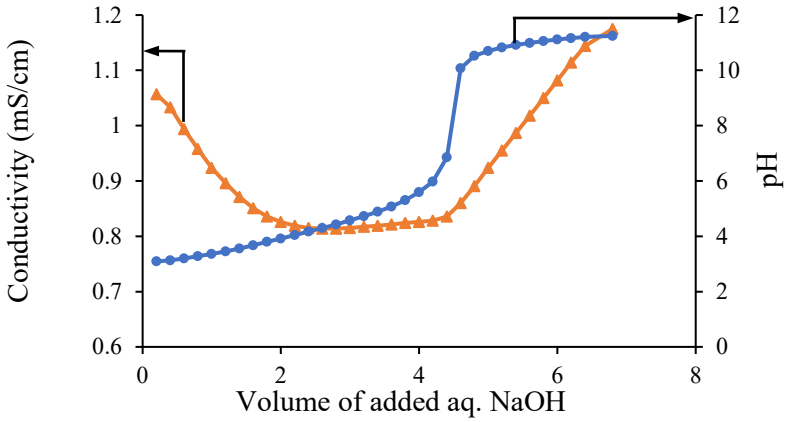

Figure 2. 3 Representative pH (circles) and electrical conductivity (triangles) curves of an aqueous suspension of TOCNF Nippon Paper Industries Co., Ltd (Tokyo, Japan).

2.3.2. Effects of cellulose nanofibrils on proline-catalyzed Michael additions

The investigation into TOCNF's application in the Michael addition started with the trial of the nanocellulose treated with various water removal procedure in the reaction. The Michael

addition of cyclohexanone (**1a**) with *trans*-β-nitrostyrene (**2a**) has been widely employed as a benchmark reaction to assess related catalytic systems [7,10]. In order to determine which nanocellulose could bring any improvement on the Michael addition, they were dispersed in DMF to constitute the reaction medium of **1a** and **2a** (**Table 2. 1**).

During this study, water was confirmed to decrease the yield of the reaction without affecting the selectivity for the Michael addition. Consequently, water was removed from CNFs water suspension samples through solvent exchange by centrifugation to give precipitated CNFs (entries 3 to 5 and 7, **Table 2. 1**), or by freeze drying (entry 6).

Table 2. 1 Nanocellulose effect in the Michael addition[a].

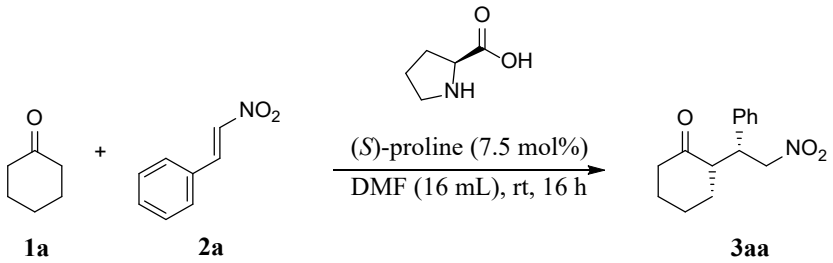

1a **2a** **3aa**

Entry	Catalysts	Yield (%)[b]	*syn*:*anti*[c]	*ee* for *syn* (%)[c]
1	Nanocellulose only	Trace	-	-
2	(*S*)-Proline only	35	89:11	32
3[d]	Precipitated CNF with (*S*)-proline	33	85:15	35
4	Precipitated TOCNF with (*S*)-proline	78	90:10	35
5	Precipitated TOCNF-H with (*S*)-proline	14	92:8	0
6[e]	Freeze-dried TOCNF with (*S*)-proline	73	94:6	25
7[f]	Precipitated TOCNF with (*S*)-proline solved in MeOH	88	90:10	43
8[g]	(*S*)-Proline only, solved in MeOH	56	96:4	34

[a] Conditions: cyclohexanone **1a** 4 mL (excess), *trans*-β-nitrostyrene **2a** 74.6 mg (0.50 mmol), (*S*)-proline 7.5 mol% (against **2a**), and TOCNF 100 mg (dry weight), in DMF (16 mL); [b] isolated yield; [c] determined by chiral stationary phase supercritical fluid chromatography (SFC) analysis; [d] precipitated means water removal from nanocellulose with MeOH by repetitive centrifugation; [e] water removal by freezing in liquid N_2 and vacuum drying; [f] (*S*)-proline solved in MeOH (2 mL) added to TOCNF dispersed in DMF (14 mL); [g] stirred for 24 h instead of 16 h.

The reaction in the presence of either TOCNF or CNF, regardless of the water removal treatment, did not yield the target product. In other words, TOCNF or CNF were catalytically inactive in the Michael addition (entry 1). Without (*S*)-proline but nanocelluloses only, the reaction did not yield any product. The reaction with (*S*)-proline alone resulted in a low yield

and poor enantioselectivity (entry 2). Adding precipitated CNF, which are lacking carboxylate groups on their surfaces compared to TOCNF, did not change the outcome of the reaction (entry 3). In contrast, the presence of precipitated TOCNFs with sodium carboxylate groups on its facet significantly enhanced the yield under the same reaction conditions (entry 4). Protonated TOCNF with carboxylic acids on its surface inhibited the Michael addition (entry 5). This is probably due to the hydrolysis of key transition states such as the iminium/nitronate that is the most probable transition state in the Michael addition [11]. This is further emphasized by the absence of enantioselectivity which suggest the reversibility of the reaction in the presence of TOCNF.

Interestingly, poorly dispersed freeze-dried TOCNFs due to severe aggregation [12], also achieved a high yield but the *ee* was lower (entry 6). These results clearly suggest that the cooperation of catalytically inactive TOCNF in sodium form and low-activity proline was critical for enhancing the reaction efficiency of this Michael addition.

Previous reports about density functional theory (DFT) calculations on the Michael addition showed that MeOH molecules from the solvent can affect the enantioselectivity [13]. In the models, MeOH stabilized a preferred orientation of the approach of the nitroolefin substrate to the enamine formed by proline and the ketone substrate. The result is a higher *ee* towards the formation of the major product **3aa**. In this study, the practical application by using MeOH as solvent was however detrimental because the reaction took several days (**Table 2. 2**). Therefore, the strategy was applied to the reaction in the presence of TOCNF by dissolving (*S*)-proline in a small portion of MeOH before addition to the nanocellulose dispersion. Consequently, the reaction time was kept the same and the yield was further increased (entry 7). Furthermore, the *ee* raised from 35 to 43%. In contrast, the same amount of MeOH for the reaction without TOCNF but (*S*)-proline only did not improve the result (entry 8).

In brief, none of the tested nanocellulose acted as a catalyst and only TOCNF with hydroxy and sodium carboxylate groups acted as a cocatalyst to (*S*)-proline for better yields and *ee*. The optimum reaction conditions were screened after establishing that TOCNFs in sodium form is the most effective nanocellulose for the Michael addition.

2.3.3. Solvent screening

The type of solvent to be used in the reaction is crucial. Indeed, the better the CNF dispersibility, the higher the surface available to the reactants to interact with the nanofibrils. Different solvents were tried to assess the most suitable for the TOCNFs-enhanced Michael addition (**Table 2. 2**). Water, in which TOCNFs have the highest degree of dispersion was first tested as a reaction media (entry 1). Although, only traces of the product could be spotted on TLC. Most of the screening was stopped after 48 h except for methanol (entry 2). The reaction in IPA proceeded substantially with (*S*)-proline only compared to with TOCNFs but the *ee* was the highest recorded for the product **3aa** (entry 3). In overall, DMF gave the best compromise in yield and enantioselectivity for the TOCNF assisted Michael addition and will be used in subsequent reactions (entry 7).

Table 2. 2 Solvent screening[a]

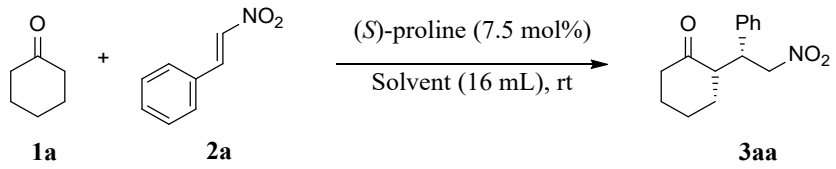

1a **2a** **3aa**

Entry	Solvent	Time (h)	TOCNF	Yield (%)[b]	*syn* : *anti*[c]	*ee* for *syn* (%)[c]
1	H_2O	48	-[d]	Trace	-	-
			+[d]	Trace	-	-
2	MeOH	96	-	11	96:4	39
			+	42	97:3	45
3	IPA	48	-	55	96:4	33
			+	17	97:3	52
4	DCM	48	-	Trace	-	-
			+	Trace	-	-
5	MeCN	48	-	Trace	-	-
			+	Trace	-	-
6	DMSO	16	-	57	95:5	32
			+	73	95:5	29
7	DMF	16	-	35	89:11	32
			+	88	90:10	43

[a] Otherwise stated, the reaction was performed using cyclohexanone (**1a**) (4 mL, excess), *trans*-β-nitrostyrene (**2a**) (74.6 mg, 0.50 mmol), (*S*)-proline (7.5 mol%), and TOCNF(if used, 100 mg in dry weight) in the adequate solvent (16 mL). Aqueous medium of TOCN suspension was replaced by MeOH by repetitive centrifugation prior to the reaction; [b] isolated yield; [c] determined by chiral stationary phase supercritical fluid chromatography (SFC) analysis; [d] reaction without TOCNF noted as '- ' and with TOCNF noted as '+'.

2.3.4. Reaction conditions optimization

The model reaction between **1a** and **2a** was conducted in DMF with different conditions: temperature, (*S*)-proline catalyst load, TOCNF matrix load. The best parameters were chosen

based on green chemistry principles as to minimize energy consumption, economize atoms and materials towards a sustainable process while achieving higher yields and enantioselectivity.

At first, different quantities of (*S*)-proline were tested (**Table 2. 3**, entry 1 and 2). An appreciable amount of the product could be formed with 5 mol% of the catalyst in 16 hours (entry 1). There was no significant change in the selectivity. On the other hand, using a higher catalyst loading (15 mol%) led to a decrease in diastereoselectivity for both reaction with and without TOCNF (entry 2). Furthermore, the yield was lower than with 7.5 mol% catalyst (77% yield vs. 89%). These two factors imply that more reactions are catalyzed by (*S*)-proline only without the assistance of the nanocellulose at higher load. Accordingly, 7.5 mol% was used as optimum load in the following experiments.

Table 2. 3 Fine-tuning of catalyst amount, reaction temperature in the TOCNF-enhanced Michael addition[a].

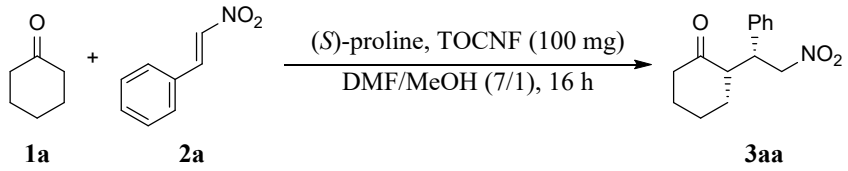

1a **2a** **3aa**

Entry	(*S*)-proline (mol%)	Temperature	TOCNF	Yield (%)[b]	*syn*:*anti*[c]	*ee* for *syn* (%)[c]
1	5	rt	-[d]	37	87:13	29
			+[d]	74	93:7	39
2	15	rt	-	58	69:31	26
			+	77	69:31	39
3	7.5	0 °C	-	9	77:23	19
			+	23	74:26	39
4[e]	7.5	40 °C	-	66	94:6	32
			+	91	94:6	42

[a] Reaction conditions: **1a** (4 mL, excess), **2a** (74.6 mg, 0.50 mmol), (*S*)-proline (7.5 mol%), and TOCNF (100 mg dry weight) in a mixture of DMF (14 mL) and MeOH (2 mL) stirred for 16 h. Aqueous medium of TOCNF suspension was replaced with MeOH by repetitive centrifugation prior to reaction; [b] isolated yield; [c] determined by chiral stationary phase SFC analysis; [d] reaction without TOCNF noted as '- ' and with TOCNF noted as '+'; [e] Stirred for 11 h.

Secondly and equally important, the temperature was lowered to seek for higher *ee* under the assumption that the reaction is under kinetic control. However, the reaction was slow at 0°C and the *ee* slightly decreased (entry 3). On the contrary, increasing the reaction temperature led to faster reaction without loss of *ee*. The best result was obtained at 40 °C for 11 h in the presence of TOCNF (entry 4). With respect to green chemistry and sustainability, further

reactions were conducted at room temperature because the (*S*)-proline/TOCNF catalytic system efficiency at this temperature was close to that at 40 °C.

Table 2. 4 Effect of different TOCNF quantities on the Michael addition[a].

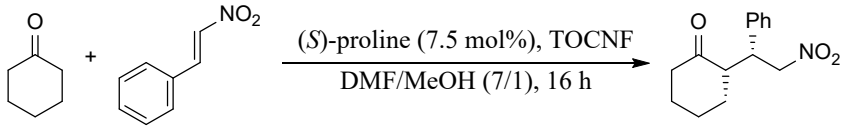

1a **2a** **3aa**

Entry	TOCNF (mg)	Yield (%)[b]	*syn*:*anti*[c]	*ee* for *syn* (%)[c]
1	25	51	92:8	41
2	50	66	94:6	43
3	100	88	90:10	41
4	150	63	71:29	41
5	200	43	83:17	43

[a] Conditions: **1a** (4 mL, excess), **2a** (74.6 mg, 0.50 mmol), (*S*)-proline (7.5 mol%), and TOCNF in a mixture of DMF (14 mL) and MeOH (2 mL) stirred for 16 h. Aqueous medium of TOCNF suspension was replaced with MeOH by repetitive centrifugation prior to reaction; [b] isolated yield; [c] determined by chiral stationary phase SFC analysis.

The results from reactions with different amount of TOCNF was also compared (**Table 2. 4**). The quantity of each substrates was kept the same as in previous reactions (4 mL for **1a**, 74.6 mg for **2a**). The tests showed that the lower the amount of nanocellulose, the lower the yield of the reaction (entries 1–3). The optimum weight ratio of nitrostyrene/TOCNF was 1:1.34 (entry 3). Further increasing the amount of fibers gradually impeded the reaction. This might be attributed to reaction mixture thickening causing crowding in the reaction medium (entries 4 and 5).

Solvent screening revealed DMF as the most suitable medium for the reactions (**Table 2. 2**). Altogether, the best parameters to achieve optimum enhancement was to conduct the reaction in DMF at room temperature with 7.5 mol% (*S*)-proline and 100 mg of TOCNF.

2.3.5. Substrate scope

Representative nitrostyrene and ketone substrates were subjected to the TOCNF/(*S*)-proline catalytic system using the optimum conditions (**Table 2. 5**).

Both electron-donating and electron-withdrawing groups on the nitrostyrene phenyl ring were compatible with the catalytic system, affording moderate to high yields and excellent diastereoselectivities in the presence of TOCNF (entries 1 and 2). The enantioselectivity was increased in both cases.

The effect of steric hindrance was also studied (entry 3). The yield of the reaction with naphthyl-substituted nitroalkene was almost the same for the reaction with and without TOCNF. Although, the presence of nanocellulose increased the enantioselectivity.

The reaction between **1a** and **2a** in the presence of TOCNF is fully kinetically controlled as the observation of the enantioselectivity over time did not show any changes. Same yield between reaction with and without TOCNF implies a same overall reaction rate. But the difference in *ee* implies that the reaction is exclusively controlled by TOCNF. The enantioselective step is the formation of the iminium nitronate. The entry 3 clearly demonstrate that TOCNF is involved in stabilizing this transition state and that the reaction exclusively occurs on the TOCNF facet.

The generality of ketones, as the nucleophile activated by proline, was also studied in the reaction with *trans*-β-nitrostyrene. A significant increase in yield was observed for 4-oxothiane, a cyclic ketone bearing a heteroatom (entry 4). Unfortunately, the reaction yield with

cyclopentanone was diminished in the presence of TOCNF, despite a markedly increased enantioselectivity (entry 5). Acetone, the simplest ketone without a cyclic structure, was also applicable to the present catalytic system (entry 6).

TOCNF clearly enhanced the reaction efficiency and stereoselectivity of proline-catalyzed Michael additions of various substrates.

Table 2. 5 Substrate scope[a].

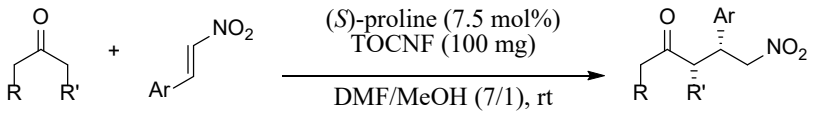

1 **2** **3**

Entry	Substrates	Product	Time (h)	TOCNF	Yield (%)[b]	*syn*:*anti*	*ee* for *syn* (%)[c]
1	**1a**/ 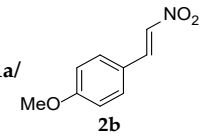 **2b**	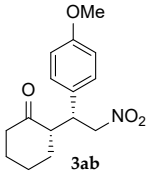 **3ab**	48	-[d]	26	90:10[e]	31
			48	+[d]	68	93:7[e]	35
2	**1a**/ 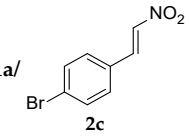 **2c**	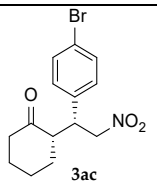 **3ac**	24	-	59	96:4[c]	28
			24	+	83	95:5[c]	50
3	**1a**/ 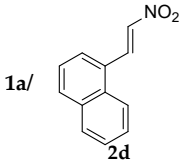 **2d**	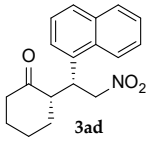 **3ad**	48	-	75	87:13[e]	10
			48	+	71	87:13[e]	21
4	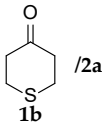 **/2a** **1b**	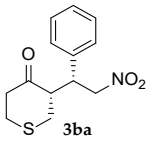 **3ba**	24	-	18	94:6[e]	24
			24	+	76	97:3[e]	38
5	 **/2a** **1c**	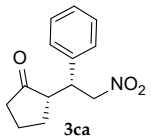 **3ca**	24	-	43	61:39[c]	29
			24	+	12	72:28[c]	59
6	 **/2a** **1d**	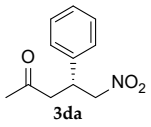 **3da**	24	-	32	-	10
			24	+	70	-	23

[a] Conditions: excess of ketone **1** (4 mL for all entries, except 10 eq. of **1b** in entry 5) and nitrostyrene (**2**) (0.50 mmol); [b] isolated yield; [c] determined by chiral stationary phase SFC analysis; [d] reaction without TOCNF noted as '- ' and with TOCNF noted as '+'; [e] determined by ^{1}H NMR.

2.3.6. Mechanistic studies

Different additives with the equivalent amount of carboxylate groups present on TOCNF (1.61 mmol/g) were used with (*S*)-proline to determine the role of the nanocellulose in the reaction (**Table 2. 6**). The first entry is the reaction with (*S*)-proline only and the second is with TOCNF which has the highest level of enhancement repeated from **Table 2. 1** for easier of comparison (**Table 2. 1** entry 7).

The requirement of a crystalline additive was evaluated by trying amorphous carboxymethylcellulose (entry 3). Despite having the same functional groups as TOCNF on its surface, carboxymethylcellulose paired with (*S*)-proline failed to promote the reaction. Furthermore, homogeneously dispersed sodium acetate with an equivalent carboxy group content to the TOCNF used only slightly augmented the reaction yield and gave nearly racemic products (entry 4). Consequently, the crystalline nature of TOCNF would be essential in the present catalytic system.

The influence of functional groups was also investigated using freshly prepared TOCNF with low carboxy contents (0.94 mmol/g, entry 5). The reaction resulted in a lower yield, but with similar improvements in enantioselectivity than the original TOCNF. In addition, using (*R*)-proline with TOCNF (1.61 mmol/g) gave the same type of enhancement with (*S*)-proline by improving the *ee* of the opposite enantiomer (entry 6). Consequently, the unique regular alignment of hydroxy and carboxylate groups present on the TOCNF facet are essentially involved in improving the catalytic efficiency and the intrinsic chirality of TOCNF might not be involved in imparting enantioselectivity.

Table 2. 6 Catalytic behavior of proline combined with TOCNF or additives in the Michael addition[a].

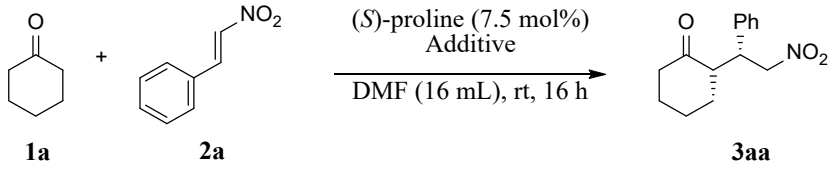

1a **2a** **3aa**

Entry	Additive	Yield (%)[b]	*syn*:*anti*[c]	*ee* for *syn* (%)[c]
1	No additive	35	89:11	32
2	TOCNF	88	90:10	43
3[d]	Carboxymethylcellulose	34	90:10	27
4	Sodium acetate	41	89:11	6
5[e]	TOCNF/low carboxylate	42	82:18	42
6[f]	TOCNF	86	93:7	(39)[g]

[a] Unless otherwise noted, the reaction was performed using cyclohexanone (**1a**) (4 mL, excess), *trans*-β-nitrostyrene (**2a**) (74.6 mg, 0.50 mmol), (*S*)-proline (7.5 mol%), and TOCNF (100 mg dry weight) in a mixture of DMF (14 mL) and MeOH (2 mL). Aqueous medium of TOCNF suspension was replaced with MeOH by repetitive centrifugation prior to reaction; [b] isolated yield; [c] determined by chiral stationary phase supercritical fluid chromatography (SFC) analysis; [d] for entries 3 and 4, additive amount adjusted to 1 eq. of $–COO^-$ groups contained in 100 mg of TOCNF of entry 2; [e] TOCNF with $–COO^-$ group content of 0.94 mmol/g; [f] (*R*)-proline was used instead of (*S*)-proline; [g] *ee* for *anti* **3aa**.

2.4. Conclusion

In conclusion, none of the nanocellulose showed catalytic activity in the reaction. They acted as a matrix to the reaction catalyzed by (*S*)-proline in which the yield is drastically improved from 35 to 86%. Solving (*S*)-proline in methanol provided an enhancement on the *ee* from 35 to 43% that is seen only when TOCNF are present in the reaction medium. The

nanocellulose's chirality was not transferred to the product because the opposite enantiomer's *ee* was also improved when (*R*)-proline was used.

References

1. Okita, Y.; Saito, T.; Isogai, A. Entire surface oxidation of various cellulose microfibrils by TEMPO-mediated oxidation. *Biomacromolecules* **2010**, *11*, 1696–1700.

2. Saito, T.; Isogai, A. TEMPO-Mediated Oxidation of Native Cellulose. The Effect of Oxidation Conditions on Chemical and Crystal Structures of the Water-Insoluble Fractions. *Biomacromolecules* **2004**, *5*, 1983–1989.

3. Segal, L.; Creely, J.J.; Martin, A.E.; Conrad, C.M. An Empirical Method for Estimating the Degree of Crystallinity of Native Cellulose Using the X-Ray Diffractometer. *Text. Res. J.* **1959**, *29*, 786–794.

4. Kondo, T.; Kose, R.; Naito, H.; Kasai, W. Aqueous counter collision using paired water jets as a novel means of preparing bio-nanofibers. *Carbohydr. Polym.* **2014**, *112*, 284–290.

5. Jalal, S.; Sarkar, S.; Bera, K.; Maiti, S.; Jana, U. Synthesis of nitroalkenes involving a cooperative catalytic action of iron(III) and piperidine: A one-pot synthetic strategy to 3-alkylindoles, 2H-chromenes and N-arylpyrrole. *European J. Org. Chem.* **2013**, *2013*, 4823–4828.

6. Syu, S.; Kao, T.-T.; Lin, W. A new type of organocatalyst for highly stereoselective Michael addition of ketones to nitroolefins on water. *Tetrahedron* **2010**, *66*, 891–897.

7. Kaplaneris, N.; Koutoulogenis, G.; Raftopoulou, M.; Kokotos, C.G. 4-Fluoro and 4-Hydroxy Pyrrolidine-thioxotetrahydropyrimidinones: Organocatalysts for Green Asymmetric Transformations in Brine. *J. Org. Chem.* **2015**, *80*, 5464–5473.

8. Daicho, K.; Saito, T.; Fujisawa, S.; Isogai, A. The Crystallinity of Nanocellulose: Dispersion-Induced Disordering of the Grain Boundary in Biologically Structured

Cellulose. *ACS Appl. Nano Mater.* **2018**, *1*, 5774–5785.

9. Ranaivoarimanana, N.; Kanomata, K.; Kitaoka, T. Concerted Catalysis by Nanocellulose and Proline in Organocatalytic Michael Additions. *Molecules* **2019**, *24*, 1231.

10. Betancort, J.M.; Sakthivel, K.; Thayumanavan, R.; Tanaka, F.; Barbas III, C.F. Catalytic Direct Asymmetric Michael Reactions: Addition of Unmodified Ketone and Aldehyde Donors to Alkylidene Malonates and Nitro Olefins. *Synthesis (Stuttg).* **2004**, *2004*, 1509–1521.

11. Yang, H.; Wong, M.W. (S)-Proline-catalyzed nitro-Michael reactions: towards a better understanding of the catalytic mechanism and enantioselectivity. *Org. Biomol. Chem.* **2012**, *10*, 3229.

12. Nemoto, J.; Saito, T.; Isogai, A. Simple Freeze-Drying Procedure for Producing Nanocellulose Aerogel-Containing, High-Performance Air Filters. *ACS Appl. Mater. Interfaces* **2015**, *7*, 19809–19815.

13. Patil, M.P.; Sunoj, R.B. The role of noninnocent solvent molecules in organocatalyzed asymmetric michael addition reactions. *Chem. Eur. J.* **2008**, *14*, 10472–10485.

Chapter 3

TEMPO-oxidized Cellulose Nanofibrils Enhanced Aldol Reactions

3.1. Introduction

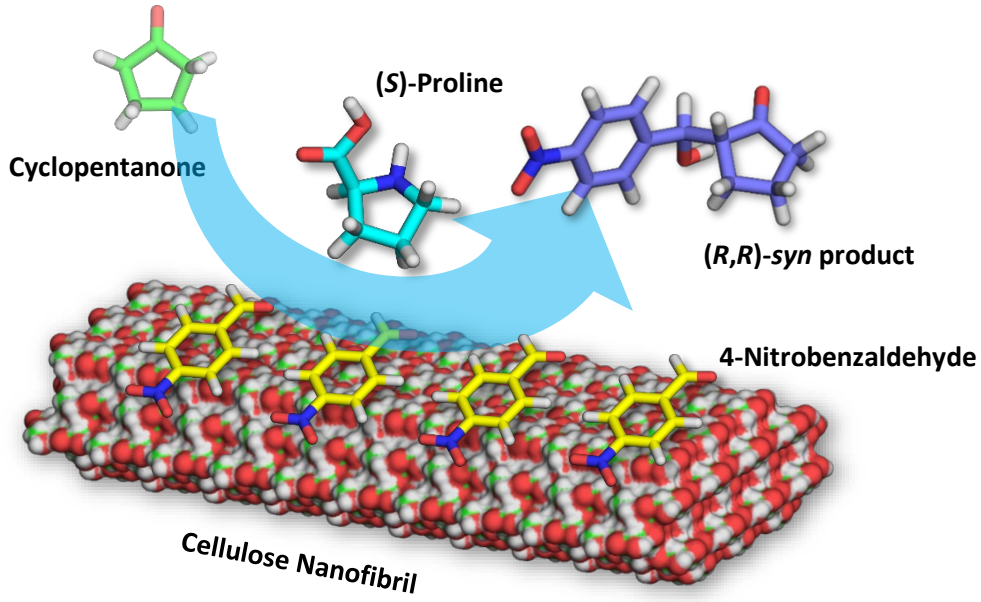

Figure 3. 1 Schematic of the approach for the TOCNF/(*S*)-proline catalyzed aldol reaction between cyclopentanone and 4-nitrobenzaldehyde.

Based on the hypothesis that CNF are able to interact with the different moieties involved in the aldol reaction (**Figure 3. 1**), the present chapter is relating the effect of different nanocelluloses on the reaction and the pairing of such materials with different amino acid catalyst. Additionally, an attempt on explaining the reaction's mechanism is provided.

3.2. Materials and Methods

The softwood-derived TOCNF used in this chapter is the same as in the Michael addition and was kindly provided by Nippon Paper Industries Co., Ltd. (Tokyo, Japan) (see chapter 2 for characterization).

3.2.1. Protonated TOCNF preparation (TOCNF-H)

A water suspension of TOCNF in sodium carboxylate form (2.01 wt%, 300 mg of dried cellulose) was mixed with 0.1 M aqueous HCl solution, shaken several times, and then centrifuged at 12,000 ×*g* for 10 min (TOMMY Suprema 21 High-Speed Refrigerated Centrifuge, TOMMY Seiko, Tokyo, Japan). The supernatant was then renewed with deionized water and the mixture was centrifuged again. This washing cycle was repeated until the supernatant pH reached 4.5.

3.2.2. TOCNF organogel preparation

TOCNF dispersion (0.5% w/v, 100 mg of dried cellulose) was poured into a mold (6 cm × 5 cm × 1 cm in size) and covered with a nylon sheet (20-µm mesh). A 0.1 M aqueous HCl solution was spread over the nylon sheet and the mold was allowed to stand overnight. The cellulose nanofibrils, which are initially dispersed due the self-repelling ionic surface carboxyl groups, partially assemble and form physical hydrogels as the carboxyl are converted to carboxylic acids upon HCl addition. The resulting stiff gel was cut into cubes (1 cm × 1 cm × 1 cm) and shaken gently in 0.01 M aqueous HCl overnight. The as-prepared hydrogel cubes were immersed in DMF and shaken gently, renewing the solvent every 8 h (five times), to

afford the TOCNF organogel of DMF. Organogel samples of other solvents were prepared using the same procedure [1,2].

3.2.3. Aldol addition representative procedure in the presence of TOCNFs

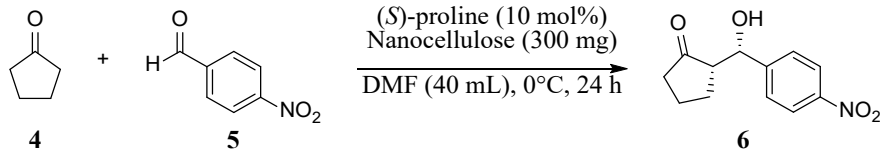

4 5 6

Scheme 3. 1 Representative reaction used in the TOCNF enhanced Michael addition.

A double-cylinder-type homogenizer probe was applied on the pretreated nanocellulose (300 mg) poured in DMF (40 mL) to homogenize the mixture. To the suspension were added 4-nitrobenzaldehyde **5** (300 mg, 2 mmol), cyclopentanone **4** (10 mL), and (*S*)-proline (0.2 mmol), and the resultant mixture was stirred at 0 °C for 24 h (**Scheme 3. 1**). The reaction was then quenched with water and extracted with CH_2Cl_2. After drying over $MgSO_4$ and concentrating, the residue was purified by silica gel column chromatography to afford the product as a colorless oil.

3.2.4. Reaction products characterization

The structure of the products was confirmed by Nuclear Magnetic Resonance spectroscopy (NMR). ^{1}H-NMR spectra were recorded on a JNM-ECZ400 spectrometer (JEOL, Tokyo, Japan). Chemical shifts in the ^{1}H-NMR spectra are reported in parts per million relatives to the

peak of tetramethylsilane (TMS, δ 0.00 ppm), used as an internal standard. All product structures were in agreement with previously reported data [3].

The diastereomeric ratio (*dr*) and enantioselectivity (*ee*) were determined using SFC (SFC; ACQUITY UPC2, Waters, Tokyo, Japan) using chiral stationary phases (Chiralpak IB-3; IPA/CO_2, 95:5; 40 °C; 254 nm). Each purified aldol product samples were solved in heptane before injection. Four isomers can be produced from the aldol reaction of cyclopentanone (**4**) with 4-nitrobenzaldehyde (**5**) (**Scheme 3. 2**). The *ee* towards the formation of the (*SS*)-*syn* main product (noted a) in **Scheme 3. 2**) is given by the following equation:

$$ee = \left|\frac{[a]-[b]}{[a]+[b]}\right| \times 100$$

where [a] is the integrated peak surface of (*SS*)-*syn* and [b] is the integrated peak surface of (*RR*)-*syn* (noted b) in **Scheme 3. 2**) on the SFC chromatograph.

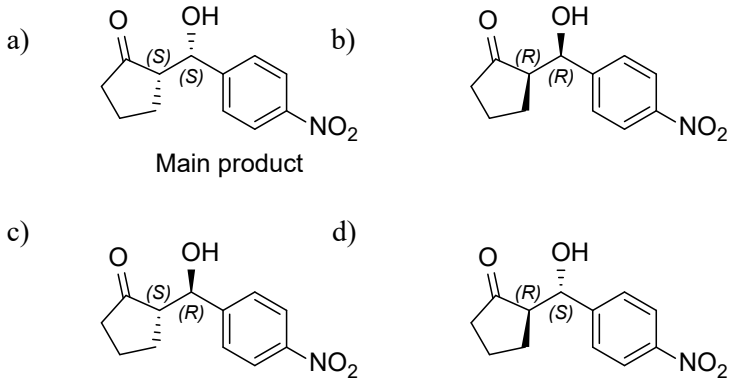

Scheme 3. 2 Products of the aldol reaction where a) and b) are the *syn* diastereomers, c) and d) are the *trans* diastereomers; a) is the mirror image of b) and form a pair of enantiomer, the same rule applies to c) and d).

The diastereoselectivity (*dr*) is the ratio between *syn* and *trans* diastereomers. The value is the ratio of the total surface of a) and b) relative to the total surface of c) and d) peaks from the SFC chromatograph.

3.2.5. Molecular dynamics (MD) simulation

The CNF model was described by the GLYCAM06 force field [4]. 4-Nitrobenzaldehyde, the enamine intermediate, and DMF solvent were modeled using the GAFF force field.[5] The QM/MM simulation was conducted using the SCC-DFTB-PA method with mio-1-1 parameters [6,7]. The particle mesh Ewald algorithm was adopted for long-range interactions, and the cutoff for nonbonding interactions in the coordinate space was fixed at 12 Å. All MD calculations were conducted using the SANDER and PMEMD.CUDA modules of the Amber 18 software package with the NVIDIA Kepler GPU system [8–10]. MD trajectory analysis was performed using the CPPTRAJ module of AmberTools 19 [11].

A CNF model with a hexagonal shape consisting of 19 chains of 10-mers in a 3×4×5×4×3 cellulose chain arrangement was built based on the crystallographic structural data of cellulose Iβ [12]. The DMF suspension system around the CNF model was constructed, including 50 molecules of either 4-nitrobenzaldehyde or the enamine intermediate equivalent to a concentration of 0.19 mol L^{-1}. The latter was an intermediate of the reaction of cyclopentanone with (*S*)-proline in DMF solution. Conventional MD calculations were performed for the system at constant temperature (300 K) and pressure (1 bar) for 2 μs. The adsorption distribution of 4-nitrobenzaldehyde and the enamine intermediate on the CNF surface was evaluated by analyzing the obtained MD trajectory.

Furthermore, a multiscale simulation combining quantum mechanics (QM) and molecular mechanics (MM) was conducted to reproduce the aldol reaction on the CNF surface. The

substrate was appropriately arranged on the CNF model based on the results obtained by MD calculation. The substrate and enamine intermediate involved in the aldol reaction were included as the QM region, and the rest of the system was treated as the MM region. The enamine intermediate was pulled toward 4-nitrobenzaldehyde arranged on the CNF model by an external force of 1,000 kcal mol^{-1} $Å^{-2}$ using a steered molecular dynamics (SMD) method [13]. The potential of mean force (PMF) of the reaction process was estimated from the exponential Boltzmann-weighted ensemble average of nonequilibrium works obtained from 1,000 SMD runs under ambient conditions (300 K and 1 bar) for 100 ps.

3.3. Results and Discussions

3.3.1. Effects of cellulose nanofibrils on proline-catalyzed Aldol reactions and reaction conditions optimization

The strategy to assess the effect of nanocellulose in the aldol reaction is similar to that used in the Michael addition. The pretreated matrix was dispersed in DMF to serve as the reaction medium. The reaction between cyclopentanone (**4**) and 4-nitrobenzaldehyde (**5**) catalyzed by (*S*)-proline in that medium at 0°C was observed for 24 h (**Table 3. 1**).

Table 3. 1 Nanocellulose effect in the Aldol reaction.[a]

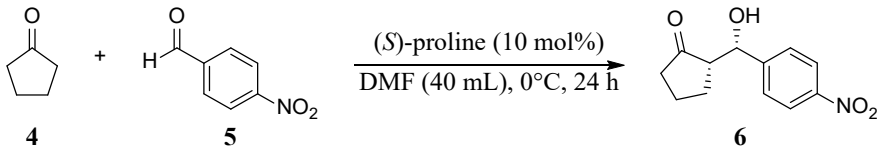

4 5 6

Entry	Catalysts	Yield (%)[b]	*syn*:*anti*[c]	*ee* for *syn* (%)[d]
1	Nanocellulose only	Trace	-	-
2	(*S*)-Proline only	18	80:20	64
3[e]	Precipitated CNF with (*S*)-proline	90	54:46	76
4	Precipitated TOCNF with (*S*)-proline	78	65:35	80
5	Precipitated TOCNF-H with (*S*)-proline	<99	78:22	89
6[f]	Precipitated TOCNF-H with (*S*)-proline solved in MeOH	89	47:53	78
7	TOCNF-H gel with (S)-proline	86	78:22	90
8	TOCNF-H gel with (S)-proline stirred at rt	85	71:29	60

[a] Conditions: cyclopentanone **4** (10 mL), 4-benzaldehyde **5** (2 mmol), (*S*)-proline (0.2 mmol), nanocellulose (300 mg, when used), DMF (40 mL); [b] isolated yield; [c] determined by ^{1}H-NMR (400 MHz, $CDCl_3$); [d] determined by chiral-phase SFC; [e] water removal from CNF or TOCNFs with DMF by repetitive centrifugation; [f] (*S*)-proline solved in MeOH (1 mL) added to TOCNF-H dispersed in DMF (39 mL).

No reactions occurred when CNF, TOCNF or TOCNF-H were used without (*S*)-proline (entry 1). The nanocellulose did not act as catalyst in the aldol reaction across different pretreatments. Low yield and moderate selectivity towards the formation of the *syn* product were recorded with (*S*)-proline alone after 24 h at 0°C (entry 2). However, adding precipitated nanocelluloses to (*S*)-proline in the reaction medium markedly increased the yield but also the enantioselectivity (entries 3 to 7). TOCNF delivered better *ee* compared to CNF (entries 3 to

5). The product was formed almost quantitatively in the presence of protonated TOCNF (entry 5). In contrast to the nanocellulose enhanced Michael addition, the presence of MeOH in the reaction medium was detrimental (entry 6). The *ee* of the *syn* product was reduced as well as the diastereoselectivity which was inversed.

In our previous studies, TOCNF precipitated in the sodium form were sensitive to aggregation in the reaction media without noticeably influencing the selectivity of the aldol reaction [14]. To prevent this, standing organogels were used, which enabled superior dispersion in the reaction media compared with that obtained by simple solvent exchange and centrifugation. Using the organogels, the reaction reached completion within 24 h (entry 7). However, the product could not be fully recovered (86% yield), probably owing to its strong adhesion to TOCNF-H surfaces. The obtained diastereoselectivity and enantioselectivity were comparable with the reaction using precipitated TOCNF-H.

The improved enantioselectivity was not solely attributed to the reaction solvent or temperature, because the reaction with TOCNF-H at room temperature delivered values comparable to that with (*S*)-proline alone at 0 °C in DMF (entries 2 and 8). Therefore, the stereoselectivity of the reaction with aromatic aldehydes was presumably improved *via* TOCNFs. The same product recovery issues from the reaction with TOCNF-H organogels at room temperature suggest that stereo control is caused by the aromatic aldehydes being restricted to adsorption to the TOCNF-H solid surfaces bearing regularly aligned chiral carbons on crystalline facets where hydrophobic and hydrophilic faces were separately located on the nanofibril's surfaces [15,16].

Solvent screening indicated that protic solvents (methanol and ethanol) and aprotic solvents (DMAc and dioxane) in which TOCNF-H aggregated were unsuitable for delivering the aldol adducts. DMF, which gave the most stable TOCNF-H dispersion, was the best solvent for the direct aldol reactions and used in subsequent experiments.

Consequently, the trial of different nanocellulose revealed that precipitated TOCNF-H are the most suitable to pair with (*S*)-proline in the aldol reaction between cyclopentanone and nitrobenzaldehyde in DMF at 0°C.

3.3.2. Catalyst load screening

The effect of the catalyst load was studied in the TOCNF-enhanced aldol reaction (**Table 3. 2**). 5 mol% of (*S*)-proline was enough to achieve 84% yield without further improvement or loss on the *ee* and *dr*. The amount of (*S*)-proline to pair with TOCNF-H in further experiment was set to 10 mol% as full completion was reached within reasonable time. In the spirit of green chemistry, but also, to prevent reactions without the assistance of TOCNF, the amount was not further increased.

Table 3. 2 Catalyst loads screening in the TOCNF-H enhanced aldol reaction.[a]

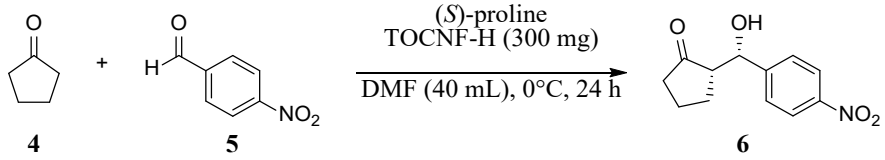

4 **5** **6**

Entry	(S)-proline load (mol%)	Yield (%)[b]	*syn*/*anti*[c]	*ee* for *syn*(%)[d]
1	10	99	78/22	89
2	5	84	78/22	89
3	1	Trace	-	-

[a] Conditions: cyclopentanone **4** (10 mL), 4-benzaldehyde **5** (2 mmol), (*S*)-proline, precipitated TOCNF-H (300 mg), DMF (40 mL); [b] isolated yield; [c] determined by ^{1}H-NMR (400 MHz, $CDCl_3$); [d] determined by chiral-phase SFC.

3.3.3. Amino acid investigations

Several amino acids are reported to catalyze the aldol reaction between aldehydes and ketones by forming enamine with the substrates in the same fashion as (*S*)-proline [17]. Therefore, a few amino acids were also tested as catalysts to determine whether they benefitted from the assistance of TOCNF-H. Most of these amino acids are known to allow reversible reactions that lower the *ee* of the product over time. This phenomenon is aggravated for long reaction times [18]. Consequently, the reactions in this section were stirred for 24 hours and quenched regardless of their advancement to prevent such undesirable effect.

Contrary to the reaction with (*S*)-proline, the reaction with all the tested amino acids did not yield product at 0°C within 24 hours. The reactions remained negative despite having TOCNF-H dispersed in the medium. The trials performed at room temperature were more fruitful (**Table 3. 3**).

Excluding (*S*)-proline, no reaction occurred during the screening time period at rt when using amino acids alone. However, when paired with TOCNF-H, an appreciable amount of product was formed within 24 h (entries 2, 4, and 6). The *ee* of the *anti*-product was generally high, similar to the case of TOCNFs combined with proline (**Table 3. 3**). Aliphatic amino acids proved to be a good match with TOCNFs (entries 1–6), while aromatic (*S*)-phenylalanine and (*S*)-tyrosine failed to catalyze the reaction (entries 7–10). This was probably because both hydrophobic catalysts and substrates were competitively adsorbed on the hydrophobic facets of the TOCNF crystals.

Table 3. 3 Scope of amino acids for cooperative catalysis in aldol reaction.[a]

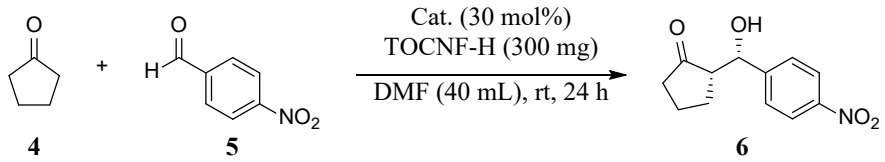

4 **5** **6**

Entry	Amino acid	TOCNF-H	Yield (%)[b]	*syn*/*anti*[c]	*ee* for *syn* (%)[d]
1	(*S*)-Alanine	–	trace	–	–
2		+	60	51:49	89
3	(*S*)-Valine	–	trace	–	–
4		+	65	49:51	91
5	(*S*)-Lysine	–	trace	–	–
6		+	54	69:31	82
7	(*S*)-Phenylalanine	–	trace	–	–
8		+	trace	–	–
9	(*S*)-Tyrosine	–	trace	–	–
10		+	trace	–	–

[a] Conditions: cyclopentanone **4** (10 mL), 4-benzaldehyde **5** (2 mmol), amino acid (0.6 mmol), TOCNF-H (300 mg, when used), solvent (40 mL); [b] isolated yield; [c] determined by ^{1}H-NMR (400 MHz, $CDCl_3$); [d] determined by chiral-phase SFC.

3.3.4. Substrate scope

Different aldehyde substrates were tested in the TOCNF-H/(*S*)-proline catalyzed aldol reaction (**Table 3. 4**). The main diastereomer had a *syn*-configuration. Surprisingly, all substrates resulted in enhanced enantioselectivity in the *anti*-product. The reaction yields gradually decreased with increasing strength of the electron-withdrawing groups on the aldehyde (entries 1 to 3). The bulky naphthaldehyde yielded the *anti*-product in a low yield

with high enantiopurity (entry 4). This effect might be attributed to both electrophilic interaction and steric hindrance between the substrates and the TOCNF solid surface bearing carboxylate groups [19], although a detailed mechanism remains to be determined.

Table 3. 4 Stereoselective aldol reaction of different aldehydes in the presence of protonated TOCNFs as a matrix using (*S*)-proline as organocatalyst[a].

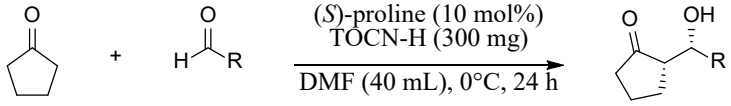

4 **5'** **6**

Entry	R	Yield[b] (%)	*syn/anti*[c]	*syn ee* (%)[d]	*anti ee* (%)[d]
1	4-NO_2-C_6H_4	98	78:22	89	87
2	4-Br-C_6H_4	60	63:37	53	88
3	4-Cl-C_6H_4	55	64:36	55	88
4	2-Naphthyl	24	64:36	51	87

[a] Conditions: cyclopentanone **4** (10 mL), aldehyde substrate **5'** (2 mmol), (*S*)-proline (0.2 mmol), TOCNF-H (300 mg), DMF (40 mL); [b] isolated yield; [c] determined by ^{1}H-NMR (400 MHz, $CDCl_3$); [d] determined by chiral-phase SFC.

3.3.5. Mechanistic studies

3.3.5.1. Catalyst deactivation inhibition

Proline is known to form an oxazolidinone byproduct with aldehyde substrates to a certain extent during reactions, which can lead to fatal catalyst deactivation. This byproduct is stable enough to be isolated and does not revert into the free proline and aldehyde forms [20]. The ^{1}H-NMR spectra of crude mixture from reactions with and without TOCNF-H were compared.

The proton signals for the deactivated catalyst form were clearly detected for the reaction in the absence of TOCNF-H (**Figure 3. 2**) [20,21]. Pleasingly, conducting the reaction in the presence of TOCNF-H drastically suppressed oxazolidinone formation, indicating effective prevention of proline decarboxylation in the reaction media. Furthermore, the baseline of the NMR spectra was distorted for reactions without TOCNFs, which indicated side polymerization reactions occurring among substrates and/or products (**Figure 3. 3**). Conversely, TOCNFs provided the target product with high purity (**Figure 3. 4**).

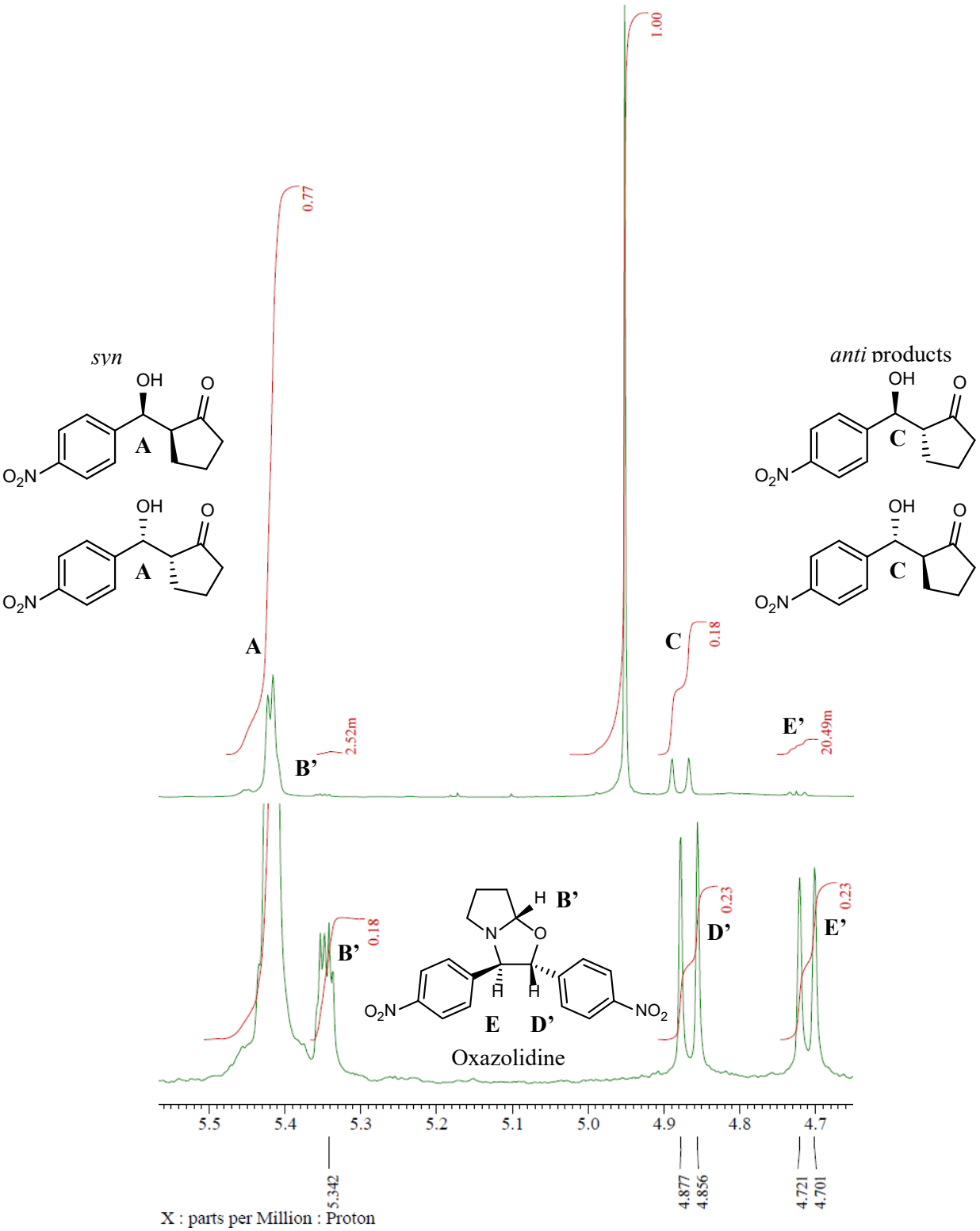

Figure 3. 2 Enlargements of ^{1}H NMR spectra (400 MHz, $CDCl_3$) shown in **Figure 3. 3** and **Figure 3. 4**, which represent the crude mixture from the aldol reaction between 4-nitrobenzaldehyde (300 mg, 2 mmol) and cyclopentanone (10 mL) catalyzed by (*S*)-proline (0.3 mmol) after stirring at 0°C for 24 h. Top spectrum, with TOCNF-H; bottom spectrum,

without TOCNF-H. Each spectrum was recorded from the combined organic layers dried in vacuo after the extraction process and before column chromatography purification.

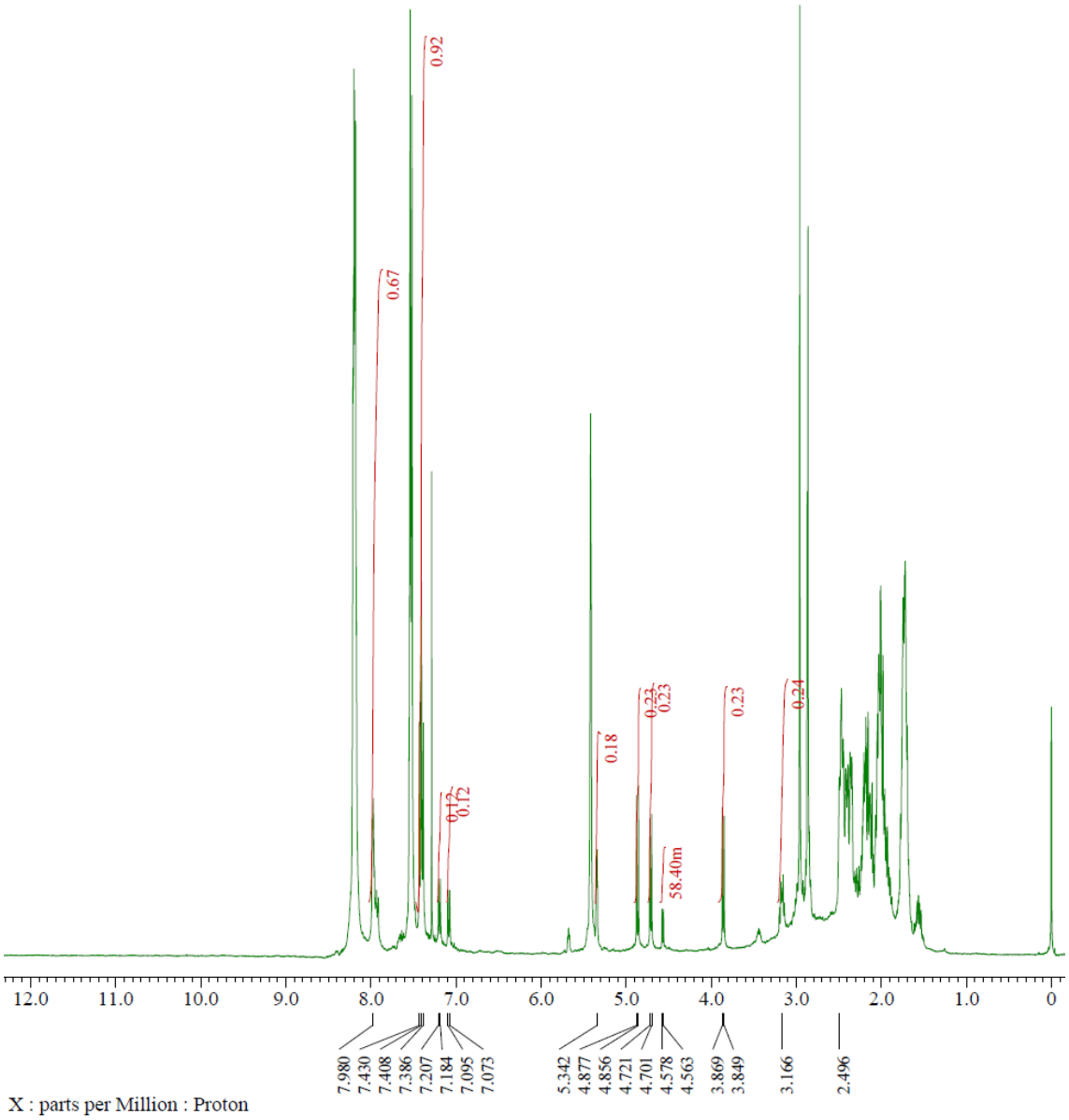

Figure 3. 3 ^{1}H NMR spectrum (400 MHz, $CDCl_3$) of the crude mixture from the aldol reaction without TOCNF-H.

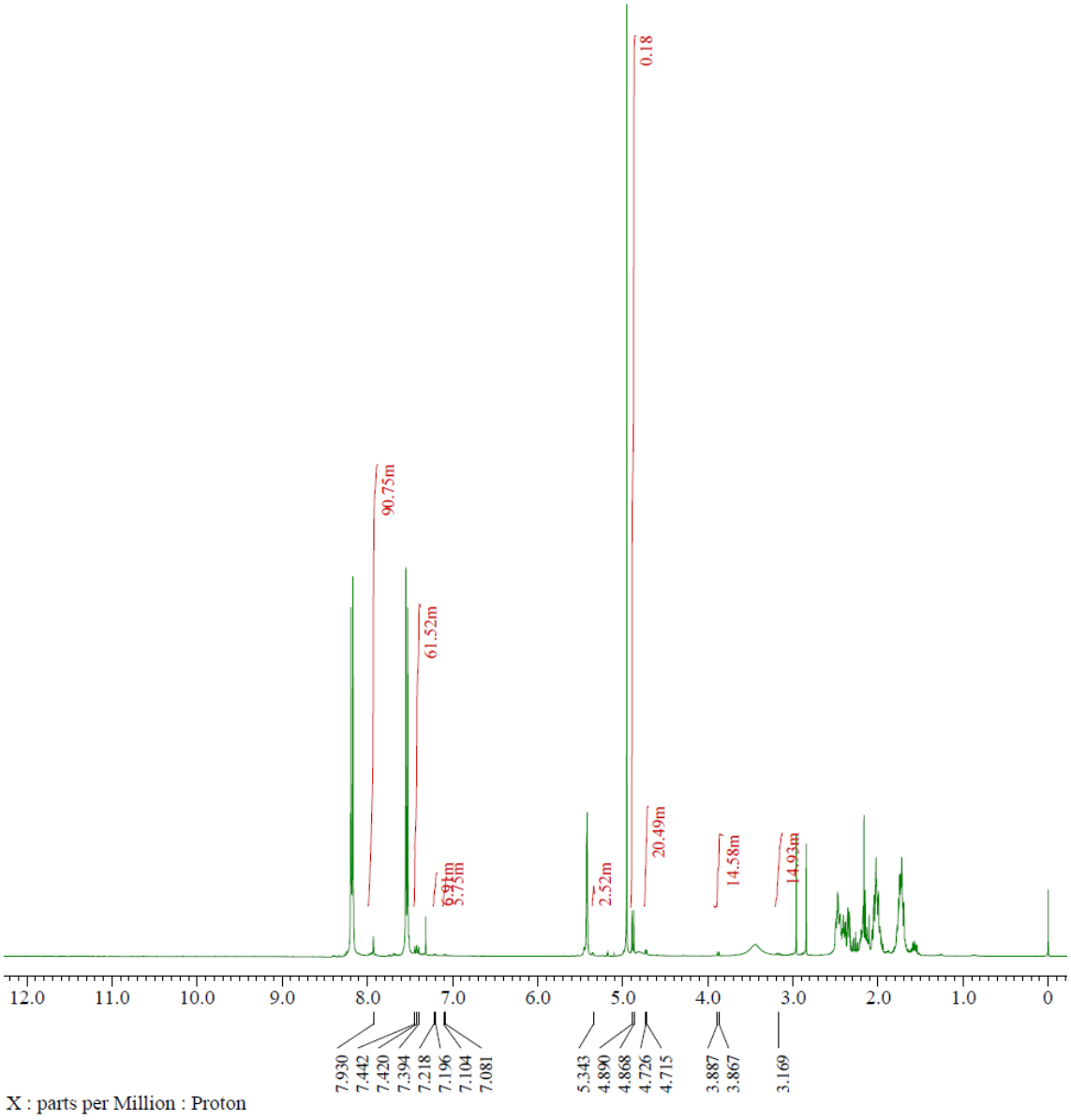

Figure 3. 4 ^{1}H NMR spectrum (400 MHz, $CDCl_3$) of the crude mixture from the aldol reaction in the presence of TOCNF-H.

3.3.5.2. Molecular dynamics

Computational chemistry was used to provide insight on the mechanism. The adsorption of substrates and intermediates onto CNFs was probably a key step in these asymmetric aldol reactions. Hydrogen bonds and van der Waals forces are considered the dominant intermolecular forces contributing to adhesion strength at the vicinity of CNF surfaces [22].

Molecular dynamics gives a simplistic but straightforward approach to explain the evolution of such forces and the interaction of macromolecular structures.

The three-dimensional structure of the product was speculated to be determined by the enantioselective mechanism occurring on the CNF surface, rather than asymmetric induction by the catalyst molecule as a unique chiral source. The adsorption behavior of the substrate and enamine intermediate on the CNF surface in the DMF solution was evaluated using conventional molecular dynamics (MD) calculations. The substrate (4-nitrobenzaldehyde) was reversibly adsorbed on the hydrophobic surface of CNF of either the (100) or (200) lattice planes of cellulose Iβ (Movie 1, **Figure 3. 5**). In particular, the molecular axis of 4-nitrobenzaldehyde preferred being perpendicular to the fiber axis of the cellulose chains, with the aromatic plane of the substrate parallel to the pyranose plane.

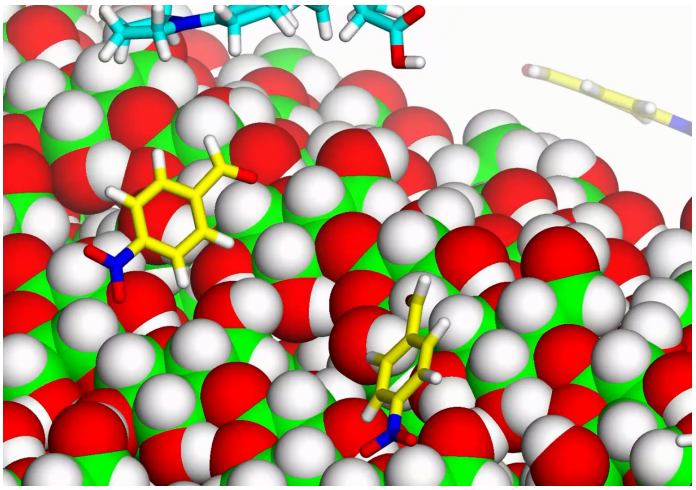

Figure 3. 5 Frame of the Movie 1 that shows reversible adsorption of 4-nitrobenzaldehyde (represented by yellow-ringed stick model) on the (100) or (200) lattice planes of cellulose Iβ (represented by Van der Waals speres).

The **Figure 3. 6** shows the distribution of substrate and intermediate on the surface of the CNF model for 2 μs, with the clear distribution of 4-nitrobenzaldehyde obtained by reflecting the aromatic ring. The regular and homogeneous high-density distribution of the substrate (red surface, **Figure 3. 6**) exclusively appeared over the cellobiose unit, reflecting the two-fold helical symmetry of a cellulose chain, which suggested that the orientation of the substrate was restricted by the surface topology of the CNF. Conversely, the enamine intermediate (blue surface, **Figure 3. 6**) showed an obscure distribution, indicating less specific adsorption behavior, albeit with a tendency to be located around the substituted groups of the adsorbed substrate. Therefore, substrate 4-nitrobenzaldehyde on the CNF surface was especially constrained by carbohydrate–aromatic CH/π and hydrophobic interactions, which possibly led to nucleophilic attack by the enamine intermediate at the aldehyde group of the adsorbed substrate from a specific direction.

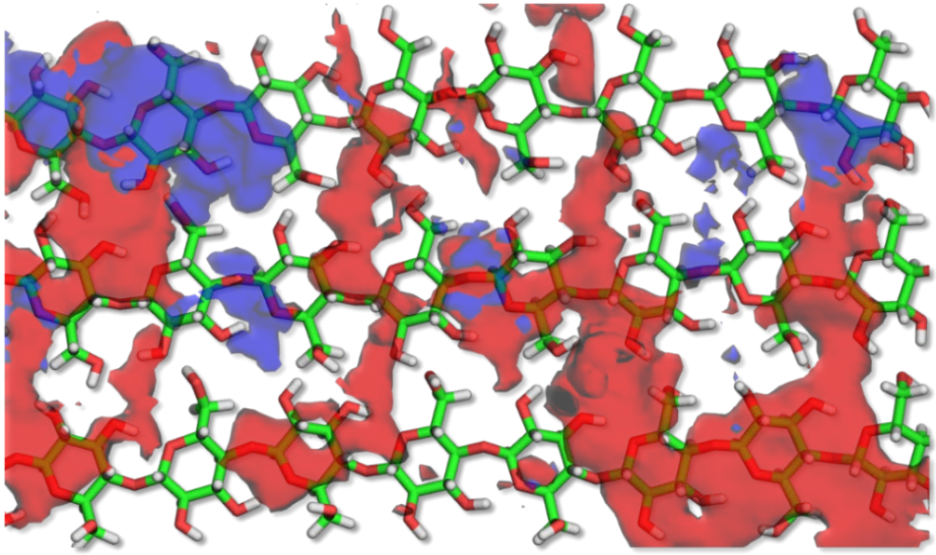

Figure 3. 6 Isocounter surfaces of the substrate and intermediate density relative to the structures of the CNF model calculated from the MD trajectories. Red and blue surfaces indicate 0.38 mol L^{-1} (corresponding to twice the bulk density) for 4-nitrobenzaldehyde and the enamine intermediate, respectively. The density was calculated for a 0.5 × 0.5 × 0.5 Å grid as the number of hits in 2,000,000 frames.

The MD simulation successfully provided pictorial elucidation of the enantioselectivity in the presence of CNF observed in the present aldol reaction. The next target was to verify whether the asymmetric aldol reaction proceeded on the substrate adsorbed on the CNF surface in the manner proposed by the MD simulation. A quantum mechanics (QM)/molecular mechanics (MM)-steered molecular dynamics (SMD) simulation was conducted to evaluate the aldol reaction on the CNF surface in a DMF solution. The QM/MM-SMD method showed that C–C bond formation was selected as the reaction coordinate leading to enantioselectivity, such that the enamine intermediate carbon (C_α) was pulled toward the carbonyl carbon (C_δ) of the substrate, giving the (*R*,*R*)-product.

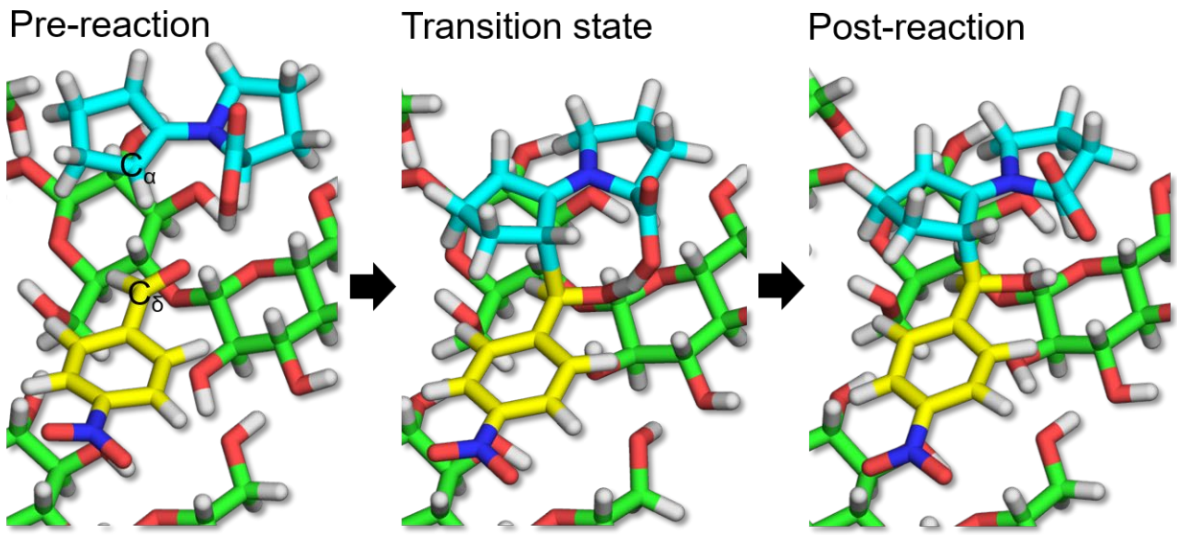

Figure 3. 7 C_α–C_δ bond forming reaction progression on CNF surface observed by QM/MM-SMD simulation.

As shown in **Figure 3. 7** and Movie 2, proton transfer occurred from the carboxy group of the enamine intermediate to the carbonyl oxygen of the substrate, accompanied by C_α–C_δ bond formation. **Figure 3. 8** shows the nonequilibrium work and potential of mean force (PMF) for

the reaction coordinate of the C_α–C_δ distance. The C–C bond forming reaction pathway of the present aldol reaction was exothermic (ΔG_r = –10.0 kcal mol^{-1}) and involved the transition state at a C_α–C_δ distance of 1.95–2.00 Å, in which the eight-membered ring structure with half-chair form contributed to stabilizing the transition state structure [23–25]. The activation energy ($\Delta G^‡$) was estimated to be 3.7 kcal mol^{-1}.

Therefore, the asymmetric aldol reaction was reasonably concluded to proceed on the CNF surface. Subsequent hydrolysis provided the reaction products, accompanied by recovery of the (*S*)-proline catalyst (**Figure 3. 9**).

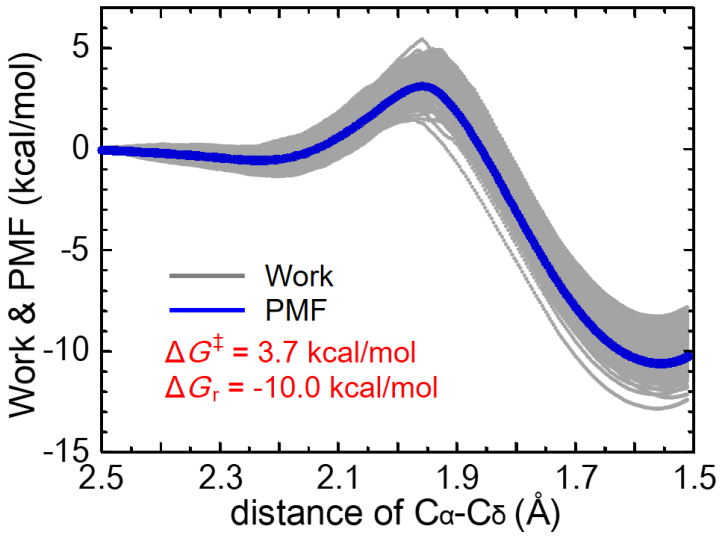

Figure 3. 8 Work distribution and potential mean force (PMF) obtained for the forced approach between the substrate (Cδ) and enamine intermediate (Cα) in DMF solvents, displayed for 0.01 Å ps–1 for pulling simulations with 1,000 trajectories.

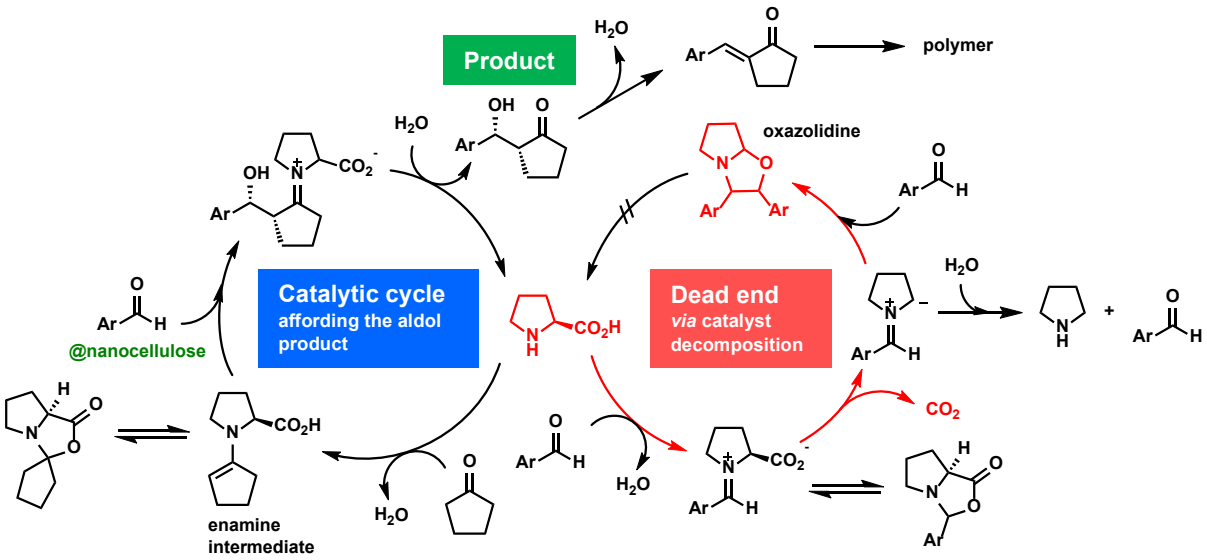

Figure 3. 9 Proposed catalytic pathway for enantioselective asymmetric aldol reactions occurring on nanocellulose surfaces in this study.

3.4. Conclusion

In summary, TOCNFs or TOCNF-H were not catalytically active in the aldol reaction between cyclopentanone and 4-nitrobenzaldehyde. Although, the nanocellulose suppressed the deactivation of the catalyst and further increase the yield. Additionally, TOCNF-H acted as a matrix to the (*S*)-proline catalyzed reaction by binding the aldehyde substrate. Constriction of the position of the substrate led to an increase in the *ee* according to molecular dynamics calculations.

References

1. Saito, T.; Uematsu, T.; Kimura, S.; Enomae, T.; Isogai, A. Self-aligned integration of native cellulose nanofibrils towards producing diverse bulk materials. *Soft Matter* **2011**, *7*, 8804–8809.

2. Kobayashi, Y.; Saito, T.; Isogai, A. Aerogels with 3D Ordered Nanofiber Skeletons of Liquid-Crystalline Nanocellulose Derivatives as Tough and Transparent Insulators. *Angew. Chemie Int. Ed.* **2014**, *53*, 10394–10397.

3. Wu, C.; Long, X.; Li, S.; Fu, X. Simple and inexpensive threonine-based organocatalysts as highly active and recoverable catalysts for large-scale asymmetric direct stoichiometric aldol reactions on water. *Tetrahedron: Asymmetry* **2012**, *23*, 315–328.

4. Kirschner, K.N.; Yongye, A.B.; Tschampel, S.M.; González-Outeiriño, J.; Daniels, C.R.; Foley, B.L.; Woods, R.J. GLYCAM06: A generalizable biomolecular force field. Carbohydrates. *J. Comput. Chem.* **2008**, *29*, 622–655.

5. Wang, J.; Wolf, R.M.; Caldwell, J.W.; Kollman, P.A.; Case, D.A. Development and testing of a general amber force field. *J. Comput. Chem.* **2004**, *25*, 1157–1174.

6. Elstner, M.; Porezag, D.; Jungnickel, G.; Elsner, J.; Haugk, M.; Frauenheim, T. Self-consistent-charge density-functional tight-binding method for simulations of complex materials properties. *Phys. Rev. B - Condens. Matter Mater. Phys.* **1998**, *58*, 7260–7268.

7. Seabra, G.D.M.; Walker, R.C.; Elstner, M.; Case, D.A.; Roitberg, A.E. Implementation of the SCC-DFTB method for hybrid QM/MM simulations within the Amber molecular dynamics package. In Proceedings of the Journal of Physical Chemistry A; *American Chemical Society* , **2007**; Vol. 111, pp. 5655–5664.

8. Salomon-Ferrer, R.; Götz, A.W.; Poole, D.; Le Grand, S.; Walker, R.C. Routine

microsecond molecular dynamics simulations with AMBER on GPUs. 2. Explicit solvent particle mesh ewald. *J. Chem. Theory Comput.* **2013**, *9*, 3878–3888.

9. Le Grand, S.; Götz, A.W.; Walker, R.C. SPFP: Speed without compromise - A mixed precision model for GPU accelerated molecular dynamics simulations. *Comput. Phys. Commun.* **2013**, *184*, 374–380.

10. Case, D.A.; Ben-Shalom, I.Y.; Brozell, S.R.; Cerutti, D.S.; Cheatham III, T.E.; Cruzeiro, V.W.D.; Darden, T.A.; Duke, R.E.; Ghoreishi, D.; Gilson, M.K. Amber 2018. *Univ. California, San Fr.* **2018**.

11. Roe, D.R.; Cheatham, T.E. PTRAJ and CPPTRAJ: Software for processing and analysis of molecular dynamics trajectory data. *J. Chem. Theory Comput.* **2013**, *9*, 3084–3095.

12. Nishiyama, Y.; Langan, P.; Chanzy, H. Crystal structure and hydrogen-bonding system in cellulose Iβ from synchrotron X-ray and neutron fiber diffraction. *J. Am. Chem. Soc.* **2002**, *124*, 9074–9082.

13. Park, S.; Khalili-Araghi, F.; Tajkhorshid, E.; Schulten, K. Free energy calculation from steered molecular dynamics simulations using Jarzynski's equality. *J. Chem. Phys.* **2003**, *119*, 3559–3566.

14. Kanomata, K.; Tatebayashi, N.; Habaki, X.; Kitaoka, T. Cooperative catalysis of cellulose nanofiber and organocatalyst in direct aldol reactions. *Sci. Rep.* **2018**, *8*, 4098.

15. Mazeau, K. On the external morphology of native cellulose microfibrils. *Carbohydr. Polym.* **2011**.

16. Mazeau, K.; Wyszomirski, M. Modelling of Congo red adsorption on the hydrophobic surface of cellulose using molecular dynamics. *Cellulose* **2012**, *19*, 1495–1506.

17. Kanemitsu, T.; Umehara, A.; Miyazaki, M.; Nagata, K.; Itoh, T. L-t-Leucine-Catalyzed

Direct Asymmetric Aldol Reaction of Cyclic Ketones. *European J. Org. Chem.* **2011**, *2011*, 993–997.

18. Orlandi, M.; Ceotto, M.; Benaglia, M. Kinetics versus thermodynamics in the proline catalyzed aldol reaction. *Chem. Sci.* **2016**, *7*, 5421–5427.

19. Rosenthal, J.; Schuster, D.I. The anomalous reactivity of fluorobenzene in electrophilic aromatic substitution and related phenomena. *J. Chem. Educ.* **2003**, *80*, 679–690.

20. Zotova, N.; Franzke, A.; Armstrong, A.; Blackmond, D.G. Clarification of the role of water in proline-mediated aldol reactions. *J. Am. Chem. Soc.* **2007**, *129*, 15100–15101.

21. Kano, T.; Takai, J.; Tokuda, O.; Maruoka, K. Design of an axially chiral amino acid with a binaphthyl backbone as an organocatalyst for a direct asymmetric aldol reaction. *Angew. Chemie - Int. Ed.* **2005**, *44*, 3055–3057.

22. Tayeb, A.H.; Amini, E.; Ghasemi, S.; Tajvidi, M. Cellulose nanomaterials-binding properties and applications: A review. *Molecules* **2018**, *23*, 2684.

23. Bahmanyar, S.; Houk, K.N. Transition states of amine-catalyzed aldol reactions involving enamine intermediates- theoretical studies of mechanism, reactivity, and stereoselectivity. *J. Am. Chem. Soc.* **2001**, *123*, 11273–11283.

24. Bahmanyar, S.; Houk, K.N. The origin of stereoselectivity in proline-catalyzed intramolecular aldol reactions. *J. Am. Chem. Soc.* **2001**, *123*, 12911–12912.

25. Bahmanyar, S.; Houk, K.N.; Martin, H.J.; List, B. Quantum mechanical predictions of the stereoselectivities of proline-catalyzed asymmetric intermolecular aldol reactions. *J. Am. Chem. Soc.* **2003**, *125*, 2475–2479.

Chapter 4

Investigation of Other Potential Organocatalytic Reactions

4.1. Introduction

During the course of this study, numerous organocatalytic reactions were tested based on the hypothesis that nanocellulose are able to interact or bind reaction intermediates or stabilize transition states. The result was drastic increase in yields and evolution in enantioselectivity in the Michael and aldol reactions. The common point for both reactions is that TOCNF acted as matrixes in the process, not catalyst themselves. The next strategy for further expanding the applicability of polysaccharide nanofibers would be their ability to act as catalyst themselves in asymmetric organic reactions. In the pursuit of this idea, attention was particularly paid to atom economic transformation such as the aldol reaction and the Michael addition. In addition, that the reactions would proceed in water, the medium in which the potential catalyst have the best dispersibility. Among reactions adhering to these criteria are the asymmetric Biginelli reaction and the asymmetric Robinson annulation.

This chapter thus depicts two interesting reactions needing a bit more trials to unlock the compatibility to polysaccharide nanofibers, with a descriptive part on phosphorylated nanocellulose (PCNF) preparation and their effect in the Biginelli reaction and chitosan nanofibers (CsNF) effect on the Robinson annulation.

4.2. Biginelli reaction

In the past years, dihydropyrimidinones (DHPM, **Scheme 4. 1**) and their derivatives attracted much attention due to their broad range of pharmacological properties such as calcium channels blockers, antioxidant, anticancer, and anti-inflammatory activity [1,2]. The Biginelli reaction is an atom efficient transformation that can be performed in a one pot process to synthesize DHPM. It is a three-component reaction between an aldehyde (**1**), urea (**2**), and a β-keto ester (**3**):

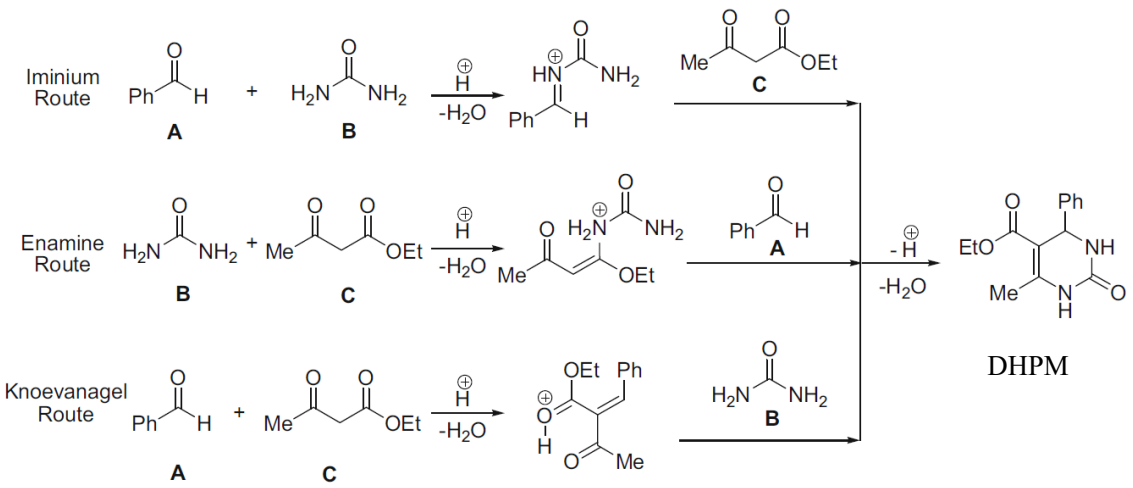

Scheme 4. 1 Commonly adopted mechanism of the Biginelli reaction.

There is a relatively few reports on the synthesis of chiral DHPM. On the other hand, highly enantioselective catalysts for the reaction often require tedious synthesis steps and several days for the reaction to complete [3]. Therefore, green and efficient methods are still desirable.

Water can be used as a solvent for the reaction, but strong acid is required as the catalyst [4]. A recent study on phosphorylated cellulose nanofibrils showed the possibility of having strongly acidic phosphate centers on the surface of the nanomaterial after surface modification

[5]. Moreover, PCNF exhibited good dispersion in water. Accordingly, PCNF was tested as an acidic chiral source in the Biginelli reaction.

4.2.1. Materials and Methods

Unless otherwise stated, solvents and reagents were of analytical grade and purchased form FUJIFILM Wako Pure Chemical Industries, Ltd. (Osaka, Japan), Sigma-Aldrich Co. LLC. (Tokyo, Japan), and Tokyo Chemical Industry Co., Ltd. (Tokyo, Japan). Soft wood bleached kraft pulp (SBKP) was purchased from Nippon Paper Industries Co., Ltd. (Tokyo, Japan). The reagents were used as received except for Benzaldehyde which was purified by distillation at reduced pressure and kept in an oxygen-free vial before its use in the reactions. Water used in this study was purified with an Arium ultrapure water system (Sartorius Co., Ltd., Tokyo, Japan).

4.2.1.1. Phosphorylated cellulose nanofibrils preparation

A previously reported method was used for the preparation of PCNF [5]. Soft wood bleached kraft pulp (SBKP) containing approximately 90% cellulose and 10% hemicelluloses was used as starting material for the preparation of PCNF. SBKP sheet (10 g) was cut in small pieces and soaked overnight in a beaker with 45 mL aqueous solution of urea (36 g) and $NH_4H_2PO_4$ (13.5 g). The soaked pulp was spread as thin as possible on a petri dish, then cured in oven at 140 °C (2 hours).

The sample was suspended in deionized water (2 wt%) with a kitchen blender then repeatedly filtered to remove unreacted reagents. NaOH (1 M) was added to the pulp slurry (2 wt%) with stirring. The pH of the slurry was controlled at 12 and left for 15 min for

neutralization purpose. Excess NaOH was removed by repeated dilution to 2 wt% and filtrations until the electric conductivity of the filtrate went lower than 100 μS/cm. The resulting phosphorylated pulp in sodium form (PP-Na) was dispersed in water (0.2 wt% slurry) and then mechanically disintegrated by aqueous counter collision with a high-pressure water jet system at 200 MPa for 10 passes (0.1-mm diameter dual-nozzle chamber; Star Burst Labo, Sugino Machine Limited, Uozu, Japan) to produce phosphorylated cellulose nanofibrils in sodium form (PCNF). The obtained suspension was then centrifuged to separate PCNF as supernatant from the unfibrillized fibers at 22,540 ×*g* for 10 min (TOMMY Suprema 21 High-Speed Refrigerated Centrifuge, TOMMY Seiko, Tokyo, Japan). The PCNF was characterized by atomic force microscope (AFM) and conductimetry.

4.2.1.2. Phosphorylated cellulose nanofibrils characterization

The phosphate content of freeze-dried phosphorylated pulp (PP) and PCNF water suspension, right after the nanofibrillation by aqueous counter collision, were measured by conductivity titration. The relevant material (100 mg) was dispersed in a mixture of aqueous HCl (10 mM, 20 mL) and H_2O (50 mL) in a beaker by sonication (10 min). The dispersion was titrated with aqueous NaOH (48 mM).

The morphology of the PCNF was analyzed by Atomic Force Microscopy (AFM) on a Dimension Icon microscope (Bruker Japan K. K., Tokyo, Japan). PCNF water dispersion (0.001% w/w, 5 μL) was dropped on a 1 cm^2 piece of freshly cleaved mica and left to dry at room temperature to prepare the analyte samples. The observation was done in tapping mode with a 40 Nm cantilever (RTESP-300, Bruker Japan K. K., Tokyo, Japan).

4.2.1.3. Protonation of phosphorylated cellulose nanofibrils

PCNF-H was prepared by the following method. A dispersion of PCNF in deionized water (0.1 wt%) was treated for 1 h with acidic ion exchange resin Amberjet 1024 (10 vol%). The sample was recovered by filtration through metal grid then treated with basic ion exchange resin Amberjet 4400 (10 vol%). Lastly, PCNF was washed then treated with acidic Amberjet 1024 and recovered. The pH of the final PCNF-H water suspension was 3.8.

4.2.1.4. Representative Biginelli reaction procedure

The catalyst amount was set to 10 mol% against **7**. When phosphorylated cellulose was used as catalyst, the amount was adjusted to 10 mol% by taking into account phosphate as the catalytic center.

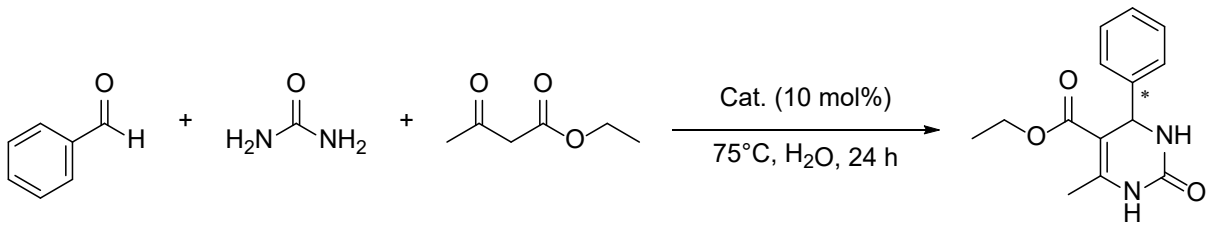

7 1 eq. **8** 1 eq. **9** 1.5 eq **10**

To an aqueous solution of urea **8** (1 eq.) was added benzaldehyde **7** (1 eq.), ethylacetoacetate **9** (1.5 eq.) and the desired catalyst (10 mol%). The reactions were stirred at 75°C for 24 h and their progress was followed by TLC. The product isolation was done by recrystallization in pure EtOH for 5 mmol scale reactions, and by extraction with EtOAc/DMSO followed by flash column chromatography for 1 mmol scale reactions. The product structure was confirmed by ^{1}HNMR (JNM-ECZ400 spectrometer, JEOL, Tokyo, Japan) and the enantioselectivity was determined by SFC (ACQUITY UPC2, Waters, Tokyo, Japan) with chiral stationary phases (Chiralpak column ID, IPA:C_2O/10:90).

4.2.2. Results and Discussion

4.2.2.1. Phosphorylated cellulose nanofibrils characterization

The obtention of nanosized phosphorylated cellulose was confirmed by the birefringence of a water suspension of the material when observed between cross polarized filter (**Figure 4. 1**).

Figure 4. 1 Birefringence test on a PCNF water suspension (0.1 wt%).

The morphology of PCNF from the AFM analysis revealed bundles of fibers of 50 nm width as well as 2 to 5 nm width short individualized fibers (**Figure 4. 2**).

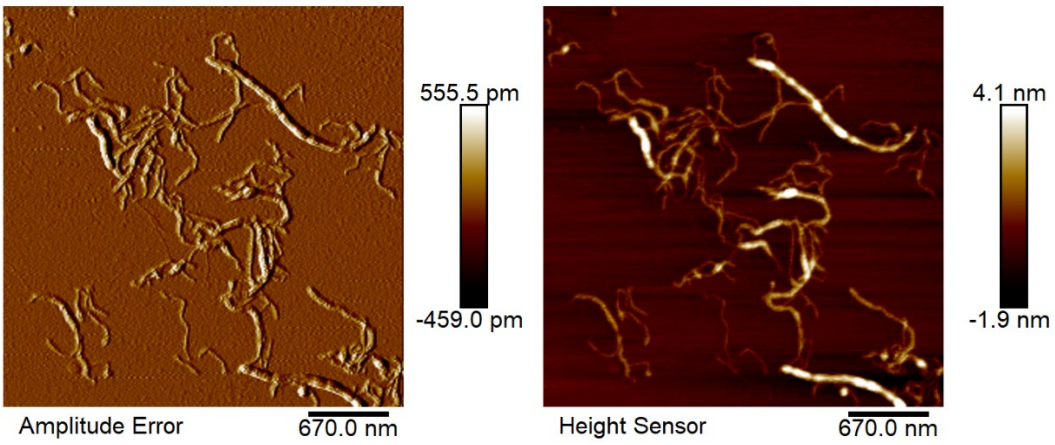

Figure 4. 2 PCNF (0.74 wt%, 1.9 mmol/g phosphate) images in tapping mode with a 40 Nm cantilever.

The electric conductivity curves of phosphorylated pulp (PP) returned 1.7 mmol/g of phosphate content. Although, PCNF's measurement gave 1.9 mmol/g (**Figure 4. 3**). The slight difference can be attributed to the titration of a less dispersed freeze-dried PP versus a well dispersed never dried PCNF water suspension.

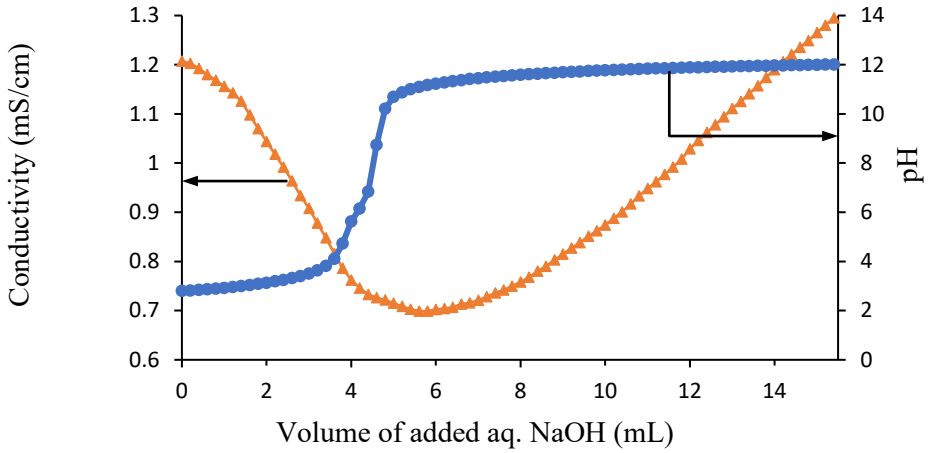

Figure 4. 3 Representative pH (circles) and electrical conductivity (triangles) curves of an aqueous suspension of PCNF. Phosphate content: 1.9 mmol/g.

The recorded characteristics of the prepared PCNF are in agreement with previously reported values [5].

4.2.2.2. Effects of phosphorylated cellulose nanofibrils on the Biginelli reaction

Table 4. 1 Comparison between strong acid and PP or PCNF in the Biginelli reaction.[a]

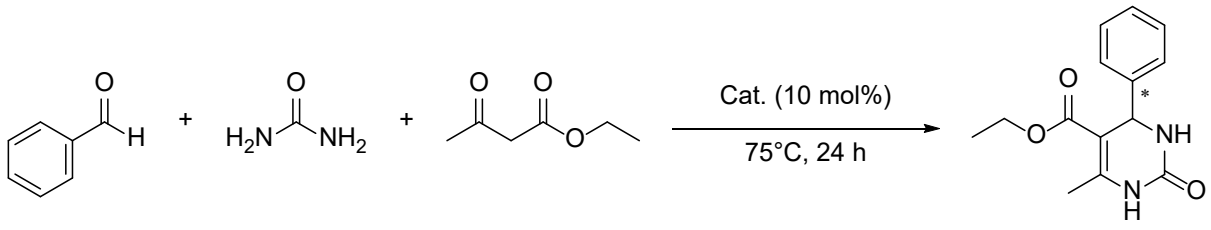

Entry	Scale (mmol)	Catalysts (mg)	Solvent (mL)	Time	Yield (%)[b]
1	1	-	H_2O (4)	24 h	3
2	1	H_3PO_4	H_2O (4)	24 h	10
3	1	H_3PO_4	EtOH (4)	24 h	42
4	5	PP (294)	H_2O (20)	24 h	11
5	5	PCNF (256)	H_2O (30)	24 h	13
6	1	PCNF-H (51)	H_2O (4)	24 h	3
7[c]	1	PCNF-H (51)	EtOH (2)/H_2O (2)	24 h	3
8[d]	1	PCNF (51)	H_2O (4)	11 d	7
9[d]	1	PCNF-H (51)	H_2O (4)	11 d	6

[a] Conditions: benzaldehyde **7** (1 mmol), urea **8** (1 mmol), ethylacetoacetate **9** (1.5 mmol), catalyst (10 mol%) stirred in the stated solvent at 75°C; [b] isolated yield; [c] EtOH (2 mL) and H_2O (2 mL) mixture as solvent; [d] stirred at rt.

Most of reactions were stopped at 24 h before full conversion for fast evaluation of a potential catalytic system (**Table 4. 1** entries 1 to 7). The Biginelli reaction proceeds slowly in

water at 75°C without catalyst (entry 1). Phosphoric acid (10 mol%) was chosen as a strong acid control to compare with PP and PCNF (entries 2 and 3). H_3PO_4 yielded a smaller amount of the product in water than in EtOH probably due to a better solubility of the substrate in the organic solvent. The products are racemic. PP and PCNF in sodium form yielded nearly as much product as H_3PO_4 in water (entries 4 and 5). Although, isolation of the product after a total of 24 h reaction gave lower yields than with H_3PO_4 in EtOH. Unfortunately, the products are also racemic. Protonated PCNF was not able to catalyze the reaction even in EtOH/H_2O mixture as solvent (entries 6 and 7). In the meantime, reactions at room temperature to seek for changes in enantioselectivity with PCNF and PCNF-H were conducted for long reaction times. The reactions were extracted as soon as enough product was formed upon TLC analysis (entries 8 and 9). The products were also racemic.

Despite not acting as chiral source in the chosen Biginelli reaction model, PP and PCNF in sodium form did catalyze the reaction in water. Different reaction conditions and substrates are still awaiting testing to expose the nanocellulose's potential.

4.3. Wieland-Miescher ketone synthesis

The discovery of (*S*)-proline catalyzed synthesis of Wieland-Miescher (WM) ketone **13** and Hajos−Parrish (HP) ketone **14** (**Figure 4. 4**) is a cornerstone of organocatalysis [6,7]. The motifs are valuable synthon for the preparation of natural molecules including sesquiterpenoids, diterpenoids, and steroids that are biologically active [8,9].

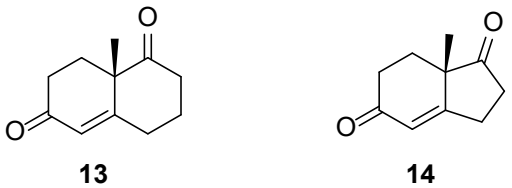

13 **14**

Figure 4. 4 Wieland−Miescher ketone (**13**) and Hajos−Parrish ketone (**14**).

Much advancement has been reported in the developpement of highly enantioselective catalyst for the reaction, the Robinson annulation, but chiral organocatalysts rarely achieve high enantioselectivity, high conversion ratio, low cost and ease of synthesis simultaneously [10,11]. Most organocatalyst structures are based on chiral amines for promoting the reaction through enamine activation mode because the Robinson annulation is a Michael Addition to an α,β-unsaturated ketone followed by an aldol condensation [12,13].

4.3.1. Materials and Methods

Chitosan powder (CsP; 80% deacetylation, 6.8 mmol/g of amine content) was purchased from FUJIFILM Wako Pure Chemical Industries, Ltd. (Osaka, Japan). Chitosan nanofibers (CsNF; 80% deacetylation, 4.3 mmol/g of amine content) prepared by mechanical nanofibrillation were purchased from Sugino Machine Limited (BiNFi-s AFo-10002, Uozu, Japan). TEMPO-oxidized cellulose nanofibrils (TOCNF, carboxylate content: 1.61 mmol/g) were kindly supplied by Nippon Paper Industries Co., Ltd. (Tokyo, Japan). Unless otherwise stated, all solvents, substrates and (*S*)-proline were of analytical grade and purchased form Sigma-Aldrich Co. LLC. (Tokyo, Japan), and Tokyo Chemical Industry Co., Ltd. (Tokyo, Japan). The reagents and polysaccharides were used as received.

4.3.1.1. Water removal process from chitosan nanofibers and TEMPO-oxidized cellulose nanofibrils

CsNF and TOCNF were subjected to water removal treatment by solvent exchange with DMSO. A water suspension of polysaccharide nanofibers (100 mg of dry material) was mixed with DMSO (30 mL) then centrifuged at 12,000× *g* for 15 min (TOMMY Suprema 21 High-Speed Refrigerated Centrifuge, TOMMY Seiko, Tokyo, Japan). The supernatant was replaced

with fresh DMSO after each centrifugation cycle. After the last fifth cycle, the solvent was removed, and the precipitates were recovered and used in reactions.

4.3.1.2. Representative Robinson annulation reaction procedure

The amount of (*S*)-proline was set at 100 mol% against the diketone substrate **12**. The amount of chitosan was adjusted to 100 mol% by taking into account the amine group as a catalytic center. The mass of TOCNF was set equal to that of **12** (200 mg) or a half (100 mg). When used, CsNF and TOCNF precipitates were dispersed in DMSO (10 mL) with a double-cylinder-type homogenizer (2 min) to serve as the reaction medium.

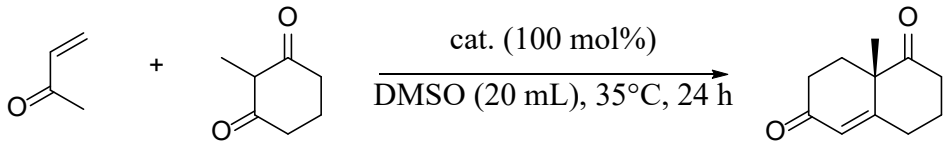

11
1.5 eq.
2.4 mmol

12
1 eq.
1.6 mmol

13

To a suspension of 2-methyl-1,3-cyclohexanedione **12** (1.6 mmol) and the catalyst (100 mol%) in DMSO (20 mL) was slowly added methyl vinyl ketone **11** (2.4 mmol) with a micropipette to start the reaction. The resulting mixture was stirred at 35°C and monitored by TLC. The plates were visualized using *p*-anisaldehyde. After for 24 h, the reaction was stopped and quenched by adding aq. NH_4Cl, extracted with ethyl acetate (30 mL × 3), and dried over Na_2SO_4. The concentrated organic layer was purified by column chromatography on an automated flash chromatography system (Smart Flash EPCLC-AI-580S, Yamazen, Osaka, Japan). Hexane and ethyl acetate were used as eluents and rendered the Wieland-Miescher ketone main product (*S*)-**13** as a brown oil after solvent evaporation.

4.3.1.3. Reaction products characterization

The structure of the product was confirmed by proton Nuclear Magnetic Resonance (^{1}H-NMR) recorded on a JNM-ECZ400 spectrometer (JEOL, Tokyo, Japan). The chemical shifts are reported in parts per million relative to the peak of tetramethylsilane (TMS, δ 0.00 ppm), used as an internal standard.

The enantioselectivity was measured by Supercritical Fluid Chromatography (SFC; ACQUITY UPC2, Waters, Tokyo, Japan) using a chiral stationary phase. The purified Wieland-Miescher ketone sample was solved in MeOH before injection. The Robinson annulation of addition of **12** with **13** gives a pair of enantiomers (**Scheme 4. 2**). The enantioselectivity (*ee*) towards the formation of the (*S*)-**13** main product (noted a) in **Scheme 4. 2**) is given by the following equation

$$ee = \left|\frac{[a]-[b]}{[a]+[b]}\right| \times 100$$

where [a] is the integrated peak surface of (*S*)-**13** and [b] is the integrated peak surface of (*R*)-**13** (noted b) in **Scheme 4. 2**) on the SFC chromatograph.

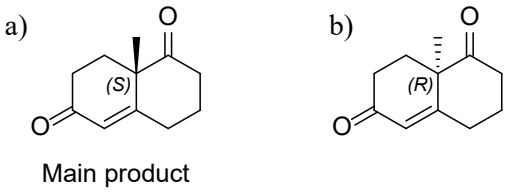

Scheme 4. 2 Pair of enantiomer products of the Robinson annulation.

4.3.2. Results and Discussion

The choice on catalyst amount was done due to the fact that the Robinson annulation is very slow and the *ee* is proportional to the amount of (*S*)-proline in previous reports.

Table 4. 2 Polysaccharide effect in the Robinson annulation reaction.[a]

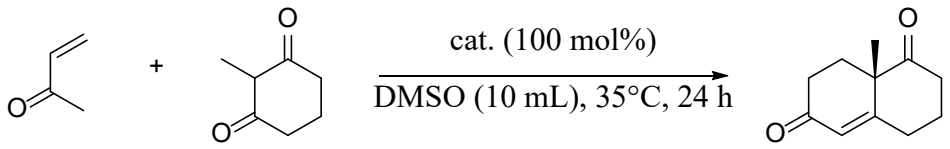

11 1.5 eq. 2.4 mmol

12 1 eq. 1.6 mmol

13

Entry	Catalysts	Time (h)	Yield (%)[b]	*ee* (%)[c]
1[d]	(*S*)-Proline only	48	77	38
2[d]	Chitosan powder	48	62	(3)[e]
3	(*S*)-Proline only	24	16	73
4	Chitosan powder	24	34	(5)
5[f]	Precipitated chitosan nanofiber	24	13	(5)
6	Precipitated TOCNF (200 mg)	24	Trace	-
7	Precipitated TOCNF-H (200 mg)	24	Trace	-
8	Precipitated TOCNF (200 mg) with (*S*)-proline	24	13	77
9	Precipitated TOCNF (100 mg) with (*S*)-proline	24	20	73
10	Precipitated TOCNF-H (100 mg) with (*S*)-proline	24	25	74

[a] Conditions: methyl vinyl ketone **11** (200 μL), 2-methyl-1,3-cyclohexanedione **12** (202 mg), catalyst (100 mmol%), DMSO (20 mL); [b] isolated yield; [c] determined by chiral-phase SFC (Chiralpak column IC-3, IPA:C_2O/15:85); [d] reaction in DMSO (5 mL)/H_2O (5 mL) mixture as solvent; [e] *ee* of the opposite enantiomer (*R*)-**13** as main product; [f] precipitated means water removal from TOCNF and CsNF by repetitive centrifugation in DMSO.

(*S*)-Proline catalyzed Robinson annulation between methyl vinyl ketone **11** and 2-methyl-1,3-cyclohexanedione **12** was used as a model for the study [6]. Due to the fact that the reaction

using the literature condition took several days to complete, all catalyst load was set at 100 mol% against **12** for faster screening.

The comparison between (*S*)-proline and chitosan powder (CsP) in DMSO/H_2O mixture as solvent showed a superior activity of the homogeneously dispersed molecule over the amorphous polymer (entries 1 and 2, **Table 4. 2**). Isolated product from proline catalysis gave a modest *ee* in the reaction (entry 1) and nearly racemic for CsP (entry 2). The lower enantioselectivity of (*S*)-proline is due to the presence of water which promotes the reversibility of the reaction towards the formation of the minor (*R*)-**13** product [14].

For the following experiments, DMSO only was used a solvent and water was removed by precipitation from water suspension of chitosan nanofibers (CsNF) and TEMPO-oxidized cellulose nanofibrils (TOCNF). CsP was more active than proline when water was not present in reaction (entries 3 and 4). This is probably due to a lower solubility of the molecule in DMSO. Precipitated CsNF yielded nearly the same amount of WM ketone as (*S*)-proline (entry 5). The enantioselectivity from CsP and CsNF catalyzed reaction are the same despite the crystalline nature of the nanofibers.

Considering the mechanism of the Robinson annulation, a Michael addition followed by an intramolecular aldol reaction, TOCNF was also tried as a potential catalyst (entries 6 to 10). Neither of the sodium or protonated form of the nanocellulose could activate the reaction when used without (*S*)-proline (entries 6 and 7). Consequently, the strategy of using precipitated TOCNF with (*S*)-proline adopted in chapters 2 and 3 was also tried. The presence of 200 mg of TOCNF in the medium did not affect the reaction (entry 8). The amount of nanocellulose was lowered to 100 mg as the reaction medium seemed thick (entry 9). Accordingly, the yield slightly improved from 13 to 20%. The use of protonated TOCNF further increased the yield to 25% (entry 10). In overall, there was no appreciable change in enantioselectivity with TOCNF or TOCNF-H/(*S*)-proline as catalytic system for the tested reaction conditions.

4.4. Conclusion

On the road to discover new and promising application of natural polysaccharides in water, phosphorylated pulp and PCNFs did not act as chiral catalyst in the Biginelli reaction, chitosan powder and CsNF also did not act as a chiral source in the Robinson annulation. The same strategy adopted in the previous chapters by combining TOCNF and (*S*)-proline showed an enhancement of the Wieland-Miescher ketone yield without loss of enantioselectivity. It is important to note that only few conditions were tested and more needs to be done to unravel other potentials of polysaccharide nanofibers.

References

1. Shaikh, I.R. Organocatalysis: Key Trends in Green Synthetic Chemistry, Challenges, Scope towards Heterogenization, and Importance from Research and Industrial Point of View. *J. Catal.* **2014**, *2014*, 1–35.

2. Sunagar, V.; Dixit, S.R.; Chougala, B.M.; Samundeeswari, S.; Holiyachi, M.; Shaikh, F.; Madar, J.; Kulkarni, R. 3,4-Dihydropyrimidinone-coumarin analogues as a new class of selective agent against S. aureus: Synthesis, biological evaluation and molecular modelling study. *Bioorganic Med. Chem.* **2017**, *25*, 1413–1422.

3. Heravi, M.M.; Moradi, R.; Mohammadkhani, L.; Moradi, B. Current progress in asymmetric Biginelli reaction: an update. *Mol. Divers.* **2018**, *22*, 751–767.

4. Clark, J.H.; Macquarrie, D.J.; Sherwood, J. The Combined Role of Catalysis and Solvent Effects on the Biginelli Reaction: Improving Efficiency and Sustainability. *Chem. - A Eur. J.* **2013**, *19*, 5174–5182.

5. Noguchi, Y.; Homma, I.; Matsubara, Y. Complete nanofibrillation of cellulose prepared by phosphorylation. *Cellulose* **2017**, *24*, 1295–1305.

6. Bui, T.; Barbas, C.F. A proline-catalyzed asymmetric Robinson annulation reaction. *Tetrahedron Lett.* **2000**, *41*, 6951–6954.

7. Hajos, Z.G.; Parrish, D.R. Asymmetric Synthesis of Bicyclic Intermediates of Natural product chemistry. *J. Org. Chem.* **1974**, *39*, 1615–1621.

8. Bradshaw, B.; Etxebarria-Jardi, G.; Bonjoch, J.; Viózquez, S.F.; Guillena, G.; Nájera, C. Efficient solvent-free robinson annulation protocols for the highly enantioselective synthesis of the wieland-miescher ketone and analogues. *Adv. Synth. Catal.* **2009**, *351*, 2482–2490.

9. Bradshaw, B.; Bonjoch, J. The Wieland-Miescher ketone: A journey from organocatalysis to natural product synthesis. *Synlett* **2012**, 337–356.

10. Chemistry, B.; Ramachary, D.B.; Sakthidevi, R. Combining multi-catalysis and multi-component systems for the development of one-pot asymmetric reactions : stereoselective synthesis of highly. **2008**, 2488–2492.

11. Bañón-Caballero, A.; Guillena, G.; Nájera, C.; Faggi, E.; Sebastián, R.M.; Vallribera, A. Recoverable silica-gel supported binam-prolinamides as organocatalysts for the enantioselective solvent-free intra- and intermolecular aldol reaction. *Tetrahedron* **2013**, *69*, 1307–1315.

12. Zhou, P.; Zhang, L.; Luo, S.; Cheng, J.-P. Asymmetric Synthesis of Wieland–Miescher and Hajos–Parrish Ketones Catalyzed by an Amino-Acid-Derived Chiral Primary Amine. *J. Org. Chem.* **2012**, *77*, 2526–2530.

13. Zeng, X.P.; Cao, Z.Y.; Wang, Y.H.; Zhou, F.; Zhou, J. Catalytic Enantioselective Desymmetrization Reactions to All-Carbon Quaternary Stereocenters. *Chem. Rev.* **2016**, *116*, 7330–7396.

14. List, B.; Hoang, L.; Martin, H.J. Asymmetric Catalysis Special Feature Part II: New mechanistic studies on the proline-catalyzed aldol reaction. *Proc. Natl. Acad. Sci.* **2004**, *101*, 5839–5842.

Chapter 5

Concluding remarks

A novel method to enhance the catalytic efficiency and to enrich enantiomers in direct asymmetric Michael reactions was developed owing to green natural nanofibers obtained from wood pulp by aqueous TEMPO-mediated oxidation. The crystalline nature of TOCNF with densely packed surface carboxylate groups presumably played a significant role in increasing the catalytic activity because TOCNF with low carboxylate content only gave a small yield enhancement. In addition, molecular carboxylates originating from sodium acetate gave a modestly improved yield, while amorphous carboxylated cellulose derivative was not effective. Furthermore, the efficiency of the catalytic system was directly related to the amount of nanocellulose used. The method was successfully applied to different ketones and nitroalkene substrates.

Protonated TOCNF permitted highly efficient and enantioselective aldol reactions between cyclopentanone and various aldehydes. Mechanistic investigations through NMR experiments showed that TOCNF-H drastically suppressed oxazolidinone formation. The effect is indicative of effective prevention of proline decarboxylation in the reaction media and avoidance of undesirable side polymerization reactions among substrates and/or products. Computer-aided simulations proved that the aldehyde substrate orientation was controlled by carbohydrate–aromatic CH/π and hydrophobic interactions on the CNF surfaces. Furthermore, the reaction proceeded in the direct vicinity of the cellulose surface, as suggested by QM/MM-SMD calculation results. The same phenomenon is expected to occur in the TOCNF enhanced

Michael addition in which the nitroalkene substrate is possibly constricted on the nanocellulose's surface during the rate limiting step of the reaction to enable high yields. TOCNFs acted as a matrix for (*S*)-proline catalysis in both reactions.

Further investigation on organocatalytic reactions, namely Biginelli reaction and Robinson annulations were attempted. All tested polysaccharide nanofibers, phosphorylated nanocellulose and chitosan nanofibers, did not act as chiral enhancers. Once, more TOCNF/(*S*)-proline combination showed a slightly promising outcome by keeping the *ee* and improving the yield in the Robinson annulation. Albeit only a few reaction conditions were tried for both reactions, additional trials would unravel the nanomaterial's potentials.

Given these points, the successful application of green natural nanofibers in two major carbon–carbon bond forming organocatalytic reactions could be achieved. Essentially, the process involved the simple dispersion of nanocellulose in the reaction medium with reduced proline catalytic load and conducted in mild conditions. Concerted catalysis using nanocelluloses and organocatalysts provides new research avenues for both emerging applications of nanocellulose and green sustainable chemistry and will open up the development of a new type of heterogeneous catalysis.

Appendix

6.1. TOCNF Enhanced Michael Additions

6.1.1. Synthesized substrate characterization

^{1}H-NMR data are reported as follows: chemical shift, multiplicity (s = singlet, d = doublet, t = triplet, q = quartet, m = multiplet), coupling constants (Hz), and integration.

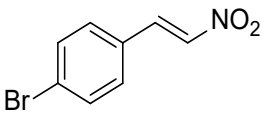

(E)-1-Bromo-4-(2-nitrovinyl)benzene (**2c**). Brown solid; ^{1}H-NMR (400 MHz, $CDCl_3$): δ_H = 7.95 (d, J = 13.7 Hz, 1H), 7.61−7.58 (m, 3H), 7.43−7.40 (d, J = 8.7 Hz, 2H); ^{13}C-NMR (100.5 MHz, $CDCl_3$): δ_C = 137.8, 137.4, 132.7, 130.4, 128.9, 126.7.

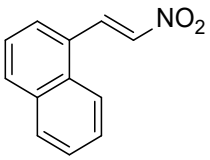

(E)-1-Bromo-4-(2-nitrovinyl)naphthalene (**2d**). Yellow solid; ^{1}H-NMR (400 MHz, $CDCl_3$): δ_H = 8.10 (d, J = 13.7 Hz, 1H), 7.94 (s, 1H), 7.87−7.82 (m, 3H), 7.65 (d, J = 13.7 Hz, 1H), 7.59−7.52 (m, 3H); ^{13}C-NMR (100.5 MHz, $CDCl_3$): δ_C = 139.1, 137.0, 134.8, 133.02 132.2, 129.3, 128.8, 128.3, 127.9, 127.4, 127.2, 123.2.

6.1.2. ^{1}H NMR data of Michael products

(S)-2-((R)-2-Nitro-1-phenylethyl)cyclohexanone (**3aa**) [1]. White solid (108.8 mg, 88%); ^{1}H-NMR (400 MHz, $CDCl_3$) *syn*-**3aa**: δ 7.34–7.28 (m, 3H), 7.18–7.15 (m, 2H), 4.94 (dd, J =

12.4, 4.4 Hz, 1H), 4.64 (dd, *J* = 12.4, 10.0 Hz, 1H), 3.76 (dd, *J* = 10.0, 4.8 Hz, 1H), 2.73–2.66 (m, 1H), 2.51–2.35 (m, 2H), 2.12–2.04 (m, 1H), 1.82–1.51 (m, 4H), 1.29–1.19 (m, 1H); detectable peaks of *anti*-**3aa**: δ 4.89–4.81 (m, 0.1H), 4.04–3.99 (m, 0.05H), 2.76–2.75 (m, overlapped with *syn*-**3aa**, 0.04H), 2.30–2.24 (m, overlapped with *syn*-**3aa**, 0.02H), 1.92–1.84 (m, 0.04H), 1.43–1.34 (m, 0.05H); ^{13}C-NMR (100.5 MHz, $CDCl_3$) *syn*-**3aa**: δ 211.9, 137.7, 128.8, 128.1, 127.6, 78.8, 52.4, 43.8, 42.6, 33.1, 28.4, 24.9; detectable peaks of *anti*-**3aa**: δ 210.4, 138.3, 128.6, 128.2, 127.4, 76.4, 53.7, 42.9, 42.2, 29.8, 27.3; SFC: Daicel Chiralpak IC-3 (λ = 210 nm, CO_2/2-propanol, 93:7, 1.0 mL/min, 30 °C), t_r (*major*) = 3.56 min, t_r (*minor*) = 4.70 min.

(S)-2-((R)-1-(4-Methoxyphenyl)-2-nitroethyl)cyclohexanone (**3ab**) [1]. Yellow solid (94.6 mg, 68%); ^{1}H-NMR (400 MHz, $CDCl_3$) *syn*-**3ab**: δ 7.08 (d, *J* = 8.4 Hz, 2H), 6.85 (d, *J* = 8.8 Hz, 2H), 4.91 (dd, *J* = 12.4, 4.8 Hz, 1H), 4.58 (dd, *J* = 12.4, 10.0 Hz, 1H), 3.78 (s, 3H), 3.74–3.68 (m, 1H), 2.68–2.61 (m, 1H), 2.50–2.34 (m, 2H), 2.11–2.04 (m, 1H), 1.82–1.52 (m, 4H), 1.28–1.18 (m, 1H); detectable peaks of *anti*-**3ab:** δ 7.20–7.16 (m, 0.09H), 4.87–4.71 (m, 0.13H), 3.96–3.88 (m, 0.06H); ^{13}C-NMR (100.5 MHz, $CDCl_3$) *syn*-**3ab**: δ 212.0, 158.8, 129.4, 129.0, 114.1, 79.0, 55.1, 52.5, 43.1, 42.6, 33.0, 28.4, 24.9; detectable peaks of *anti*-**3ab**: δ 210.6, 158.7, 129.3, 113.9, 76.9, 53.7, 42.4, 42.2, 30.0, 27.2; SFC: Daicel Chiralpak AD-3, (λ = 220 nm, CO_2/methanol, 95:5, 1.0 mL/min, 30 °C), t_r (*minor*) = 5.90 min, t_r (*major*) = 8.61 min.

(S)-2-((R)-1-(4-Bromophenyl)-2-nitroethyl)cyclohexanone (**3ac**) [1]. White solid (135.7 mg, 83%); ^{1}H-NMR (400 MHz, $CDCl_3$) *syn*-**3ac**: δ 7.48–7.43 (m, 2H), 7.20–7.04 (m, 2H), 4.93 (dd, *J* = 12.8, 4.6 Hz, 1H), 4.60 (dd, *J* = 12.8, 10.1 Hz, 1H), 3.75 (td, *J* = 9.8, 4.4 Hz, 1H), 2.68–2.62 (m, 1H), 2.50–2.45 (m, 1H), 2.42–2.33 (m, 1H), 2.12–2.06 (m, 1H), 1.83–1.55 (m, 4H),

1.23 (qd, *J* = 12.4, 3.5 Hz, 1H); detectable peaks of *anti*-**3ac**: δ 7.44–7.43 (m, 0.26H), 7.16–7.14 (m, 0.21H), 4.89–4.78 (m, 0.21H), 3.94–3.89 (m, 0.12H), 2.75–2.70 (m, overlapped with *syn*-**3ac**, 0.11H), 1.94–1.87 (m, 0.13H), 1.42–1.31 (m, 0.11H); ^{13}C-NMR (100.5 MHz, $CDCl_3$) *syn*-**3ac**: δ 211.4, 136.8, 131.9, 129.8, 121.5, 78.4, 52.1, 43.3, 42.6, 33.0, 28.3, 24.9; detectable peaks of *anti*-**3ac**: δ 210.2, 137.3, 131.7, 130.1, 76.4, 53.4, 42.2, 30.0, 27.2; SFC: Daicel Chiralpak IC-3, (λ = 220 nm, CO_2/2-propanol, 95:5, 1.0 mL/min, 30 °C), t_r (*major*) = 6.22 min, t_r (*minor*) = 9.62 min.

(S)-2-((R)-1-Naphthyl-2-nitroethyl)cyclohexanone (**3ad**) [1]. Off-white solid (105.1 mg, 71%); ^{1}H-NMR (400 MHz, $CDCl_3$) *syn*-**3ad**: δ 7.82–7.77 (m, 3H), 7.67 (d, *J* = 26.5 Hz, 1H), 7.49–7.44 (m, 2H), 7.30–7.25 (m, 1H), 5.03 (dd, *J* = 12.6, 4.3 Hz, 1H), 4.72 (dd, *J* = 12.8, 10.1 Hz, 1H), 3.95 (td, *J* = 10.1, 4.1 Hz, 1H), 2.76 (td, *J* = 11.1, 4.6 Hz, 1H), 2.49–2.32 (m, 2H), 2.05–2.00 (m, 1H), 1.71–1.49 (m, 4H), 1.28–1.19 (m, 1H); detectable peaks of *anti*-**3ad**: δ 7.69 (s, 0.12H), 7.39–7.36 (m, 0.11H), 4.96–4.93 (m, 0.13H), 4.20–4.15 (m, 0.08H), 2.24 (m, 0.07H), 1.85–1.76 (m, 0.08H), 1.42–1.29 (m, overlapped with *syn*-**3ad**, 0.04H); ^{13}C-NMR (100.5 MHz, $CDCl_3$) *syn*-**3ad**: δ 211.8, 135.0, 133.2, 132.7, 128.7, 127.7, 127.5, 126.3, 126.0, 125.1, 78.7, 52.3, 44.0, 42.6, 33.2, 28.4, 24.9; detectable peaks of *anti*-**3ad**: δ 210.4, 135.8, 133.1, 132.5, 128.4, 127.5, 126.9, 126.4, 126.2, 126.0, 76.4, 53.7, 42.9, 42.2, 29.8, 27.2; SFC: Daicel Chiralpak OD-3, (λ = 210 nm, CO_2/2-propanol, 82:18, 1.0 mL/min, 30 °C), t_r (*major*) = 1.34 min, t_r (*minor*) = 1.73 min.

(S)-3-((R)-2-Nitro-1-phenylethyl)tetrahydro-4H-thiopyran-4-one (**3ba**) [2]. White solid (100.8 mg, 76%); ^{1}H-NMR (400 MHz, $CDCl_3$) *syn*-**3ba**: δ 7.36–7.17 (m, 5H), 4.73 (dd, *J* = 12.8, 4.6 Hz, 1H), 4.61 (dd, *J* = 12.8, 9.6 Hz, 1H), 3.96 (td, *J* = 10.3, 4.7 Hz, 1H), 3.06–2.93

(m, 3H), 2.87–2.77 (m, 2H), 2.62–2.41 (m, 2H); detectable peaks of *anti*-**3ba**: δ 4.90–4.81 (m, 0.02H), 4.18–4.13 (m, 0.03H), 2.94–2.92 (m, overlapped with *syn*-**3ba**, 0.06H); ^{13}C-NMR (100.5 MHz, $CDCl_3$) *syn*-**3ba**: δ 209.5, 136.4, 129.3, 128.3, 128.1, 78.6, 54.9, 44.5, 43.4, 35.1, 31.6; detectable peak of *anti*-**3ba**: δ 129.0; SFC: Daicel Chiralpak IC-3, (λ = 210 nm, CO_2/methanol, 96:4, 1.0 mL/min, 30 °C), t_r (*major*) = 2.41 min, t_r (*minor*) = 2.75 min.

(S)-2-((R)-2-Nitro-1-phenylethyl)cyclopentan-1-one (**3ca**) [1]. Off-white solid (13.7 mg, 12%); ^{1}H-NMR (400 MHz, $CDCl_3$) *syn*-**3ca**: δ 7.32 (s, 3H), 7.14 (s, 2H), 5.32 (dd, *J* = 12.8, 5.5 Hz, 1H), 5.00 (d, *J* = 7.8 Hz, 1H), 4.70 (dd, *J* = 12.8, 10.1 Hz, 1H), 3.82 (dd, *J* = 11.9, 7.8 Hz, 1H), 3.71–3.65 (m, 1H), 2.36 (d, *J* = 43.9 Hz, 1H), 2.12 (d, *J* = 41.6 Hz, 1H), 1.89 (d, *J* = 49.4 Hz, 1H), 1.70 (d, *J* = 34.8 Hz, 1H), 1.47 (d, *J* = 41.6 Hz, 1H); detectable peaks of *anti*-**3ca**: δ 7.42–7.41 (m, 0.12H), 7.13–7.05 (m, 0.18H), 3.83 (td, *J* = 7.8, 4.1 Hz, 0.34H), 2.29–2.25 (m, overlapped with *syn*-**3ca**, 0.16H), 1.41–1.20 (m, 0.17H); ^{13}C-NMR (100.1 MHz, $CDCl_3$) *syn*-**3ca**: δ 218.5, 137.7, 128.9, 128.4, 127.9, 78.2, 50.4, 44.1, 38.6, 28.3, 20.0; detectable peaks of *anti*-**3ca**: δ 219.1, 137.3, 128.9 (overlapped with *syn*-**3ca**), 77.1, 51.4, 44.0, 39.2, 27.0, 20.5; SFC: Daicel Chiralpak IA-3, (λ = 210 nm, CO_2/2-propanol, 95:5, 1.0 mL/min, 30 °C), t_r (*minor*) = 1.70 min, t_r (*major*) = 2.56 min.

(R)-5-Nitro-4-phenylpentan-2-one (**3da**) [2]. White solid (72.3 mg, 70%); ^{1}H-NMR (400 MHz, $CDCl_3$): δ 7.33–7.19 (m, 5H), 4.62 (ddd, *J* = 40.0, 12.3, 7.5 Hz, 2H), 4.03–3.95 (m, 1H), 2.89 (d, *J* = 7.3 Hz, 2H), 2.09 (s, 3H); ^{13}C-NMR (100.5 MHz, $CDCl_3$): δ 205.4, 138.8, 128.9, 127.7, 127.3, 79.3, 46.0, 38.9, 30.2; SFC: Daicel Chiralpak IC-3, (λ = 210 nm, CO_2/2-propanol, 93:7, 1.0 mL/min, 30 °C), t_r (*major*) = 3.05 min, t_r (*minor*) = 3.50 min.

6.1.3. Supercritical fluid chromatography profiles

Each product is described with a set of two SFC profiles. The first is of the racemic product, and the second, the asymmetric. The vertical axis is the absorbance in atomic units (AU) and the horizontal axis is the retention time in minute (min).

(S)-2-((R)-2-Nitro-1-phenylethyl)cyclohexanone (**3aa**)

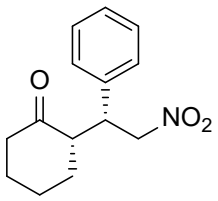

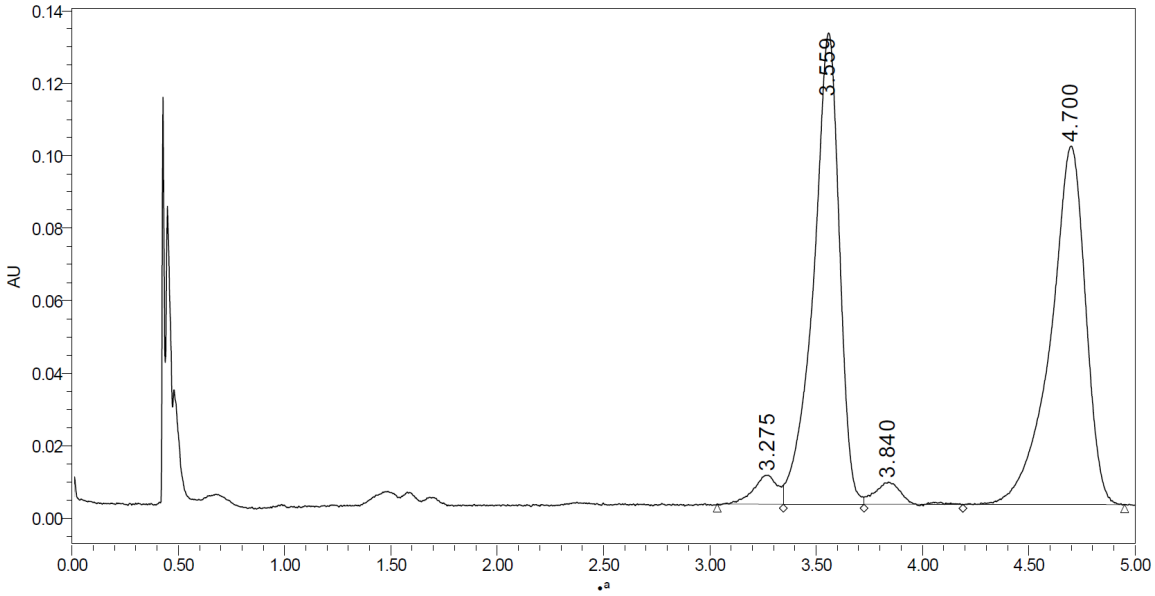

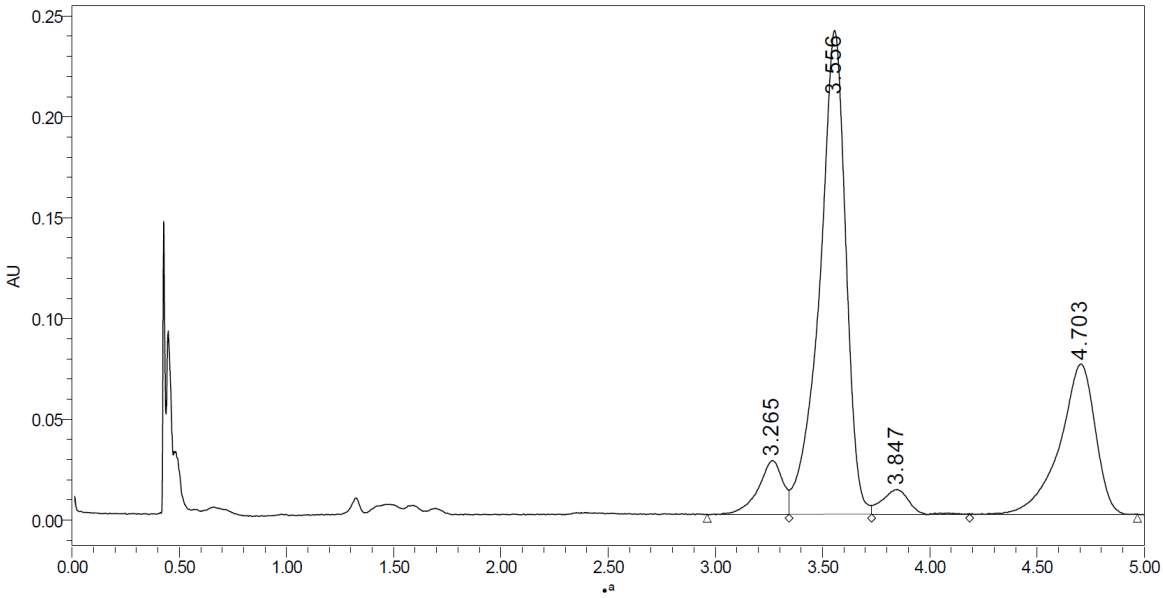
AU
0.25
0.20
0.15
0.10
0.05
0.00
3.265
3.556
3.847
4.703
0.00
0.50
1.00
1.50
2.00
2.50
3.00
3.50
4.00
4.50
5.00
min

(S)-2-((R)-1-(4-Methoxyphenyl)-2-nitroethyl)cyclohexanone (**3ab**)

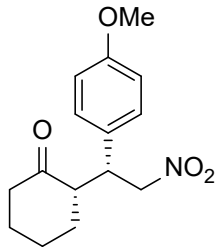

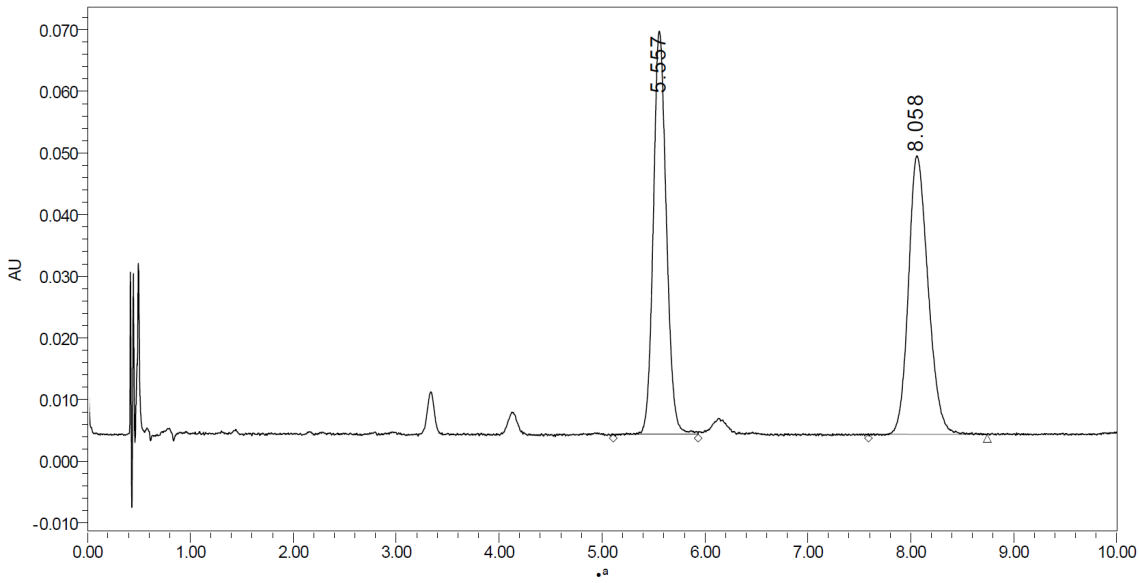

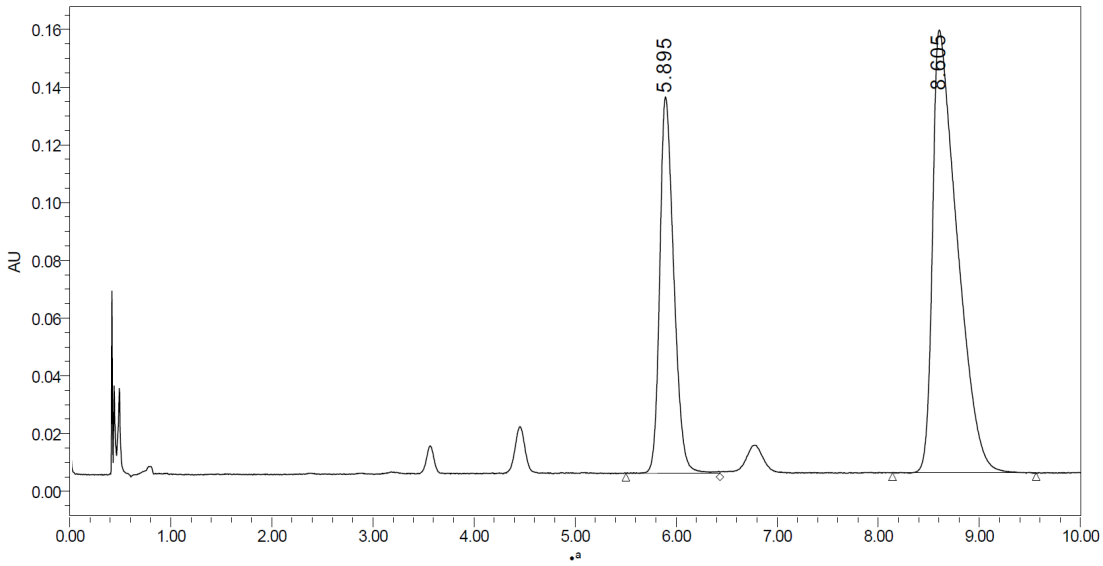

(S)-2-((R)-1-(4-Bromophenyl)-2-nitroethyl)cyclohexanone (**3ac**)

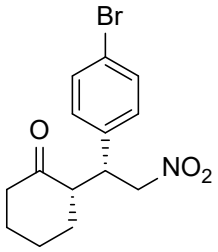

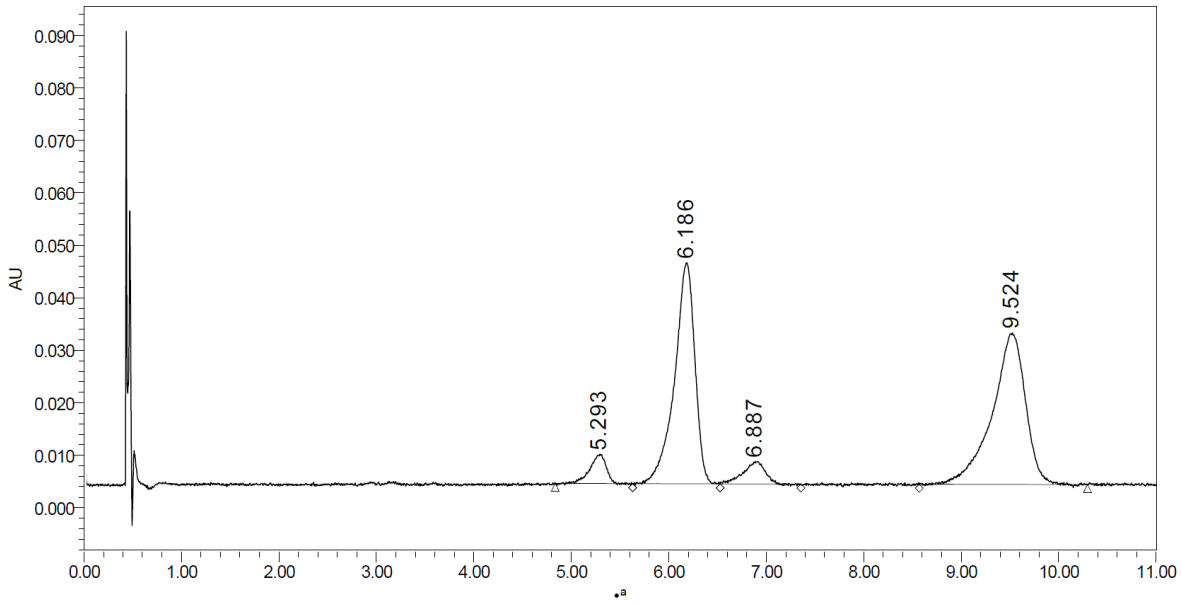

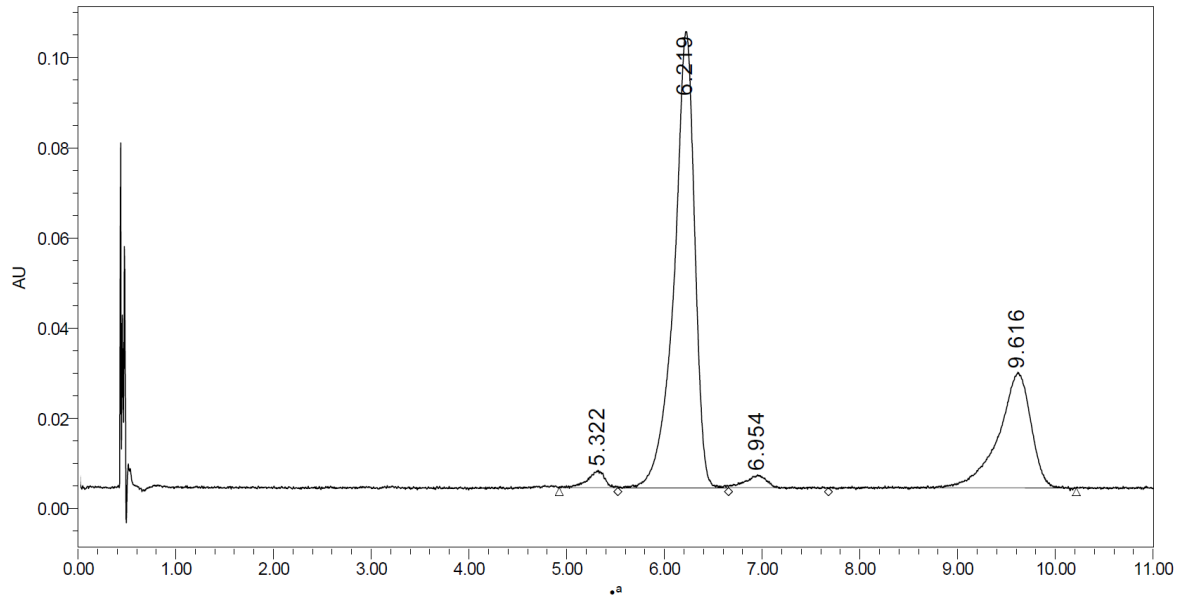

(S)-2-((R)-1-Naphthyl-2-nitroethyl)cyclohexanone (**3ad**)

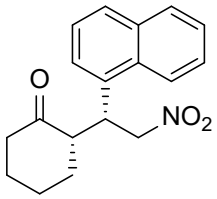

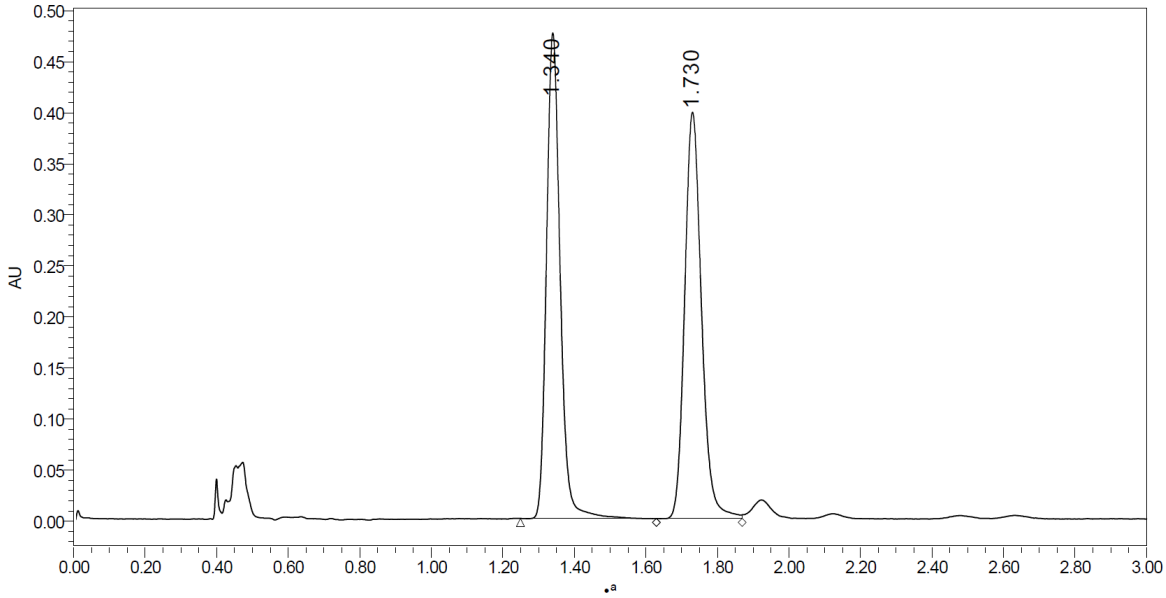

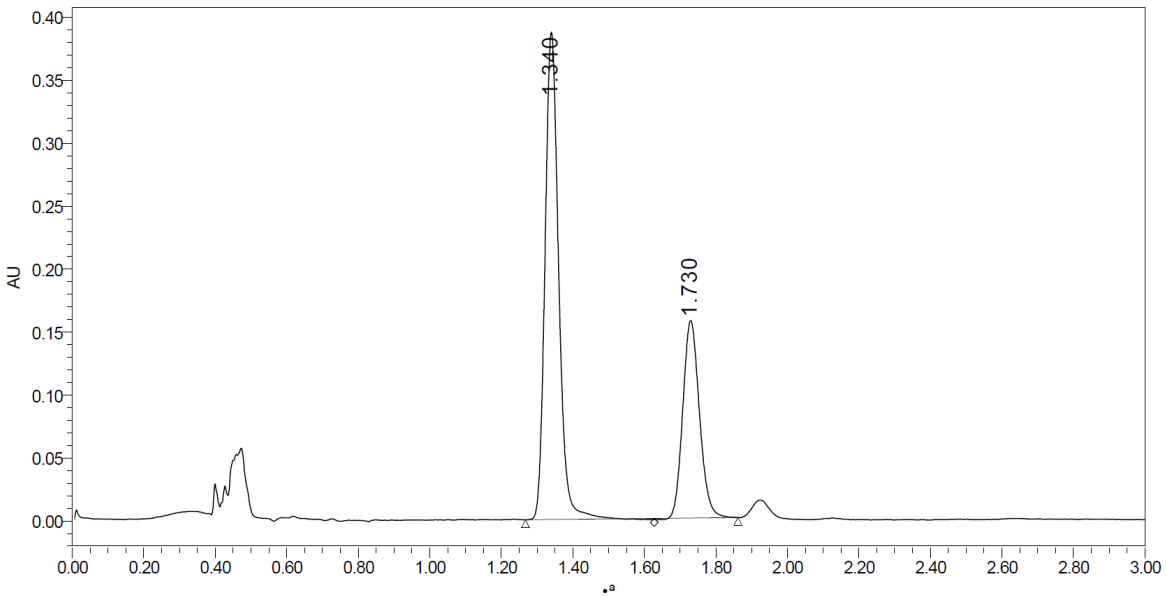

(S)-3-((R)-2-Nitro-1-phenylethyl)tetrahydro-4H-thiopyran-4-one (**3ba**)

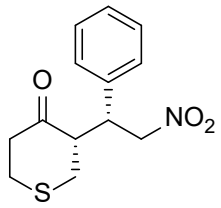

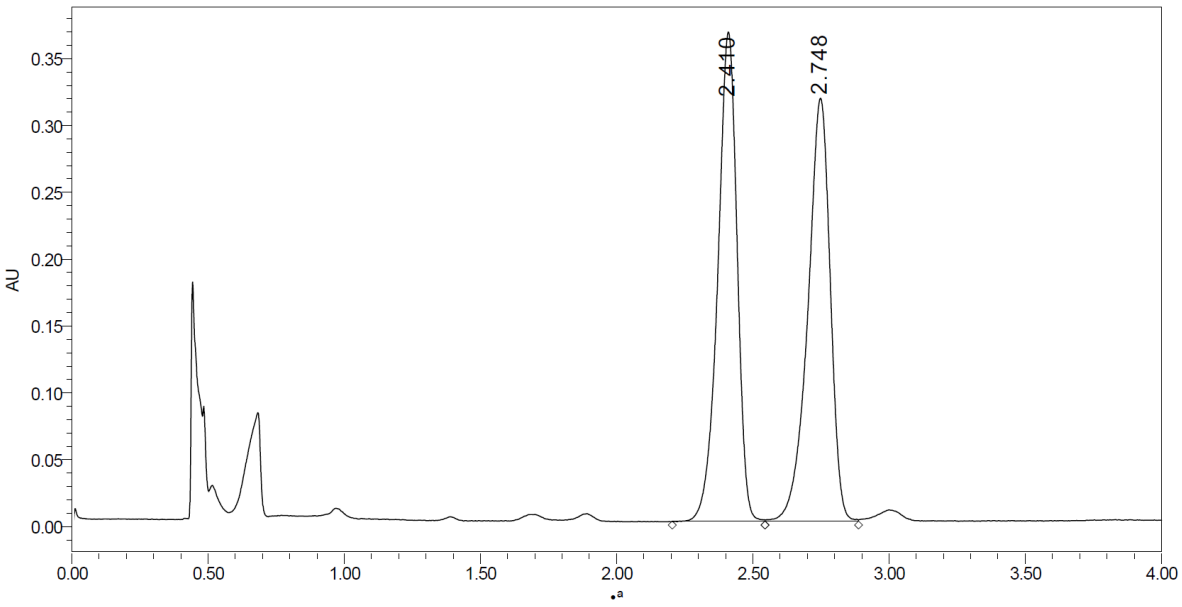

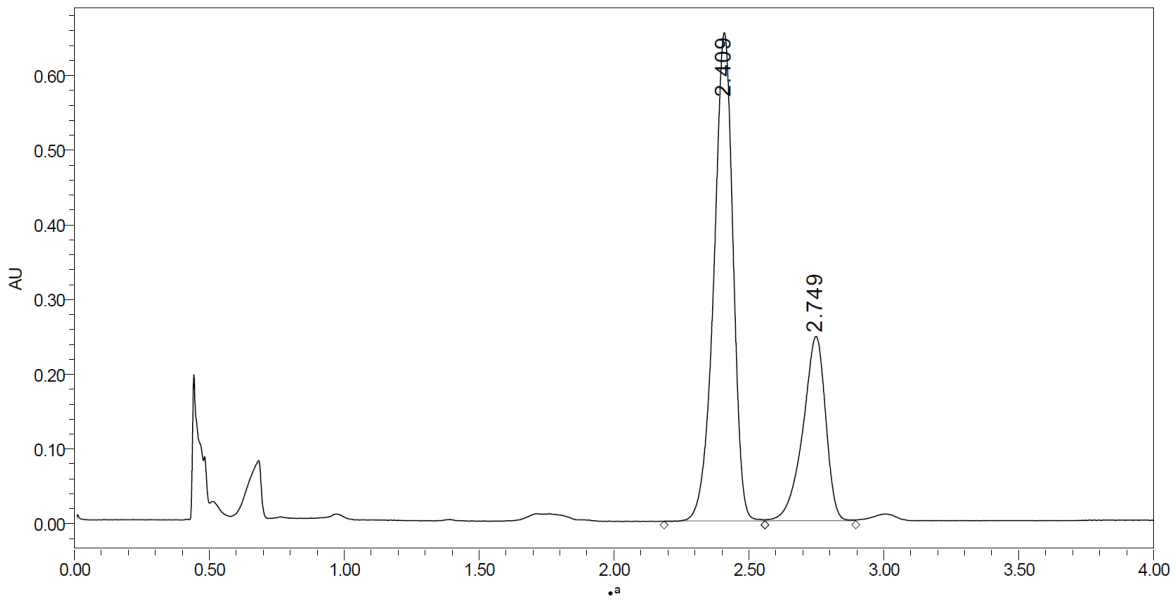

(S)-2-((R)-2-nitro-1-phenylethyl)cyclopentan-1-one (**3ca**)

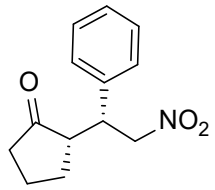

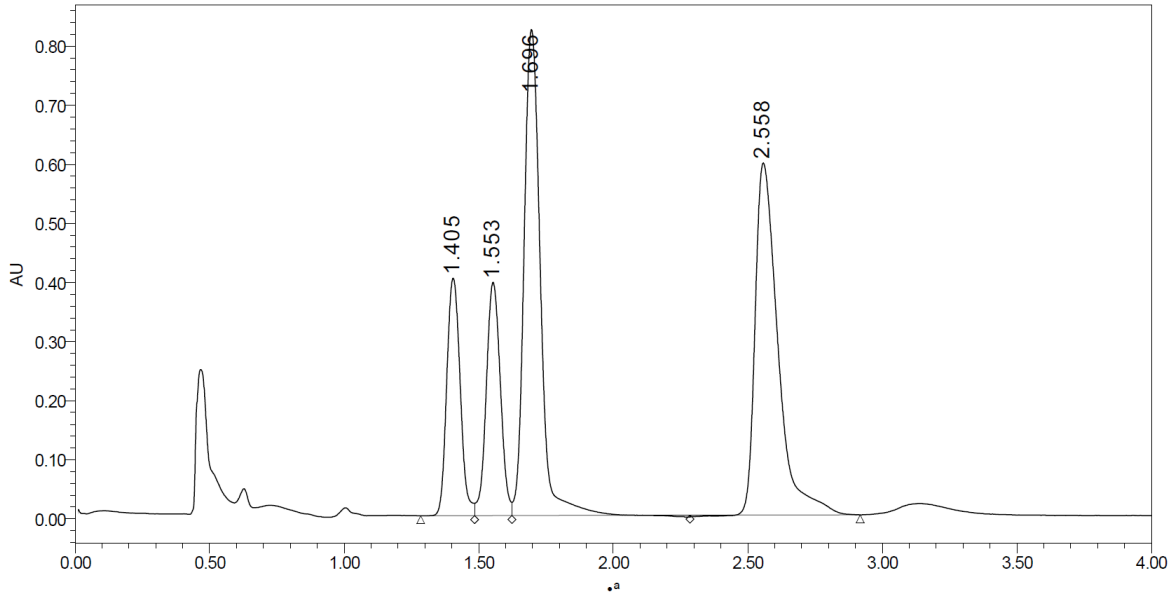

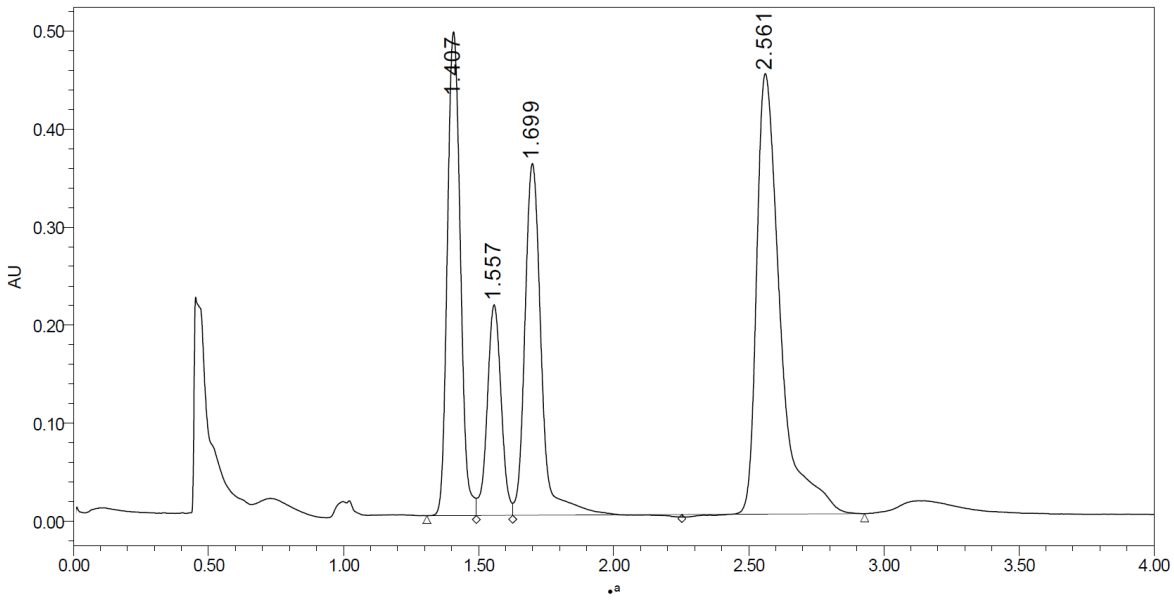

(R)-5-nitro-4-phenylpentan-2-one (**3da**)

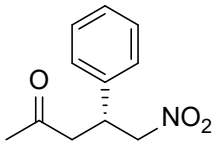

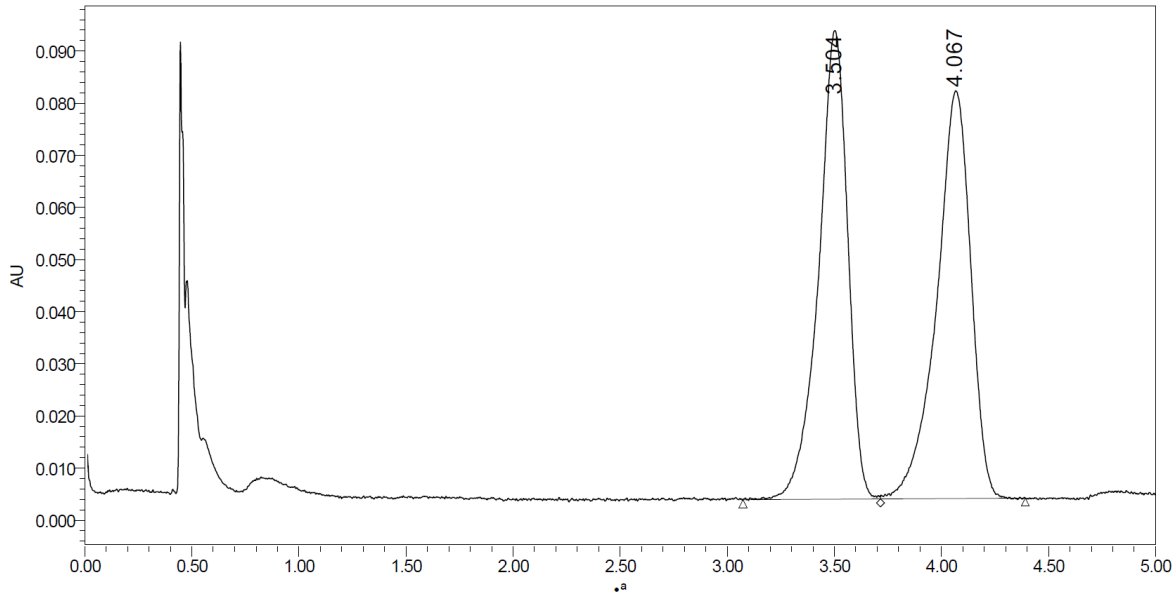

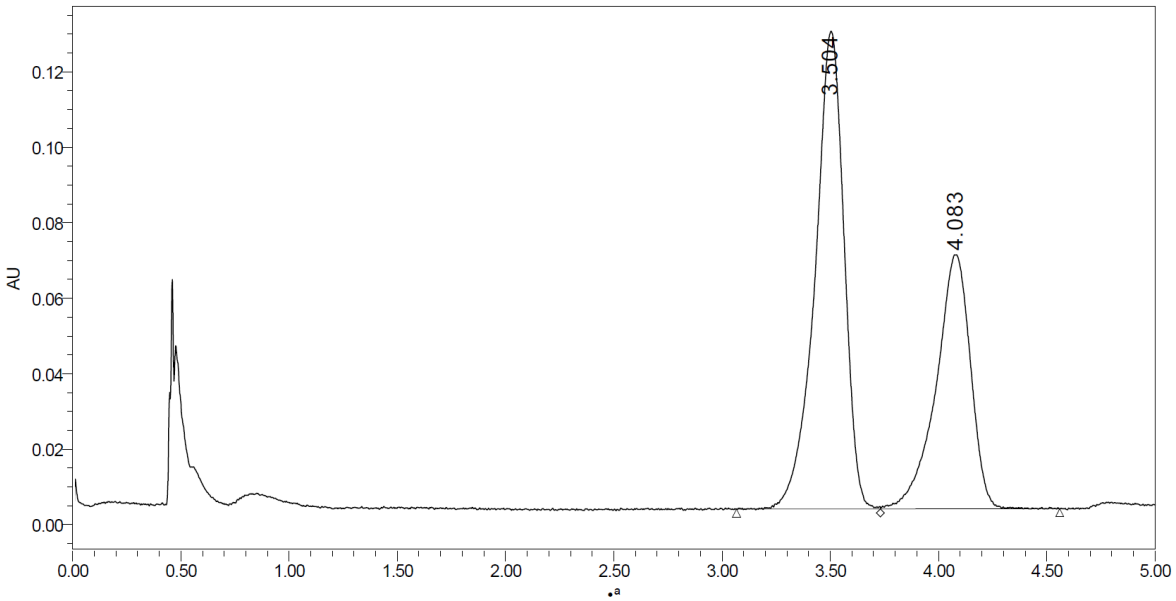

6.2. TOCNF Enhanced Aldol reaction

6.2.1. ^{1}H NMR spectra of aldol products

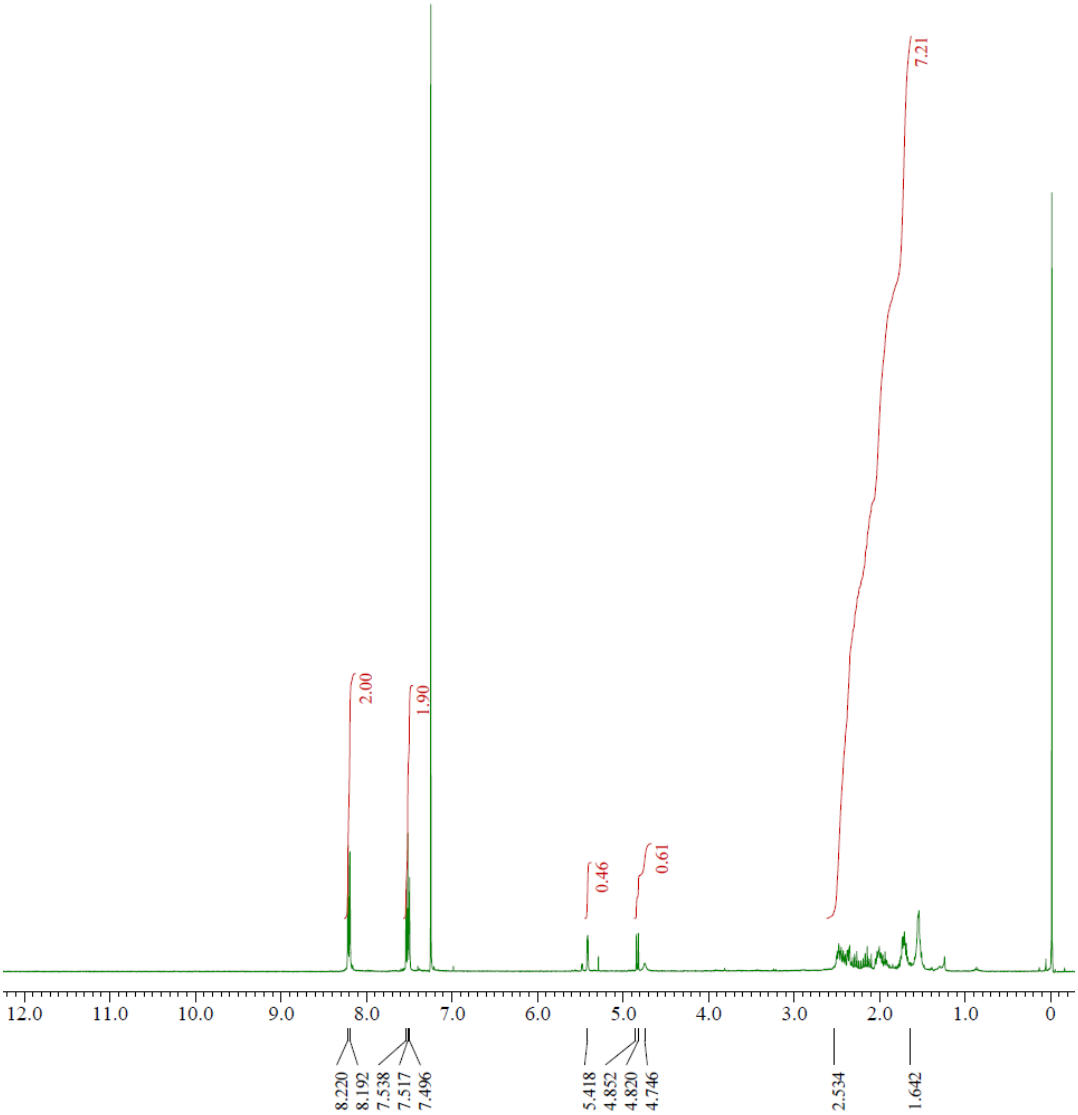

Figure 6. 1 ^{1}H NMR spectrum (400 MHz, $CDCl_3$) of (*R*)-2-((*R*)-hydroxy(4-nitrophenyl)methyl)cyclopentan-1-one.

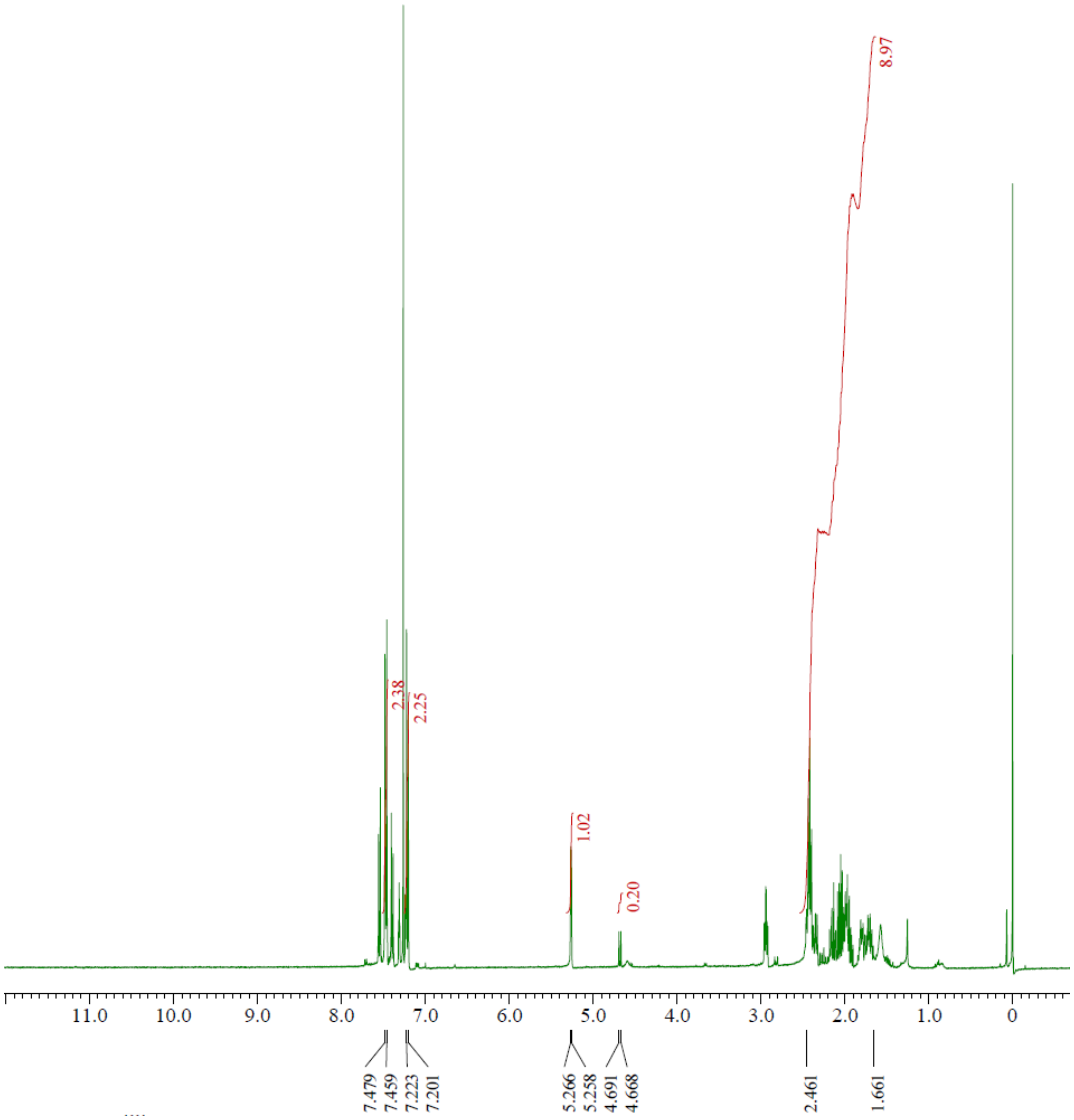

Figure 6. 2 ^{1}H NMR spectrum (400 MHz, $CDCl_3$) of (*R*)-2-((*R*)-hydroxy(4-bromophenyl)methyl)cyclopentan-1-one.

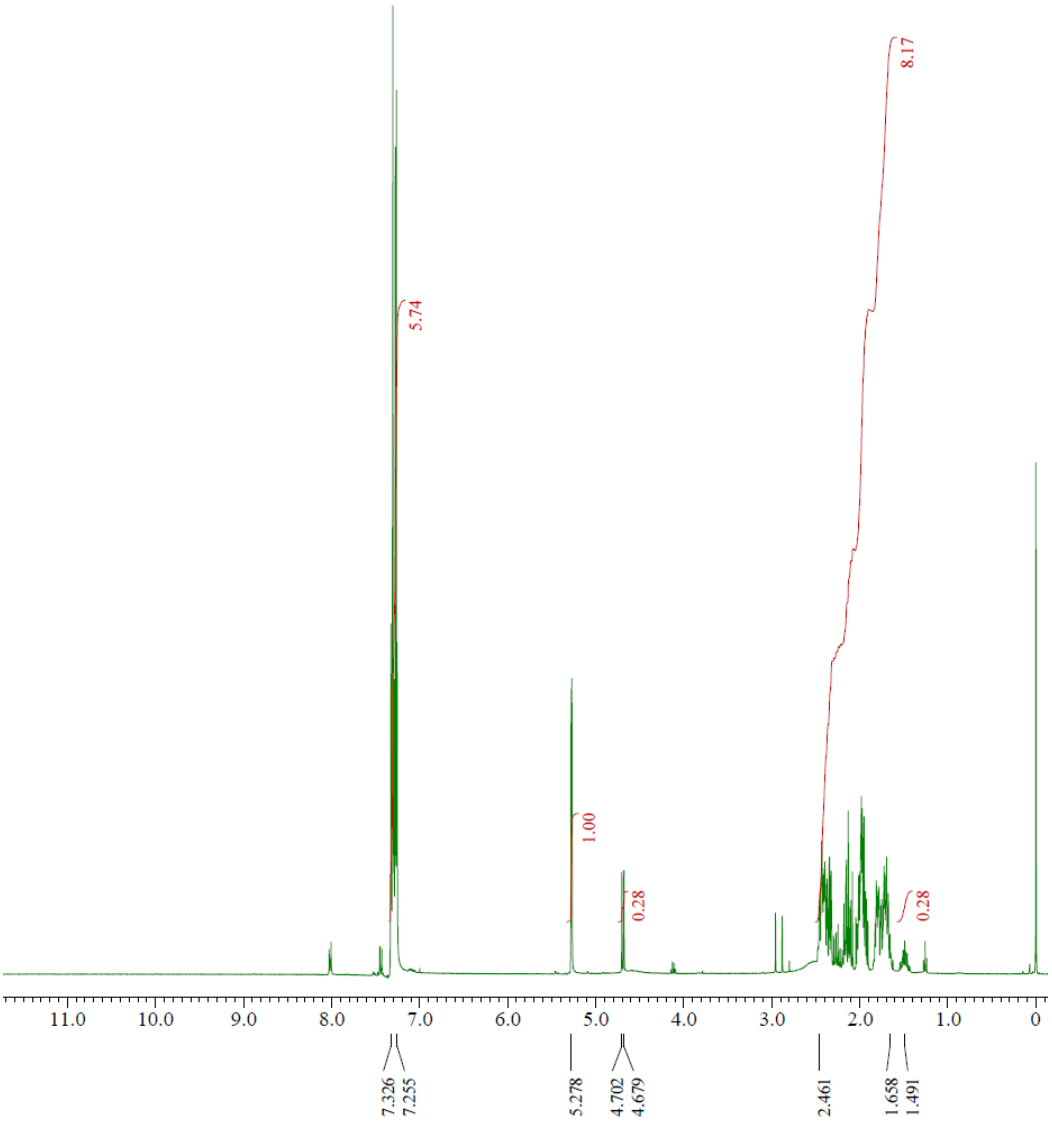

Figure 6. 3 ^{1}H NMR spectrum (400 MHz, $CDCl_3$) of (*R*)-2-((*R*)-hydroxy(4-chlorophenyl)methyl)cyclopentan-1-one.

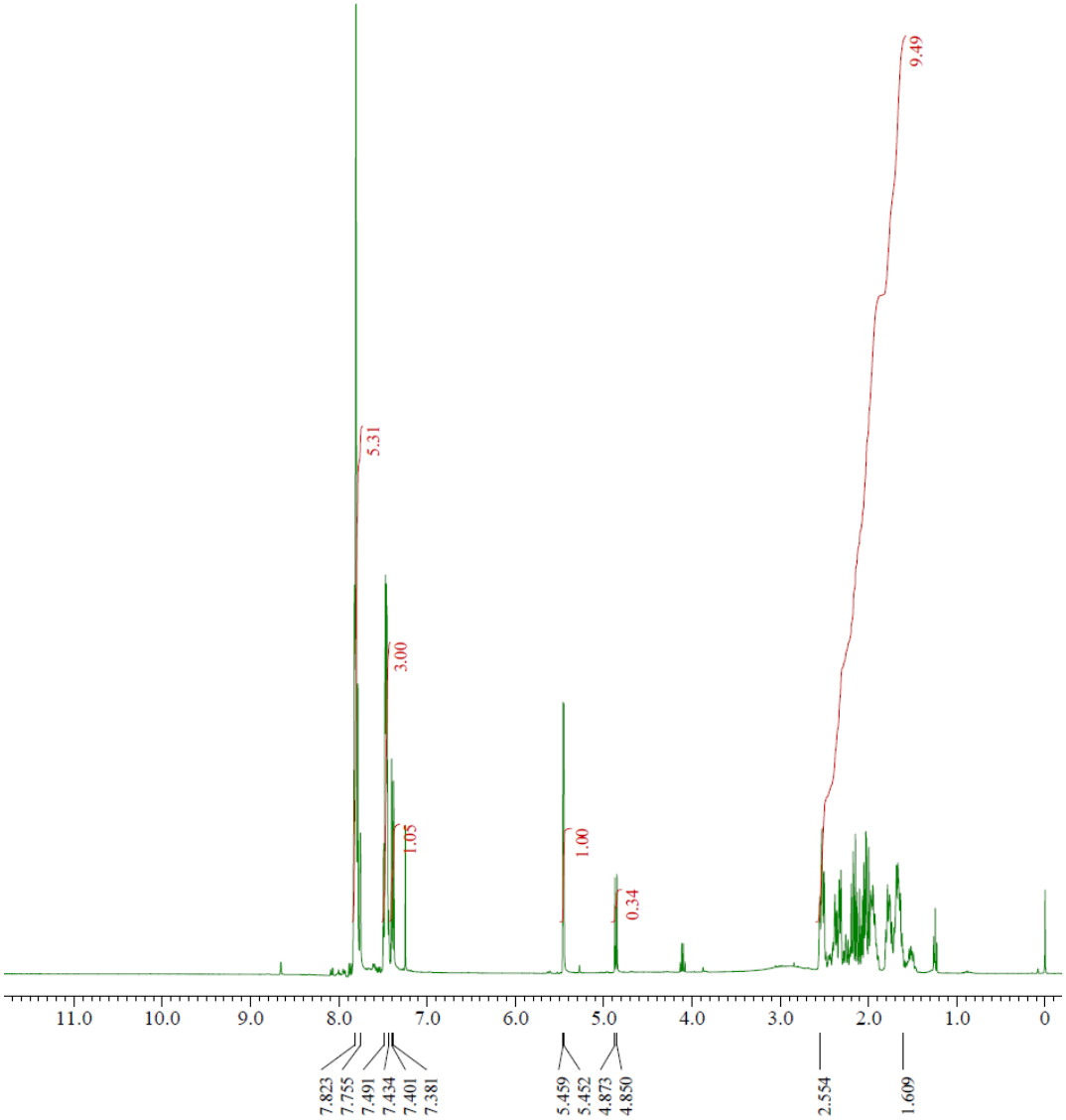

Figure 6. 4 ^{1}H NMR spectrum (400 MHz, $CDCl_3$) of (*R*)-2-((*R*)-hydroxy(naphthalen-2-yl)methyl)cyclopentan-1-one.

6.2.2. Supercritical fluid chromatography profiles

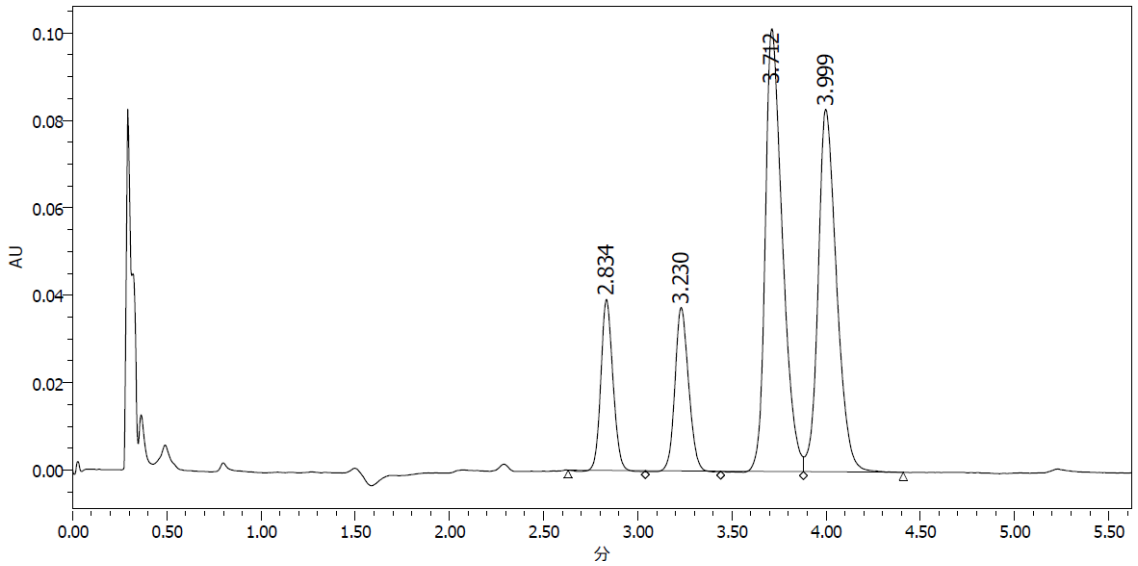

	RT (min)	Area	% Area	Height
1	2.834	175291	11.15	39153
2	3.230	188773	12.00	37384
3	3.712	643366	40.91	101261
4	3.999	565176	35.94	82912

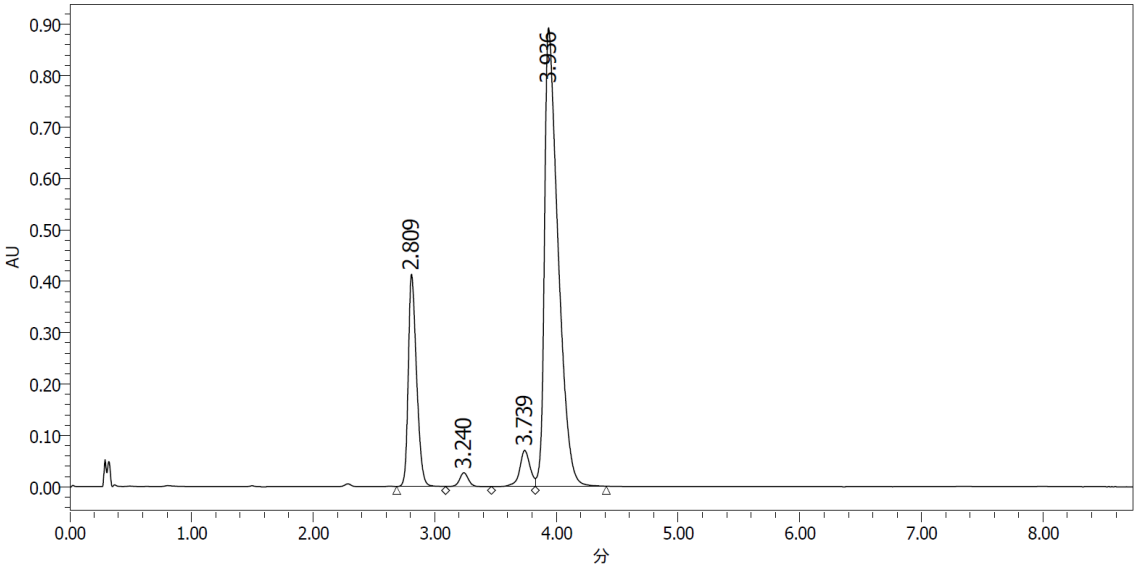

	RT (min)	Area	% Area	Height
1	2.809	1955482	20.74	412926
2	3.240	132665	1.41	26662
3	3.739	414365	4.39	70045
4	3.936	6926253	73.46	891915

Figure 6. 5 SFC chromatogram of (*R*)-2-((*R*)-hydroxy(4-nitrophenyl)methyl)cyclopentan-1-one. Daicel Chiralpak IB-3, CO_2/2-propanol = 95:5, flow = 1.0 mL min^{-1}, 30 °C, λ = 264 nm, t_r(minor) = 3.7 min, t_r(major) = 3.9 min, *er* (*syn*) = 95:5.

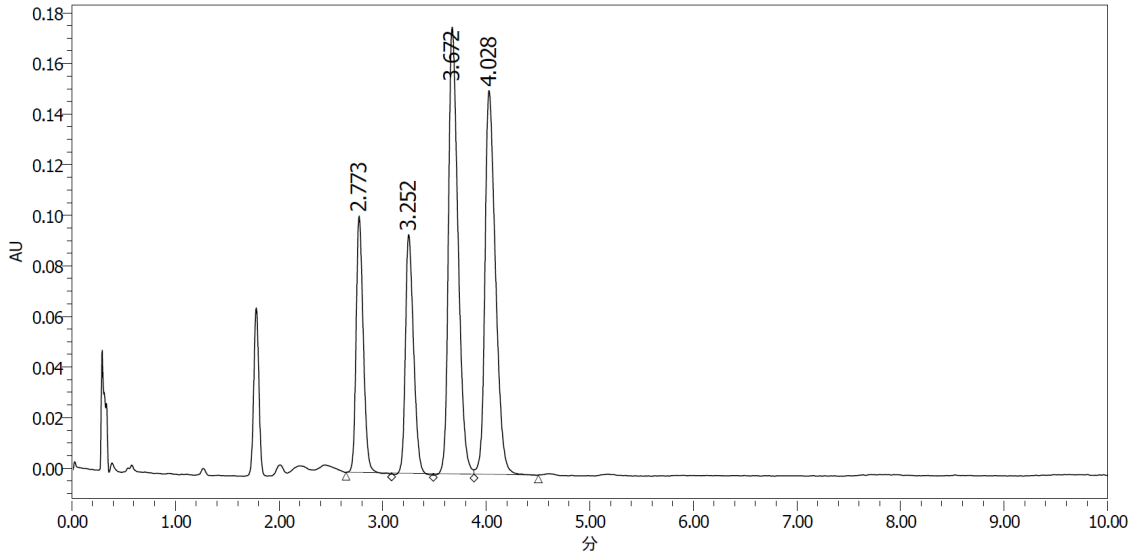

	RT (min)	Area	% Area	Height
1	2.773	486888	15.12	101342
2	3.252	515380	16.00	94398
3	3.672	1143529	33.51	176658
4	4.028	1074444	33.37	151693

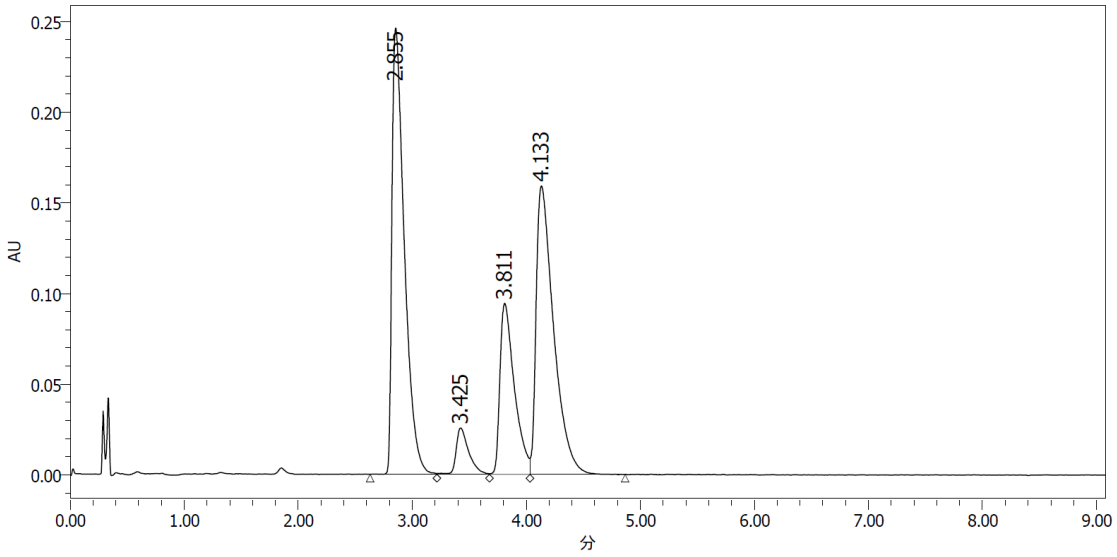

	RT (min)	Area	% Area	Height
1	2.855	1856592	40.52	246170
2	3.425	196013	4.28	25608
3	3.811	832806	18.18	94363
4	4.133	1696210	37.02	159080

Figure 6. 6 SFC chromatogram of (*R*)-2-((*R*)-hydroxy(4-bromophenyl)methyl)cyclopentan-1-one. Daicel Chiralpak IB-3, CO_2/2-propanol = 97:3, flow = 1.0 mL min^{-1}, 30 °C, λ = 220 nm, t_r(major) = 2.9 min, t_r(minor) = 3.4 min, *er* (*anti*) = 94:6.

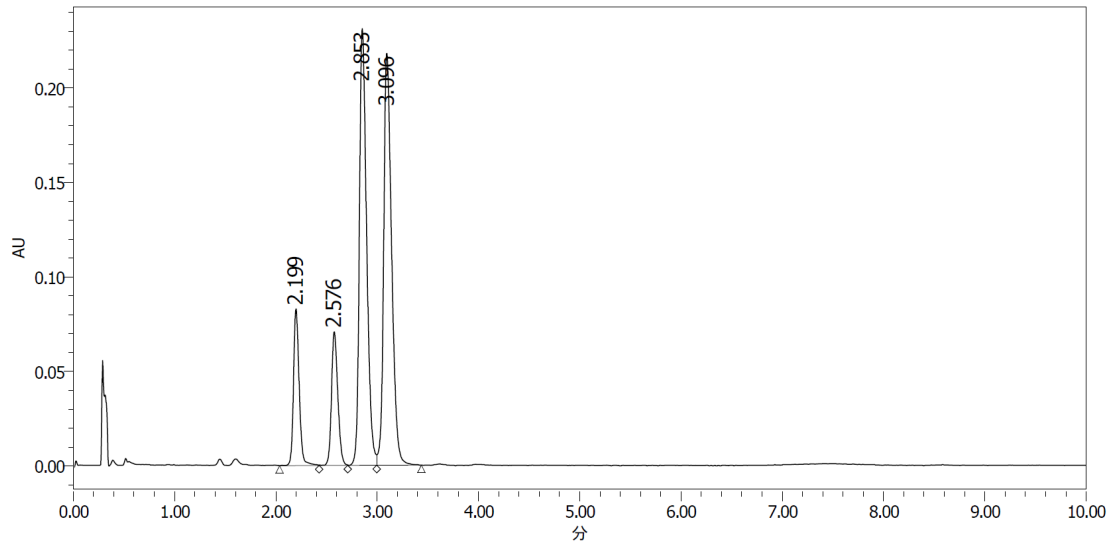

	RT (min)	Area	% Area	Height
1	2.199	322072	10.88	82955
2	2.576	305446	10.31	70786
3	2.853	1150472	38.85	231064
4	3.096	1183328	39.96	218123

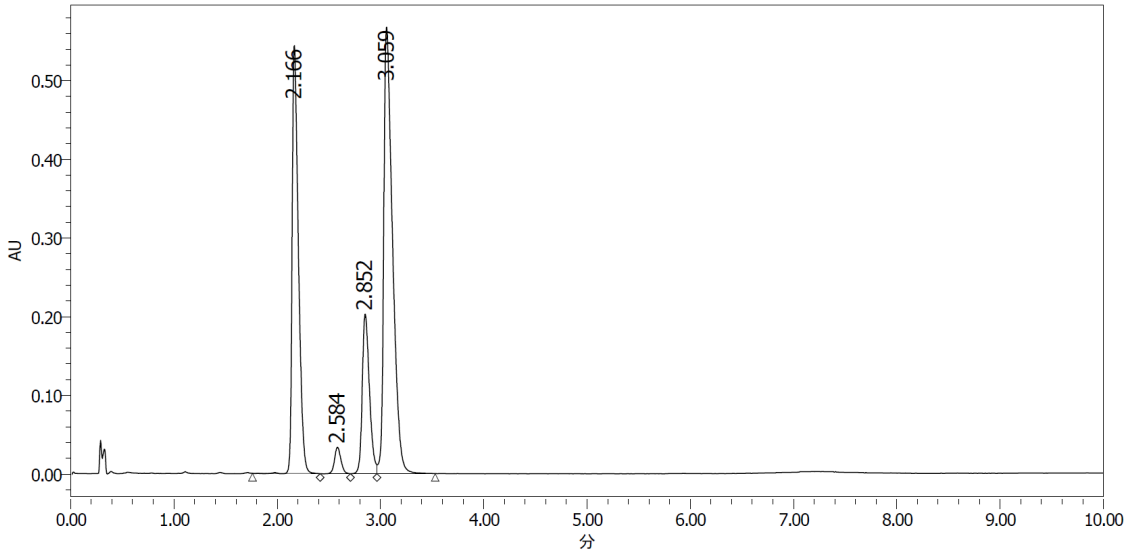

	RT (min)	Area	% Area	Height
1	2.166	2285507	33.87	544277
2	2.584	142768	2.12	33483
3	2.852	978669	14.50	202918
4	3.059	3340448	4951	567628

Figure 6. 7 SFC chromatogram of (*R*)-2-((*R*)-hydroxy(4-chlorophenyl)methyl)cyclopentan-1-one. Daicel Chiralpak IB-3, CO_2/2-propanol = 97:3, flow = 1.0 mL min^{-1}, 30 °C, λ = 220 nm, t_r(major) = 2.2 min, t_r(minor) = 2.6 min, *er* (*anti*) = 94:6.

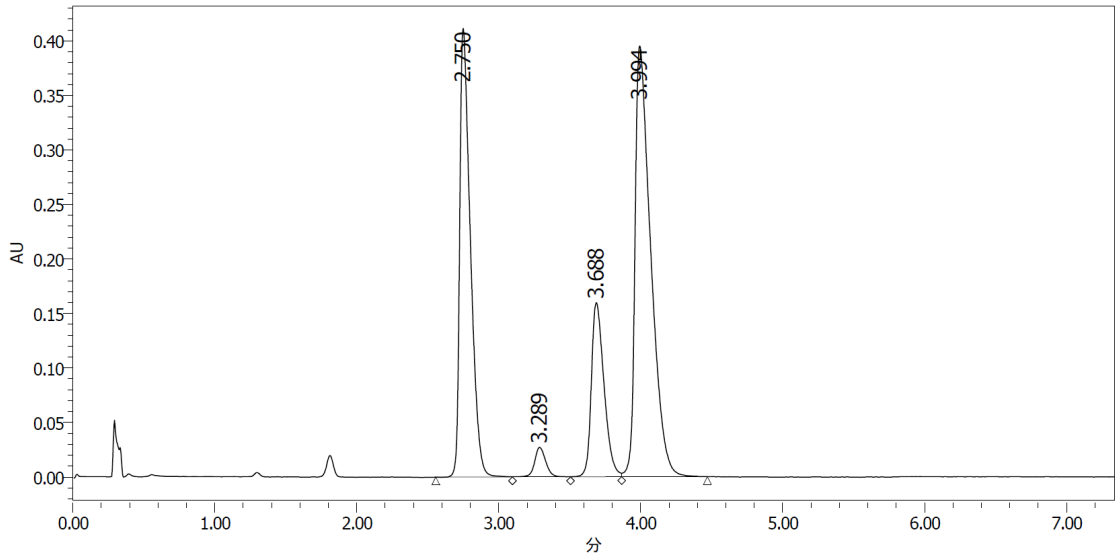

	RT (min)	Area	% Area	Height
1	2.750	2149161	33.97	411413
2	3.289	146172	2.31	27096
3	3.688	987495	15.61	159671
4	3.994	3044236	48.11	395270

Figure 6. 8 SFC chromatogram of (*R*)-2-((*R*)-hydroxy(naphthalen-2-yl)methyl)cyclopentan-1-one. Daicel Chiralpak IB-3, CO_2/2-propanol = 97:3, flow = 1.0 mL min^{-1}, 30 °C, λ = 220 nm, t_r(major) = 2.8 min, t_r(minor) = 3.3 min, *er* (*anti*) = 94:6.

6.3. Biginelli reaction

6.3.1. ^{1}H NMR spectra of Biginelli product

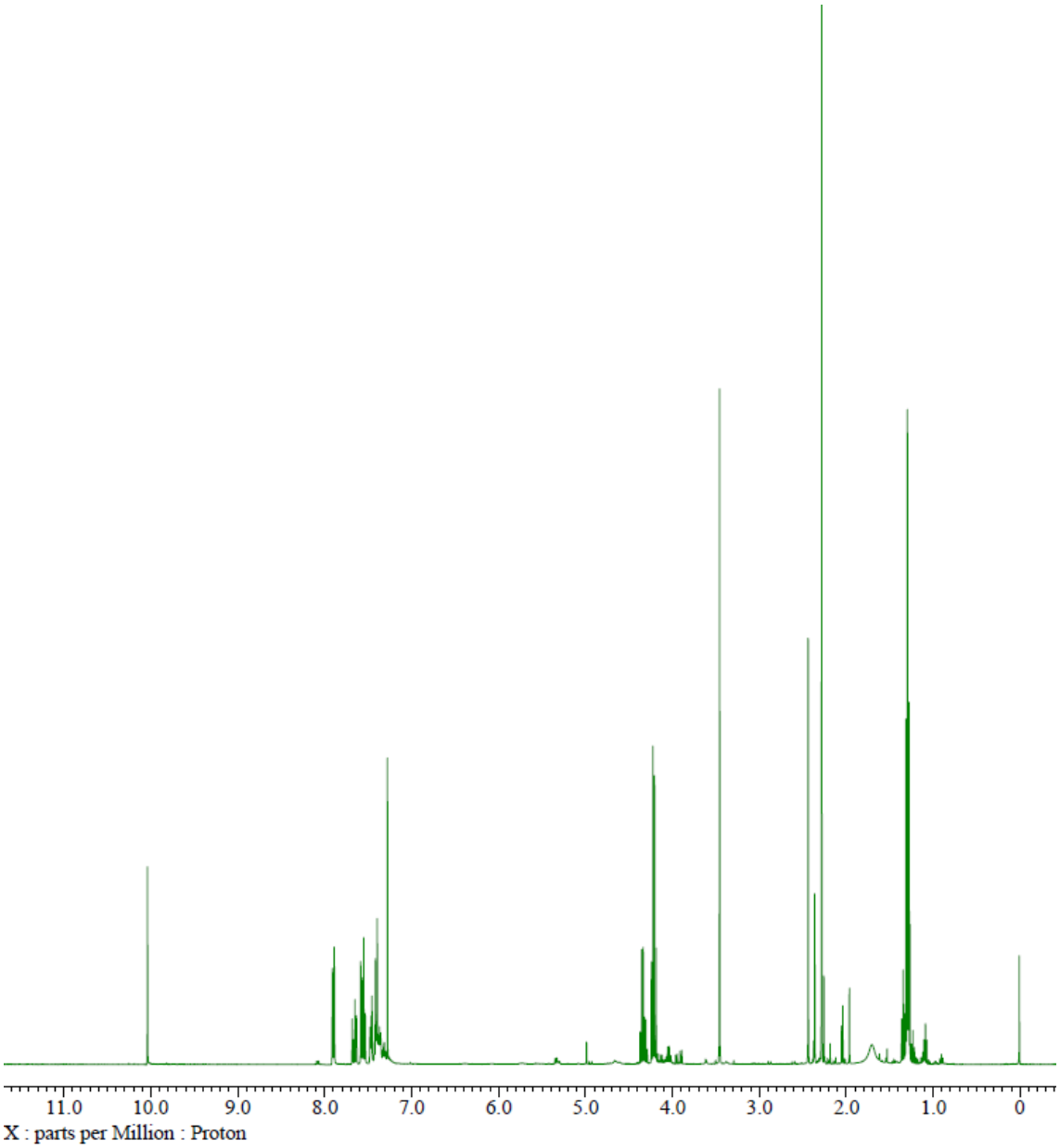

6.3.2. Supercritical fluid chromatography profile

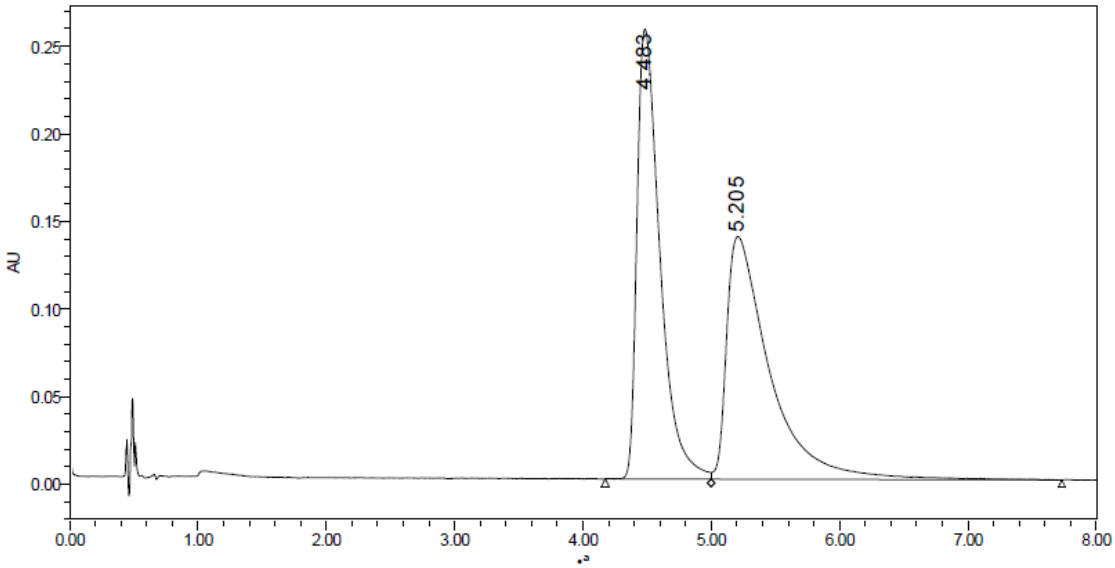

	RT (min)	Area	% Area	Height
1	4.483	3192153	49.71	256952
2	5.205	3229656	50.29	138630

Figure 6. 9 SFC chromatogram of ethyl 6-methyl-2-oxo-4-phenyl-1,2,3,4-tetrahydro-4l3-pyrimidine-5-carboxylate. Daicel Chiralpak AD, CO_2/2-propanol = 80:10, flow = 1.0 mL min^{-1}, 30 °C, λ = 220 nm, *er* = 50:50.

6.4. Wieland-Miescher ketone synthesis

6.4.1. ^{1}H NMR spectra of the Wieland-Miescher ketone

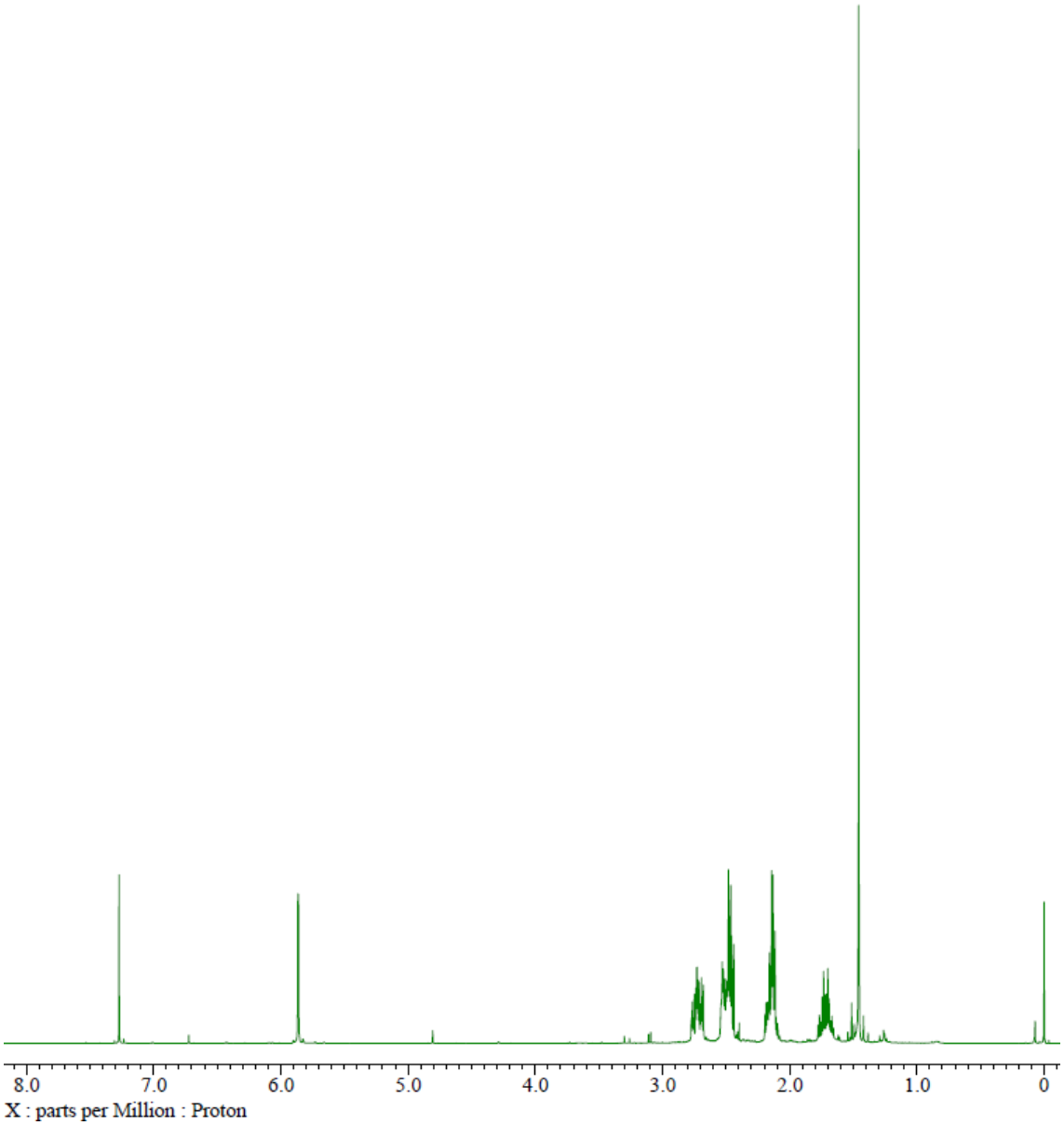

6.4.2. Supercritical fluid chromatography profile

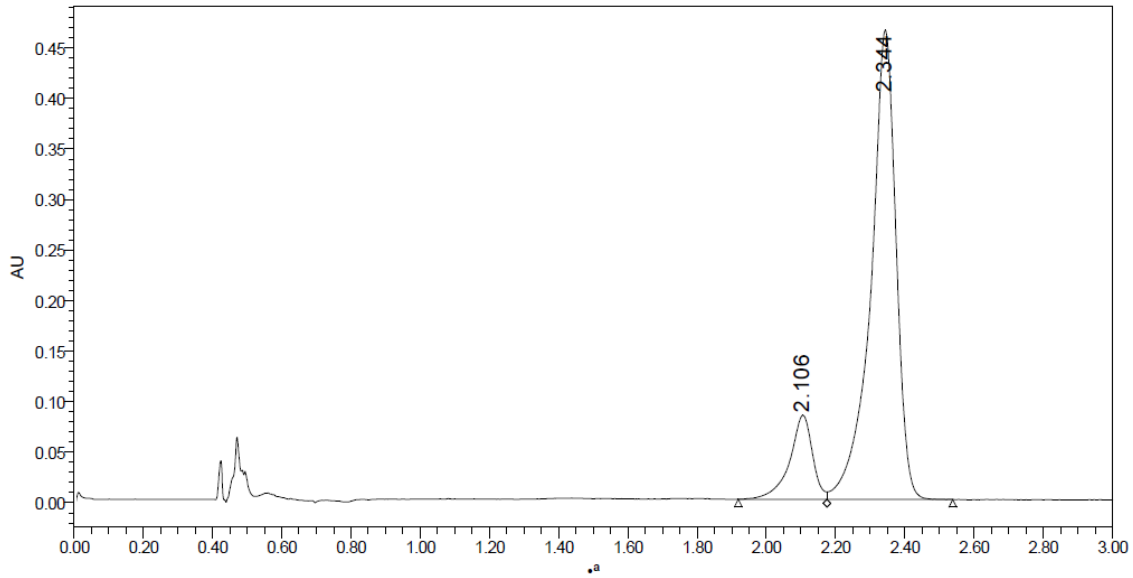

	RT (min)	Area	% Area	Height
1	2.106	381519	13.94	83087
2	2.344	2355787	86.06	464218

Figure 6. 10 SFC chromatogram of (*S*)-8a-methyl-3,4,8,8a-tetrahydronaphthalene-1,6(2H,7H)-dione. Daicel Chiralpak ID, CO_2/2-propanol = 85:15, flow = 1.0 mL min^{-1}, 30 °C, λ = 236 nm, t_r(minor) = 2.1 min, t_r(major) = 2.3 min, *er* (*syn*) = 14:86.

References

1. Syu, S.; Kao, T.-T.; Lin, W. A new type of organocatalyst for highly stereoselective Michael addition of ketones to nitroolefins on water. *Tetrahedron* **2010**, *66*, 891–897.

2. Kaplaneris, N.; Koutoulogenis, G.; Raftopoulou, M.; Kokotos, C.G. 4-Fluoro and 4-Hydroxy Pyrrolidine-thioxotetrahydropyrimidinones: Organocatalysts for Green Asymmetric Transformations in Brine. *J. Org. Chem.* **2015**, *80*, 5464–5473.